Copyright Warning & Restrictions

The copyright law of the United States (Title 17, United States Code) governs the making of photocopies or other reproductions of copyrighted material.

Under certain conditions specified in the law, libraries and archives are authorized to furnish a photocopy or other reproduction. One of these specified conditions is that the photocopy or reproduction is not to be "used for any purpose other than private study, scholarship, or research." If a, user makes a request for, or later uses, a photocopy or reproduction for purposes in excess of "fair use" that user may be liable for copyright infringement,

This institution reserves the right to refuse to accept a copying order if, in its judgment, fulfillment of the order would involve violation of copyright law.

Please Note: The author retains the copyright while the New Jersey Institute of Technology reserves the right to distribute this thesis or dissertation

Printing note: If you do not wish to print this page, then select "Pages from: first page # to: last page #" on the print dialog screen

67-14,246

BARNER, Herbert Eugen, 1936-

KINETICS OF HYDROGEN REDUCTION OF MANGANESE DIOXIDE.

Newark College of Engineering, D. Eng. Sc., 1967
Engineering, chemical

University Microfilms, Inc., Ann Arbor, Michigan

KINETICS OF HYDROGEN REDUCTION OF MANGANESE DIOXIDE

BY

HERBERT E. BARNER

A DISSERTATION

PRESENTED IN PARTIAL FULFILLMENT OF

THE REQUIREMENTS FOR THE DEGREE

OF

DOCTOR OF ENGINEERING SCIENCE IN CHEMICAL ENGINEERING

AT

NEWARK COLLEGE OF ENGINEERING

Newark, New Jersey

1967

ABSTRACT

Samples of synthetic pyrolusite were reduced in hydrogen at various partial pressures in the temperature range of 200° to 500°C. Most reduction experiments were conducted using a Pyrex vertical-tube reactor, in which small beds of porous particles (0.07 to 0.21 mm.) or single porous pellets of the oxide were suspended. The reaction kinetics were followed by recovering and weighing the water product formed during measured time intervals, and the intermediate reduction products were identified by X-ray diffraction analysis.

The data show that reduction proceeds through the sequence $MnO_2 \rightarrow Mn_2O_3 \rightarrow Mn_3O_4 \rightarrow MnO$. Below 250°C no MnO was detected, and the reaction practically terminated with the formation of Mn_3O_4. Above 250°C the Mn_3O_4 became progressively more protective, and the reduction of Mn_3O_4 to MnO became appreciable. Above 300°C all four oxides were detected in the partially reduced products, although the MnO_2 and MnO phases were usually the major components. The kinetic data were conveniently divided into two temperature regimes.

Below 250°C the reaction was found to practically subside with the formation of Mn_3O_4. The apparent activation energy for pellets and particles was, respectively,

26.8 and 22.2 kcal./mole at a hydrogen pressure of 800 mm. Hg and in the temperature range of 200° to 240°C. The rate at 226°C increased nonlinearly with hydrogen partial pressure and was sharply retarded by the presence of water vapor.

Above 300°C the reduction was always characterized by an exceedingly high initial rate; this is attributed to a rapid build-up of layers of Mn_2O_3 and Mn_3O_4. The Mn_3O_4 became protective but was itself further reduced to MnO at measurable rates. The apparent activation energy (for particles) at conversions above 20%, at hydrogen partial pressures between 80 and 800 mm. Hg, and in the temperature range of 325° to 425°C, was approximately 26 to 30 kcal./mole. The rate increased nonlinearly with hydrogen partial pressure, and at 375°C was sharply retarded by the presence of water vapor.

The low-temperature pellet data were correlated with a core reaction model, in which the reacting solid was assumed to approximate the system, MnO_2(core)-Mn_3O_4(product layer). The thickness of the intermediate Mn_2O_3 layer was neglected, and the solid-gas reaction at the Mn_2O_3/Mn_3O_4 interface was taken as the rate-controlling step. Similarly, the high-temperature particle data were correlated by a core model in which the reacting solid was assumed

to approximate the MnO_2(core)-MnO(product layer) system. The intermediate oxides were assumed to be of negligible thickness, and the solid-gas reaction at the Mn_3O_4/MnO interface was taken as the rate-limiting step. The kinetic data in both regimes were consistent with the concept that the solid-gas reactions involve adsorption of hydrogen, surface reaction, and desorption of water, the surface rearrangement being rate-controlling.

Reduction experiments were also conducted using a natural pyrolusite ore. These data showed characteristics similar to those of the synthetic pyrolusite.

APPROVAL OF DISSERTATION

KINETICS OF HYDROGEN REDUCTION OF

MANGANESE DIOXIDE

BY

HERBERT E. BARNER

FOR

DEPARTMENT OF CHEMICAL ENGINEERING

NEWARK COLLEGE OF ENGINEERING

BY

FACULTY COMMITTEE

APPROVED: _____ Chairman

_____

_____

_____

_____

NEWARK, NEW JERSEY

JUNE, 1967

ACKNOWLEDGMENTS

The author would like to express his sincere gratitude and appreciation to the following persons and organizations for their assistance and support in this work:

Dr. Charles L. Mantell, thesis advisor -- for his guidance and encouragement in all phases of this work.

Dr. Joseph Joffe -- for his assistance in translating some of the Russian literature related to this investigation.

Mr. Edwin Keel and The M. W. Kellogg Company -- for conducting the X-ray analyses reported in this thesis.

Mr. A. J. Haley and the Research and Development Division of Engelhard Industries, Incorporated -- for conducting the surface area and pore volume measurements on the pyrolusite samples.

The Union Carbide Corporation (Metals Division) -- for supplying the Belgian Congo pyrolusite ore specimens.

TABLE OF CONTENTS

LIST OF FIGURES

LIST OF TABLES

CHAPTER I

INTRODUCTION

Purpose of Study

The only commercial source of pure manganese is based on the electrolysis of manganese sulfate solutions. One of the important steps of this process is the reduction of oxidized ores to make them soluble in the recycled anolyte. This is usually accomplished by roasting the ore in a reducing atmosphere at high temperatures. It has long been known that the manganese content can be readily reduced in this manner to the divalent form. Very little, however, is known about either the kinetics of the reduction reactions or the nature of the intermediate reduction products. This situation contrasts sharply with the state of knowledge pertaining to the reduction of other oxides, such as those of iron, copper, tin and nickel.

The consumption of manganese metal in the United States has doubled during the period from 1959 to 1964[20, 21]. It may therefore be anticipated that in the future there will be a much greater economic incentive to optimize current roasting processes, as well as to develop more economical reduction and roasting techniques. In recent years, the intermediate oxides, Mn_2O_3 and Mn_3O_4, have also gained commercial importance; consequently, it is of interest to determine whether either of

these oxides can be obtained in relatively pure form as an intermediate reduction product of manganese dioxide. Accordingly, the purpose of this work was to study the reduction of manganese dioxide, both with respect to the kinetics and to the identification and stability of the reduction products. Hydrogen was used as the reducing gas, and particular attention was focused on the effects of temperature, hydrogen partial pressure, and water vapor content in the hydrogen stream.

Mineralogical Forms of Manganese Dioxide

Manganese dioxide is not a simple compound of constant structural configuration and constant properties. On the contrary, a number of structurally distinct forms have been identified either in natural ore deposits or in artificial products. In 1961 Gattow and Glemser[10, 11, 12] presented the most complete survey of the state of knowledge of the various manganese dioxides, including the interconversions and relations among them. They have classified the synthetically prepared dioxides, as well as some of the more important natural minerals. An earlier review and classification was published in 1948 by McMurdie and Golovato[19].

Gattow and Glemser classified the known manganese dioxides into seven major groups on the basis of their X-ray diffraction patterns, and within most groups they

proposed further breakdown according to crystallinity (as judged from the relative intensities of the X-ray reflections). Inasmuch as the interest of the present work is in the reduction of a dioxide form which is found in nature, the following survey is restricted to the better known manganese dioxides which have mineralogical origins.

The most common manganese dioxide is the well-crystallized form identified by the mineralogical name pyrolusite. In terms of the Gattow and Glemser classification it is known as beta-MnO_2. It is the most stable of the several forms, and the other dioxides gradually transform into this modification when they are heated. The literature is in agreement that its structure is tetragonal (rutile group) with unit cell dimensions a = 4.38 to 4.44 Å and c = 2.85 to 2.90 Å. Beta-MnO_2 is said to have a definite solubility range of $MnO_{1.89}$ to $MnO_{2.00}$.[11]

The mineralogical name polianite was sometimes used to identify a dioxide form originally thought to be distinct from pyrolusite. X-ray studies, however, have since shown that the two forms are identical and the name polianite is now rarely used.

A second well-crystallized form is known as ramsdellite. Its structure is said to be orthorhombic. This form has apparently not been prepared synthetically and

it occurs only rarely in nature.

The gamma form of manganese dioxide is found both in natural ores and in artificial products. While it is often considered to be a poorly crystallized form of pyrolusite[19], Gattow and Glemser maintain that this form contains chemically bound water which is lost at 120°C. The well-known Gold Coast ore is said to be largely of this modification.

The mineralogical form, cryptomelane, is characterized by the presence of K or Na in the lattice. Likewise the terms coronadite and hollandite apply to natural minerals containing, respectively, Pb and Ba. These forms can be prepared synthetically and they are all of the alpha variety in terms of the Gattow and Glemser classification.

Various formulas have apparently been proposed for the mineral, psilomelane, but according to McMurdie and Golovato, modern usage is restricted to $BaMnMn_8O_{16}(OH)_4$.

The term "wad" has been used to designate an earthy mixture that is largely MnO_2, but it often contains large amounts of H_2O and BaO. According to McMurdie and Golovato, it has no distinct mineralogical definition and actually consists of pyrolusite, psilomelane, cryptomelane, and other minerals.

Since pyrolusite is the most important industrial manganese dioxide mineral, it was decided to use synthetic samples of pyrolusite in this work.

CHAPTER II

PREVIOUS INVESTIGATIONS

Very few data on the reduction of manganese dioxide have been published. The only serious kinetic study heretofore made is the Russian work of Chufarov and coworkers[2, 33, 34]. In the first[34] of three related publications, powder samples of MnO_2 (the beta form), Mn_2O_3 and Mn_3O_4 were reduced to MnO with hydrogen in a closed recirculating apparatus. Product water vapor was removed in a cold trap and the kinetics were followed by noting the decrease in hydrogen pressure with time. Initial hydrogen pressures of 50, 100, and 200 mm. Hg were used, and temperatures in the range of 300° to 500°C were studied. The reduction rate of MnO_2 was observed to vary approximately linearly with hydrogen pressure, and the apparent activation energy was determined to be 24 kcal./mole. The initial reduction was always characterized by a very high rate, and this was interpreted by Chufarov to correspond to the stepwise formation of the intermediate oxide, Mn_2O_3. The high initial rate was found to fall sharply with the progress of the reaction, becoming practically constant at approximately 22, 40 and 50% reduction (based on conversion to MnO) at 400°, 450°, and 500°C, respectively. The rate thereafter decreased only slightly up to about 80 or 90% reduction, after which it decreased

relatively quickly. It was concluded that this reduction behavior was indicative of stepwise reduction.

In a second paper[33] Chufarov and co-workers reported reduction data using carbon monoxide. The rate of MnO_2 reduction increased with the CO pressure in a nonlinear fashion, and the apparent activation energy was found to be 16.2 kcal./mole. The reduction proceeded faster with carbon monoxide than with hydrogen. In a third paper[2], MnO_2, Mn_2O_3, and Mn_3O_4 were reduced in mixtures of $CO-CO_2$. The reduction rates were found to be severely retarded by carbon dioxide, the rate of MnO_2 being inversely proportional to $P_{CO_2}^{0.69}$ at 350°C. Some experiments were also conducted on the reduction of Mn_2O_3 and Mn_3O_4 at 450°C using H_2-H_2O mixtures. Here the rate was severely inhibited by the presence of water vapor. No data were presented on the effect of water vapor on the reduction of MnO_2.

Chufarov's kinetic data were not supplemented by phase identification of the partial reduction products. The conclusion that the reduction of MnO_2 proceeds stepwise appears unwarranted inasmuch as it is based only on the qualitative shape of the reduction curves.

Several other publications which relate to the reduction of MnO_2, but which are of less value than the Chufarov series, will now be reviewed briefly.

The Bureau of Mines[4] has published limited data on the reduction of manganese-silver ores. Their principal object, however, was to determine the conditions for the optimum recovery of silver (by cyanidation) and not the reduction kinetics of MnO_2. It was found that for the best recovery of silver, reduction of the higher oxides of manganese to MnO was essential. Experiments showed that if the ores were reduced at relatively low temperatures, the MnO product reoxidized to a greater or less degree upon contact with air, while reduction at high temperatures produced a stable MnO product. Consequently, considerable attention was directed toward determining the stability of the completely reduced product (i.e., MnO) as a function of reducing temperature. However, quantitative kinetic data were reported for two runs on a Sumatra ore, in which the MnO_2 was indicated to occur as "wad". The ore was reduced using CO in one case and H_2 in the other, for periods of two hours at successive temperatures ranging from approximately 100° to 465°C. The initial reduction was somewhat faster with CO, but at later stages very little difference between the two reducing gases was observed. No attempt was made to study the reduction kinetics in any detail.

Dunoyer[6] reduced several specimens of manganese dioxide, including a single sample of beta-MnO_2, with hydrogen. A closed system was used and the temperature

was progressively increased during the course of the reaction. He plotted the change in hydrogen pressure versus temperature, and from this plot concluded that the reduction started at approximately 220°C with the formation of Mn_2O_3, which was further reduced at approximately 260°C, the final product being MnO (at 400°C). The conclusions relating to the nature of the intermediate products were deduced from the qualitative shape of the pressure-temperature curve. Dunoyer's data serve merely to indicate the approximate temperature range in which MnO_2 can be reduced.

Anikeev et al.[1] reduced samples of ore and pure MnO_2 with hydrogen and carbon monoxide. A vertical-tube furnace was used and the pressure was maintained at approximately one atmosphere. A number of temperatures in the range of 150° to 400°C were investigated. Below 350°C, CO was found to reduce faster than did H_2, while at higher temperatures the reverse was true. Because of this it was concluded that the process was kinetic-controlled below 350°C and diffusion-controlled above this temperature. However, the observed rates in this study were found to vary with the flow rate of the reducing gas, even at low temperatures. Obviously, then, these data contain appreciable gas-to-particle mass transport resistance. The authors do not show an Arrhenius plot, nor do they report an apparent activation energy.

Cismaru and Vass[3] reduced powder samples of manganese dioxide in a vertical-tube furnace using hydrogen at one atmosphere pressure. Data for only four runs (350° to 490°C) are reported. Contrary to other investigators, these authors claim that under their conditions the reduction terminates with the formation of Mn_3O_4. Once again, apparently no phase identification work was conducted to support this conclusion. An apparent activation energy of 22.627 kcal./mole based on the four runs is reported.

Soldatkin[29] concentrated his efforts on reducing agglomerates prepared by fusing natural ore specimens with various additions of lime and coke at approximately 1500°C. Inasmuch as the manganese dioxide was converted to Mn_3O_4 (by dissociation) during this process, Soldatkin's study has little direct bearing on the present work.

It becomes apparent from this review that any new study of the reduction kinetics should be supported by phase identification studies.

CHAPTER III

THEORY

Stable Oxides of Manganese

X-ray evidence[22] indicates that there are four stable compounds of manganese and oxygen between the stoichiometric limits of $MnO_{1.0}$ to 2.0: MnO_2, Mn_2O_3, Mn_3O_4, and MnO. There are, however, polymorphic and disperse forms of some of these oxides. Furthermore, rather wide deviations from stoichiometric proportions have been observed. For example, Rode[26] has reported that oxidation of manganous oxide yields a homogeneous solid solution in the range of MnO to $MnO_{1.15}$. On the other hand, Moore[22] found (by X-ray studies) that the MnO structure alone was retained in oxidation up to $MnO_{1.43}$, after which the MnO pattern disappeared completely and that for Mn_2O_3 appeared. The other manganese oxides are also known to form in nonstoichiometric proportions. However, the solubility limits are not well enough established to prepare a reliable manganese-oxygen equilibrium diagram at this time.

Mn-H-O Reduction Equilibria

The oxide phases which are in equilibrium with gas mixtures of H_2 and H_2O are shown in a convenient manner in Figure 1, where the equilibrium constants calculated from the free energy data[7] are plotted against temperature.

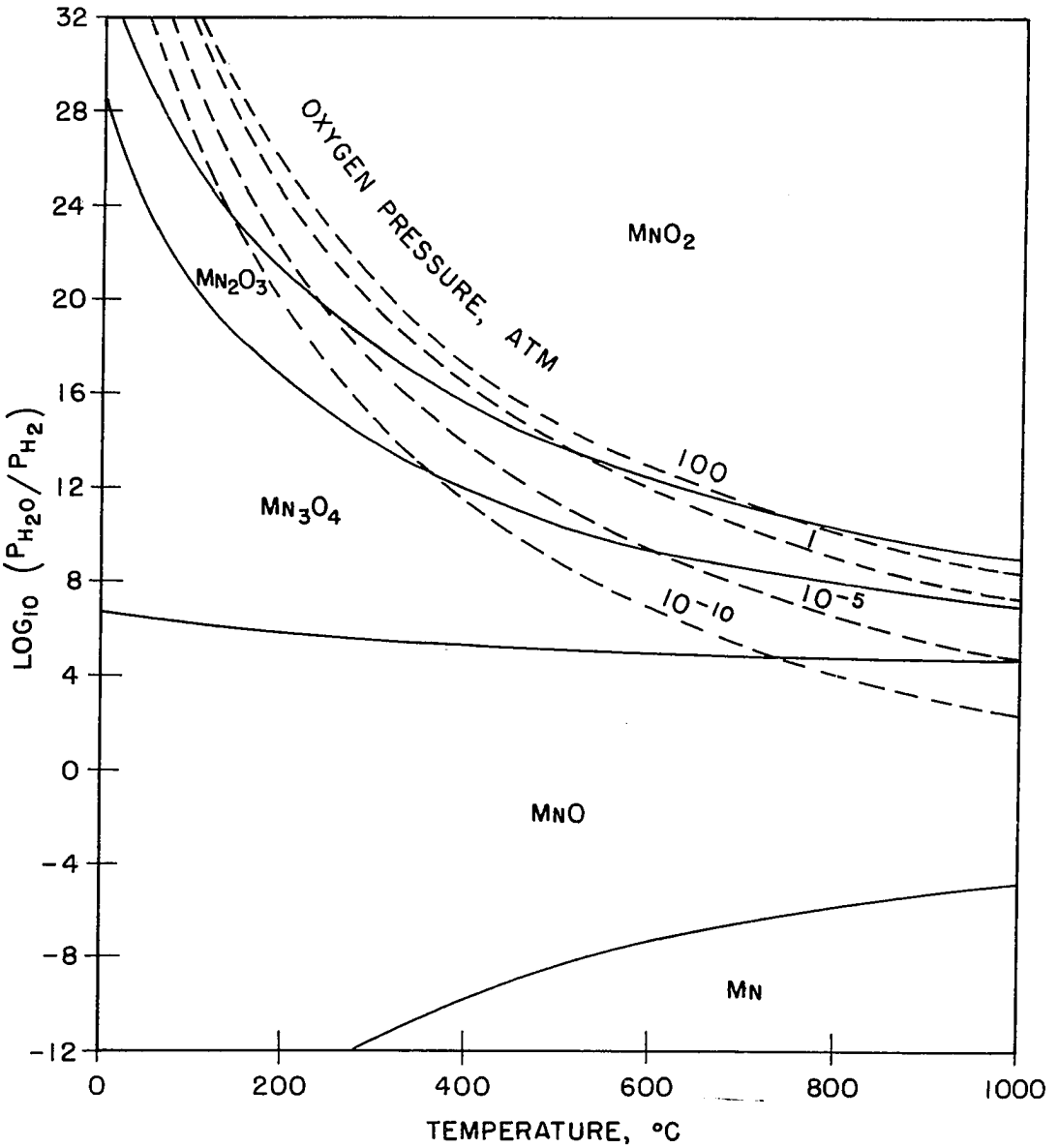

FIG. 1 Mn - H - O REDUCTION EQUILIBRIA

The broken curves are discussed at a later point and the reader may disregard them for the moment. The uppermost solid curve represents the equilibrium reaction,

$$2MnO_2 + H_2 = Mn_2O_3 + H_2O \qquad (1)$$

Similarly, the three lower solid curves represent, in turn, the equilibrium reactions,

$$3Mn_2O_3 + H_2 = 2Mn_3O_4 + H_2O \qquad (2)$$

$$Mn_3O_4 + H_2 = 3MnO + H_2O \qquad (3)$$

$$MnO + H_2 = Mn + H_2O \qquad (4)$$

Each area in the diagram represents a stable phase, as marked. Thus, if MnO_2 is exposed to a H_2-H_2O gas mixture at 500°C, and if the ratio P_{H_2O}/P_{H_2} is maintained greater than about 1×10^{14}, no reduction can occur; if, on the other hand, the ratio is less, reduction to Mn_2O_3 is thermodynamically feasible. Similar considerations apply to the other equilibrium curves. It is evident that reduction to MnO is feasible in the entire temperature range of the chart, even with very low hydrogen partial pressures. Indeed, reduction of MnO_2 down to MnO is possible as long as the ratio P_{H_2O}/P_{H_2} is less than approximately 1×10^{5}. There is then a very high thermodynamic potential for the reduction of any of the higher oxides to MnO.

Quite the opposite is true for the reduction of the monoxide to manganese metal. In this case, reduction at 500°C can proceed only if the ratio P_{H_2O}/P_{H_2} is maintained less than approximately 5×10^{-9}. Even at 1600°K (above the melting point of manganese) P_{H_2O}/P_{H_2} must be maintained below 3×10^{-4} in order to make the reduction to Mn thermodynamically possible. Consequently, further reduction of the monoxide to the metal does not occur to any appreciable extent in the realm of practical temperatures. Hence, equilibrium considerations predict that the reduction of MnO_2 with hydrogen terminates with the monoxide.

In the foregoing analysis the gas phase was assumed to contain only hydrogen and water vapor. Since manganese dioxide has a relatively high dissociation pressure, a more comprehensive approach would be not only to account for reactions (1) through (4), but to consider simultaneously the dissociation reaction, equation (5).

$$2MnO_2 = Mn_2O_3 + \tfrac{1}{2}O_2 \qquad (5)$$

Equivalently, it is sufficient to account for reaction (6).

$$H_2 + \tfrac{1}{2}O_2 = H_2O \qquad (6)$$

If the equilibrium constant of reaction (6) is given by K

$$K = \frac{P_{H_2O}}{P_{H_2} P_{O_2}^{\frac{1}{2}}} \qquad (7)$$

the equilibrium oxygen pressures in the presence of

hydrogen and water vapor may be calculated in the following manner. Rearranging equation (7),

$$P_{H_2O}/P_{H_2} = K\, P_{O_2}^{\frac{1}{2}} \qquad (8)$$

Equation (8) can be solved for the ratio P_{H_2O}/P_{H_2} at arbitrarily selected oxygen partial pressures. This calculation was carried out at various temperatures and the results are shown in Figure 1, where each dashed curve represents a constant level of oxygen pressure. The solid and dashed curves together can be used to calculate the composition of the gas in equilibrium with an oxide pair.

The calculation of the composition of the gas in equilibrium with an oxide pair is perhaps best illustrated with a specific example. For this purpose consider the gas in equilibrium with the solid phases MnO_2 and Mn_2O_3 at 530°C, at a total pressure of 1.5 atmospheres. From Figure 1, $P_{O_2} = 1.0$ atm., and $\log P_{H_2O}/P_{H_2} = 13.3$, or $P_{H_2O}/P_{H_2} = 2 \times 10^{13}$. Since the total pressure is 1.5 atm.,

$$P_{O_2} + P_{H_2} + P_{H_2O} = 1.5$$

$$1.0 + P_{H_2} + 2\times10^{13} P_{H_2} = 1.5$$

Therefore, $P_{H_2} \cong 2.5 \times 10^{-14}$ atm., and $P_{H_2O} \cong 0.5$ atm. Inasmuch as the equilibrium oxygen pressure is approximately one atmosphere, it is possible that dissociation and reduction of MnO_2 could occur simultaneously at this temperature. Of course, the relative reaction rates will determine

whether reduction and dissociation can actually proceed simultaneously.

An examination of the other constant P_{O_2} curves in Figure 1 indicates that the dissociation driving force is clearly very small below about 450°C. Nevertheless it should be borne in mind that dissociation and reduction could proceed simultaneously at the higher temperatures.

Rate Steps in the Reduction Process

The gaseous reduction of a solid oxide is usually thought to occur in topochemical fashion; that is, the gas-solid reaction is generally believed to occur at a boundary separating two solid phases. Indeed, Langmuir[17] has shown that if a solid phase and gas react to form a second solid phase, the reaction can occur only at the interface separating the two solid phases. Furthermore, a nucleus of the second phase must initiate the reaction. Once the interface has been established, the reducing gas must diffuse through a layer of the reaction product. Consequently, the overall reduction process for a nonporous particle of oxide may be separated into the following steps:

Step 1. Transfer of reducing gas from the bulk gas stream through the gas boundary layer to the exterior surface of the particle, and reverse transfer of product gas.

Step 2. Inward diffusion of reducing gas across the

outer reduced layer (metal, or a lower oxide, as the case may be) to the reaction interface, and reverse diffusion of product gas.

Step 3. Gas-solid chemical reaction at the interface separating the reduced outer layer from the unreacted oxide. This step includes any associated adsorption and desorption phenomena which may occur.

There is additional complication when the reacting particle is porous, for then the reducing gas may diffuse into the porous volume with steps 2 and 3 occurring throughout the particle along the walls of the pore structure. Because of the greater surface area available for reaction, the overall reaction rate will be higher; however, since the concentration of the reducing gas will vary throughout the particle, the reduction will not generally proceed at a uniform rate at all points. Furthermore, significant temperature gradients may be established in porous particles undergoing reduction. Hence, the combination of pore diffusion and nonisothermal effects may either increase (for an exothermic reaction only) or decrease the observed reduction rates. Methods[25, 27] have been developed to estimate the extent of these complications, but independent estimates of the effective diffusion and thermal conductivity coefficients must be made. In the laboratory these effects can usually be minimized by using sufficiently small particles, in which case concentration and temperature

gradients would be small.

Determination of Rate-Limiting Step

In the following discussion it is assumed that the particles are perfectly dense or, if porous, that they are small enough so that temperature and concentration gradients are negligible.

The concept of a rate-limiting step is very useful in interpreting heterogeneous kinetic data. In general, any or all three steps listed above may influence the observed reduction rate; however, if the resistance offered by one step is much greater than the others, it is said to be rate-determining. The other two steps then occur under very small concentration gradients, and their resistance to the overall reaction rate may be neglected. If sufficient data are available, it is a relatively simple matter to discriminate between steps 1, 2, and 3. The variation of the observed rates with temperature, pressure, and flow rate, in particular, lends insight into which of the steps is rate-controlling.

When either of the diffusion steps (1 or 2) controls, the reduction rates would be rather insensitive to temperature. Because diffusion processes have activation energies of only one or two kcal./mole, the observed activation energy would also be on the order of one or

two kcal./mole. If boundary-layer transport (step 1) controls, the observed rate would vary with the gas flow rate; whereas if diffusion across the product layer controls, the observed rate would be insensitive to the gas flow rate.

If the chemical reaction step controls, the observed rate would be insensitive to flow rate, but would be a strong function of temperature, with an apparent activation energy on the order of 10 to 60 kcal./mole. Frequently, it is found that chemical reaction controls at relatively low temperatures; but as the temperature is raised, a point is often reached where significant diffusional resistances begin to appear. Such behavior characteristically involves a break in the linearity of an Arrhenius plot, with a consequent decrease in the apparent activation energy.

The influence of pressure will also vary, depending on which step controls the reduction process. Although the discussion which follows assumes that hydrogen is the reducing gas, the conclusions apply equally well to any other reducing gas.

If step 1, boundary-layer transport, controls, an increase in the hydrogen partial pressure at constant total pressure increases the driving force for gas transport; the reduction rate accordingly increases in direct proportion to the increase in hydrogen partial pressure.

On the other hand, the reduction rate will remain essentially constant if the total gas pressure is increased while the percentage of hydrogen in the stream is maintained constant. In this case the increase in driving force across the boundary layer due to an increase in hydrogen partial pressure is very nearly counterbalanced by the decrease in the mass transfer coefficient. The latter decreases because the molecular diffusivity is inversely proportional to the total pressure.

If step 2, diffusion through the solid reduction product, controls, the gas pressure will influence the rate in a manner dependent on whether the transport is by ordinary molecular diffusion or by Knudsen diffusion. (In Knudsen diffusion, the mean free path of the molecules is much larger than the pore diameters; consequently, diffusion in this regime does not proceed in the ordinary manner.) In the first case, behavior is the same as when step 1 controls; that is, an increase in total pressure at constant hydrogen composition will not appreciably influence the reduction rate. If, however, the pores are small enough so that transport is by Knudsen diffusion, an increase in pressure at constant hydrogen composition will increase the reduction rate. This is so because the Knudsen diffusion coefficient is independent of pressure. In either extreme case, an increase in hydrogen partial pressure at constant

total pressure increases the driving force for transport, and the reduction rate would also increase.

When chemical reaction controls, the reduction rate will vary with hydrogen pressure in a more complicated fashion. Generally speaking, at very low hydrogen partial pressures, the reaction interface will be relatively sparsely covered with adsorbed hydrogen, and the reduction rate will be directly proportional to P_{H_2}; at high hydrogen partial pressures the rate will increase less and less as P_{H_2} is increased further, until, in the limit when the reacting surface is completely saturated with adsorbed hydrogen, the reduction rate approaches a maximum. Product gas (H_2O in the case of H_2) can retard the rate if the reaction is reversible, or if the surface is poisoned in some manner by the product gas. Other gas molecules can also retard the rate if they interact with the surface at the reaction interface.

Models for the Reduction Process

Although it is seldom possible to deduce the reaction mechanism from kinetic data alone, it is often possible to characterize the reaction in terms of a physical model which represents the actual rate phenomena reasonably well. A model seldom sheds any new light on the kinetics of the reaction that could not be deduced by other means, but it does provide a convenient framework in which to correlate

the experimental data. In the following sections mathematical rate expressions are presented for models in which the oxide is pictured as a dense, nonporous particle in the shape of a cube, and in which one of the three steps is taken as rate-controlling. To illustrate the technique, the derivation is carried out in detail for the case where step 3, the gas-solid reaction at the interface, is assumed to be rate-controlling. Similar expressions for models in which either of the diffusion steps is rate-controlling are also summarized. Finally, the conditions under which the same expressions may also be applied to porous oxides are considered.

Chemical reaction controls. The model is based upon several assumptions:

(1). The oxide particle is a nonporous cube of edge length x_o.

(2). The reduction reaction is of the type,

$$A(g) + B(s) \longrightarrow C(g) + D(s),$$

is irreversible, and proceeds at the interface boundary separating phases B and D.

(3). Temperature gradients within the particle are negligible.

(4). Overall particle dimensions do not vary during reduction.

Once the reduction has proceeded to a finite extent, a layer of solid D will have formed, and the edge length of

the unreacted core of B will have decreased to x ($x < x_o$). The rate of reduction of B, in moles per unit of time, will be proportional to the interfacial surface area, $6x^2$.

$$-\frac{dN_B}{dt} = r_s (6x^2) \tag{9}$$

The reaction rate r_s, in moles per unit area of unreacted B, is a function of temperature, and reducing gas composition and pressure. Relating the rate of disappearance of B to the inward advance of the interface,

$$N_B = \rho_B x^3$$

where ρ_B is the molar density of B. Differentiating with respect to time,

$$\frac{dN_B}{dt} = 3\rho_B x^2 \frac{dx}{dt} \tag{10}$$

Substituting (10) into (9), we have

$$-3\rho_B \frac{dx}{dt} = 6 r_s \tag{11}$$

The length of the cube edge, x, may be related to Z, the fractional conversion of B.

$$Z = \frac{\text{Volume of B reacted}}{\text{Total volume}} = \frac{x_o^3 - x^3}{x_o^3}$$

Therefore,

$$x = x_o (1 - Z)^{1/3}$$

Differentiating with respect to time,

$$\frac{dx}{dt} = -\frac{1}{3} x_o (1 - Z)^{-2/3} \frac{dZ}{dt} \tag{12}$$

Substituting (12) into (11), rearranging, and specifying the integration limits,

$$\rho_B x_o \int_{Z=0}^{Z=Z} (1 - Z)^{-2/3} \, dZ = 6 \, r_s \int_{t=0}^{t=t} dt$$

Integrating, one finds:

$$t = \frac{\rho_B \, x_o}{2 \, r_s} \left[1 - (1 - Z)^{1/3}\right] \qquad (13)$$

The time for complete reaction, θ, is given by setting $Z = 1$,

$$\theta = \frac{\rho_B x_o}{2 \, r_s}$$

In dimensionless form equation (13) becomes

$$\frac{t}{\theta} = 1 - (1 - Z)^{1/3} = \frac{x_o - x}{x_o} \qquad (14)$$

Equation (14) is also obtained for a dense sphere of radius $x_o/2$.

It is seen from equation (13) or (14) that if chemical reaction controls, a plot of $1 - (1 - Z)^{1/3}$ versus time should be linear and should pass through the origin. The slope of the line would be proportional to the rate per unit area, r_s. Furthermore, r_s, or the quantity $1/\theta$, should be a strong function of temperature, with an apparent activation energy characteristic of a chemical reaction.

Boundary-layer transport controls. In a similar manner it may be shown[18] that, if boundary-layer transport controls, the reduced time of reaction is equal to the fractional conversion, i. e.,

$$\frac{t}{\theta_1} = Z \qquad (15)$$

where θ_1 is a function of the boundary-layer mass transfer coefficient. Hence, if this step is rate-controlling, a plot of conversion versus time should be linear, and the slope, $1/\theta_1$, should be relatively insensitive to temperature.

Diffusion through product layer controls. When step 2 is assumed to be rate-controlling, it may be shown[18] that

$$\frac{t}{\theta_2} = 1 - 3(1 - Z)^{2/3} + 2(1 - Z) \qquad (16)$$

where θ_2 is a function of the effective diffusivity of the reducing gas in the reaction product layer. In this case the term $1/\theta_2$ should be relatively insensitive to temperature.

Equations (14), (15), and (16) and the temperature dependencies of θ, θ_1, and θ_2 provide a convenient means of testing for the rate-controlling step.

Resistances of comparable value. Mathematical expressions for models in which the resistances of two or three steps are of comparable value have also been derived[24, 28]. These expressions are somewhat involved to use, and unless independent estimates for the boundary-layer mass transfer coefficient and effective diffusion

coefficient in the reaction-product layer are available, some rather extensive curve-fitting is required to evaluate the various parameters. In most gas-solid kinetic investigations one of the three rate steps predominates, and the data can usually be correlated by completely neglecting the other two resistances. This should not be interpreted to mean that two of the three rate steps are always completely insignificant. Nevertheless, in most cases the resistance contribution of two of the steps is quite small compared to the third, and unless independent estimates of the mass transfer parameters are available, there is probably little justification for going to the more complex expressions.

Application of models to porous particles. In the laboratory it is often possible to eliminate boundary-layer (step 1) mass transport resistance by using sufficiently large flow rates and small particles. If, again, small enough particles are used, pore diffusion resistance and particle temperature gradients may be practically eliminated. Under such conditions the reduction proceeds almost uniformly on all available surface, and the model expressions based on controlling step 2 or 3 may still be used. To do this, the porous oxide particle is pictured as a hypothetical agglomeration of numerous identical, nonporous microparticles in the shape of cubes, each of

edge x_o. The entire surfaces of all cubes are imagined to be exposed to reactant gas at a concentration essentially equal to the bulk gas concentration. In such a model the number of cubes composing a single larger aggregate, as well as the characteristic dimension x_o, have meaning only in a statistical sense. Nevertheless, it should be possible to analyze and correlate the experimental data in terms of equation (14) or (16) if the aforementioned conditions are realized.

CHAPTER IV

EXPERIMENTAL

Apparatus

The great majority of the reactions were conducted in a vertical-tube differential-flow reactor. Relatively small samples of manganese dioxide (usually about 1.5 grams) were used and reducing gas flow rates were high. In the quantitative dry hydrogen kinetic runs the water vapor content in the gases leaving the reactor was always less than 0.2%; generally, only trace amounts of water vapor were present. Product water vapor was recovered over known intervals of time, and these data formed the basis for following the kinetics of the reduction.

The essential features of the equipment are represented schematically in Figure 2. The apparatus was made primarily of Pyrex glass with Tygon tubing used for the flexible connections and 1/4-inch copper tubing for the long lines. Cylinder hydrogen was metered through a ball flowmeter into a purification column containing palladium-coated alumina, where traces of oxygen were converted to water vapor. The hydrogen was then directed through either the dryer or water saturator, depending on whether a dry or moist stream was desired. The reducing gas then flowed through the heated reaction tube in which the oxide specimen was supported. For the dry hydrogen runs, product gas was directed

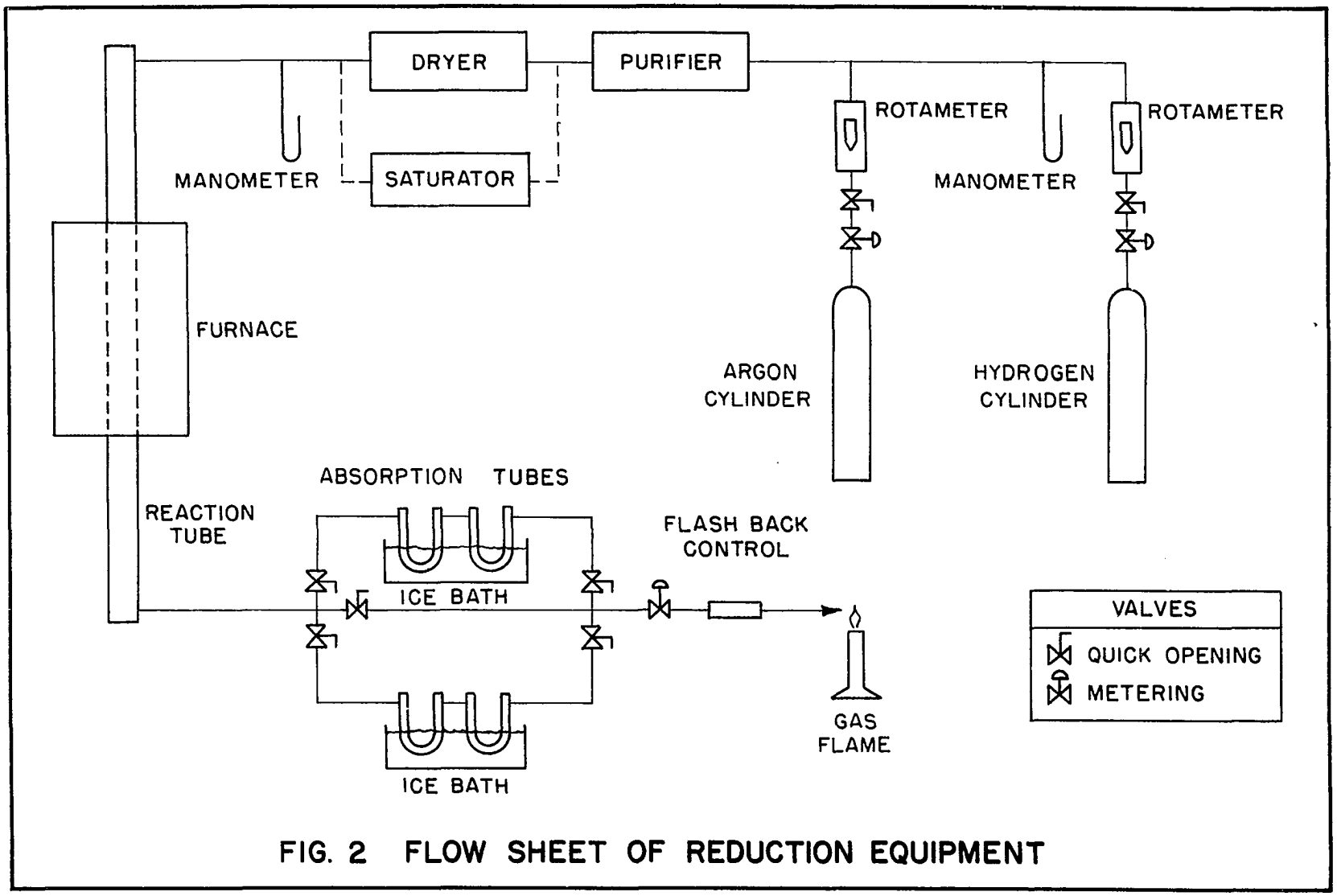

FIG. 2 FLOW SHEET OF REDUCTION EQUIPMENT

through absorption tubes, where the water vapor formed by reaction was recovered. For the moist feed runs, conversion could not be based on water recovery because the water added to the feed (in the saturator) exceeded the small amount of water formed in the reaction by several orders of magnitude. In these cases it was necessary to base the conversion on oxide weight loss alone. In any event, the hydrogen was finally directed through a flash-back control to a gas flame where it was burned.

The dryer consisted of two towers in series, the first containing Drierite (anhydrous calcium sulfate), the second, Anhydrone (anhydrous magnesium perchlorate).

The saturator is depicted in Figure 3. Moisture was added to the hydrogen stream at a controlled concentration by bubbling the gas through a series of two flasks containing distilled water. The flasks were placed in a constant temperature bath, in which the temperature in the range of 5° to $50^{\circ}C$ was easily controlled within $\pm 0.2^{\circ}C$ by means of independent heating and refrigeration coils. In the moist hydrogen runs, the entire external system was maintained at a temperature above the water bath to prevent condensation of water vapor. This was accomplished by heating the gas lines with electrical resistance elements and by heating the upper uninsulated portion of the reaction tube by infrared lamps.

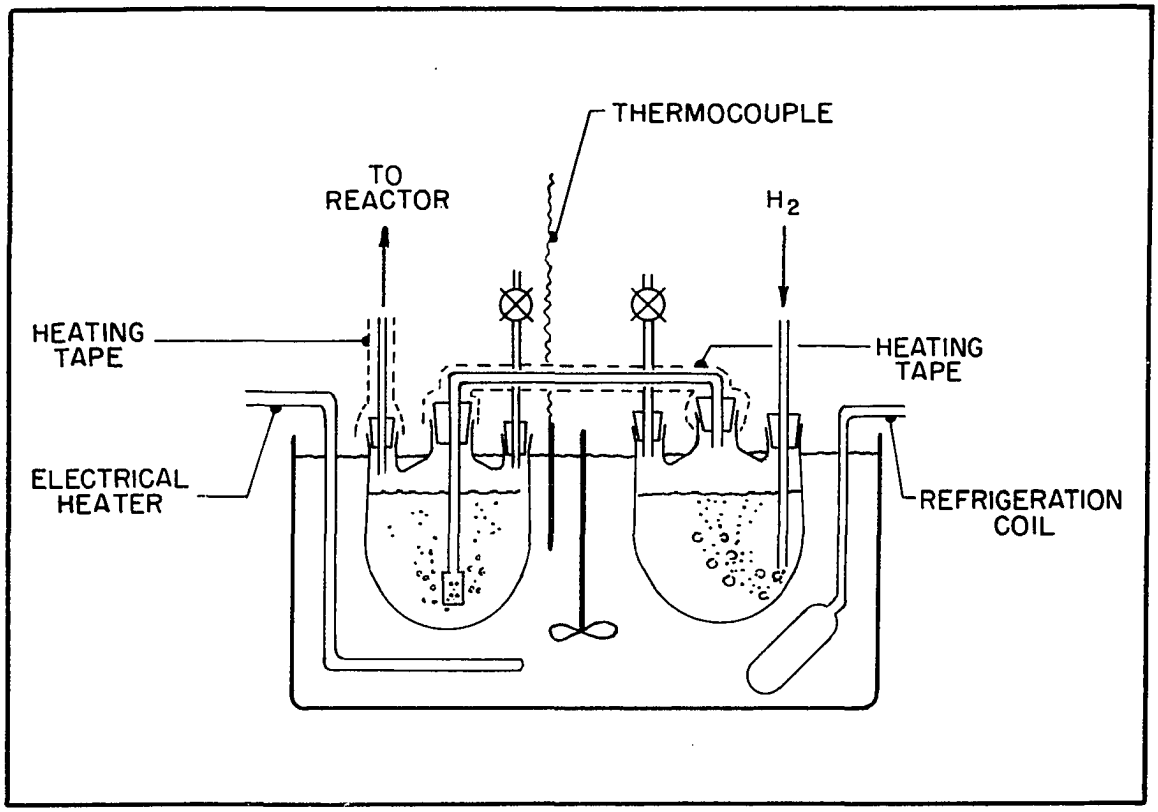

FIG. 3 SATURATOR

The water recovery system consisted of two trains of Schwartz-type U-tubes which were packed with Anhydrone. Each train contained two U-tubes in series, which were partially immersed in an ice bath. The gas stream was alternately directed from one train to the other by manipulating a number of toggle valves. The Schwartz tubes were approximately six inches in length, and the connecting side arms were equipped with high-vacuum ground glass joints containing O-ring seals. The latter eliminated the need for a sealing lubricant and facilitated quick and easy detachment so that the U-tubes could be periodically weighed during a run.

Details of the vertical-tube reactor and furnace are shown in Figure 4. A Pyrex heavy-wall reaction tube was used, measuring 1-3/16-inch I.D. and 1-1/2-inch O.D., with ground glass high-vacuum seals on either end (requiring no lubricant). The furnace core was an externally-threaded Alundum tube measuring 24 inches in length with a 1-3/4-inch bore, 2-1/4-inch O.D., and a thread pitch of 1/4 inch. Three separate windings of 24-gauge Nichrome V wire, each covering 8 inches of tube length, were placed in the grooves of the core. These were covered with a layer of Alundum cement to assure electrical insulation. The core assembly was placed in a furnace at 1000°C for a period of six hours to allow the Alundum cement to cure. The ends

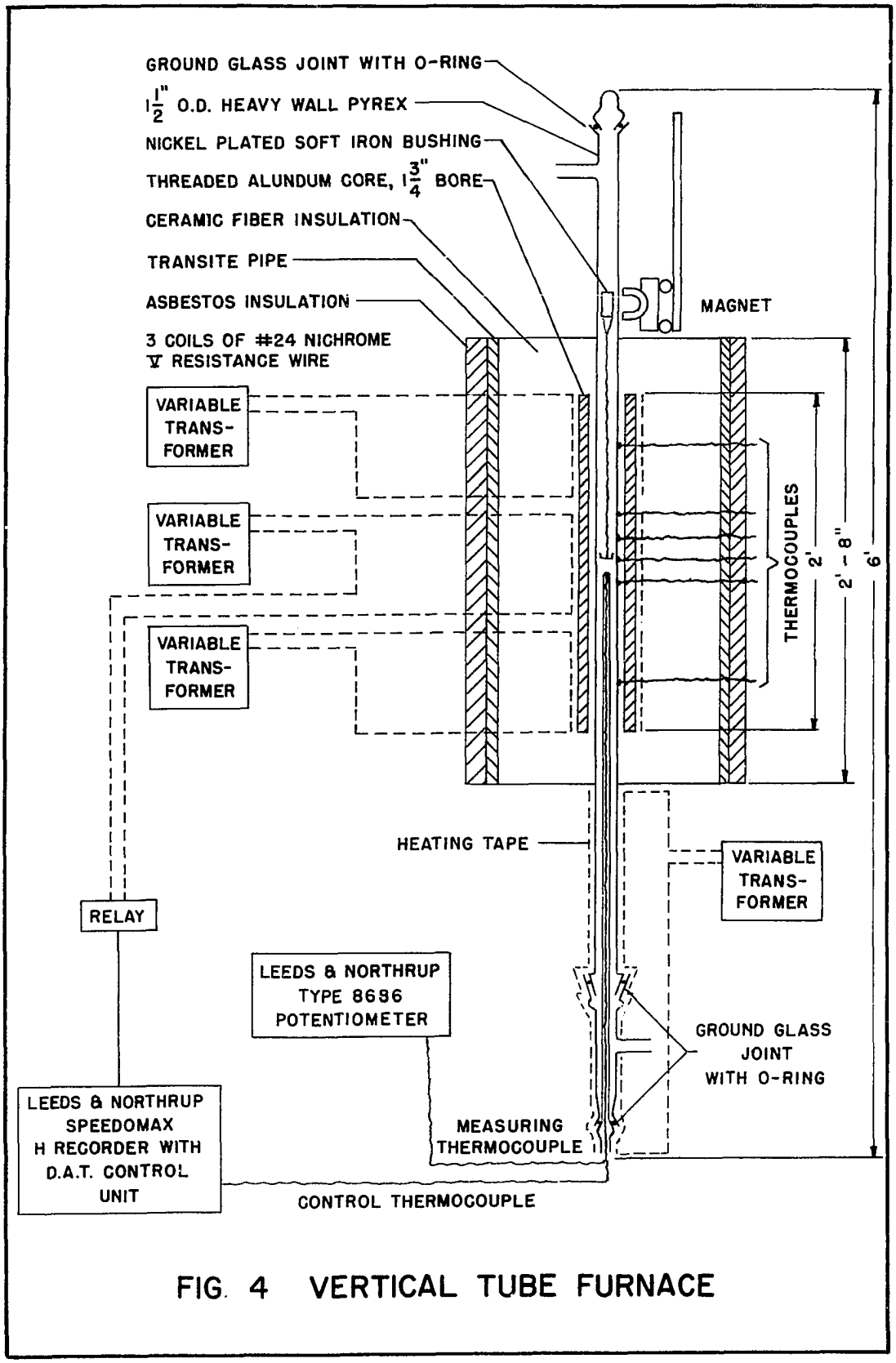

FIG. 4 VERTICAL TUBE FURNACE

of each Nichrome winding were doubled over and twisted to furnish power leads which were connected to variable transformers. Six Chromel-Alumel thermocouples were secured to the outside surface of the Pyrex reaction tube with glass fiber cord at strategic positions over the length of the furnace. One of these was located at the vertical center of the core, and a second and third were placed two inches above and below the centered thermocouple. The temperature gradient along the heated length of the reaction tube was measured by means of these thermocouples.

The furnace was surrounded by an 8-inch-diameter asbestos covered Transite pipe, and was packed with ceramic fiber insulation. The portion of the Pyrex tube exposed below the furnace, and the ground glass connections and product gas line leading to the water absorption tubes were traced with an electrical heating tape.

The oxide specimen (usually 1.5 grams) was placed in a basket constructed from 250-mesh nickel wire cloth. In some runs two or three such baskets, with a portion of the oxide in each, were used in close succession (bottom-to-bottom distance between two baskets was approximately 4 to 5 mm.). The basket assembly was attached to a chain constructed from links of nickel. The upper end of the chain was connected to a short length of glass fiber cord

which, in turn, was attached to a nickel-plated soft iron, thin-walled, hollow cylinder. The cylinder was held in position by a permanent magnet which could be raised or lowered at will, thus providing an external means of positioning the oxide specimen into or out of the heated zone while the reaction tube was sealed.

A Pyrex thermocouple probe placed in the center of the reaction tube terminated approximately 1/4 inch from the bottom of the sample basket assembly. Two identical Chromel-Alumel thermocouples were inserted in this probe; one was used as the control thermocouple and the second to measure the apparent sample temperature. The temperature as sensed by the control thermocouple was recorded and controlled by a Leeds & Northrup Speedomax H Recorder with type D. A. T. control unit. The latter controlled the power input to the central furnace coil only. Power input to the top and bottom coils was controlled manually. The measuring thermocouple and the six tube-surface thermocouples were connected through a multiple switch (not shown in Figure 4) to common terminals and thence to a Leeds & Northrup Model 8686 potentiometer. Under most experimental conditions the apparent sample temperature was controlled within $1^{\circ}C$ of the desired temperature. The longitudinal gradient along the wall of the central four-inch vertical section of the Pyrex tube seldom exceeded $2^{\circ}C$. The

temperature sensed by the thermocouples in the probe and the adjacent Pyrex wall thermocouple usually agreed within 1° or 2°C.

Because of the temperature limitations of Pyrex, the very high temperature experiments were conducted in a 25 mm. diameter, 750 mm. long Vycor tube placed horizontally in a conventional hinged-top combustion furnace (Figure 5). The ends of the tube were connected to 8 mm. Pyrex tubes by rubber stoppers sealed with Glyptal. In these runs the oxide specimens were held in Alundum boats. Hence, access of hydrogen was from the top surface only. Control and measuring thermocouples were placed in a thermocouple probe immediately above the boat; during reaction periods the apparent sample temperature was maintained within approximately ± 5° to 10°C of the desired temperature. Other aspects of the equipment (dryers, water recovery, etc.) were identical to the earlier description.

Raw Materials

Synthetic pyrolusite was derived from 50% aqueous manganese nitrate solutions purchased from the Fisher Scientific Company. The bulk of the water was first removed by evaporating the solution on water baths for approximately 2-1/2 hours. The concentrated nitrate solution was then pyrolyzed in a forced-air circulation oven at a controlled temperature of 200°C for 24 hours. The product

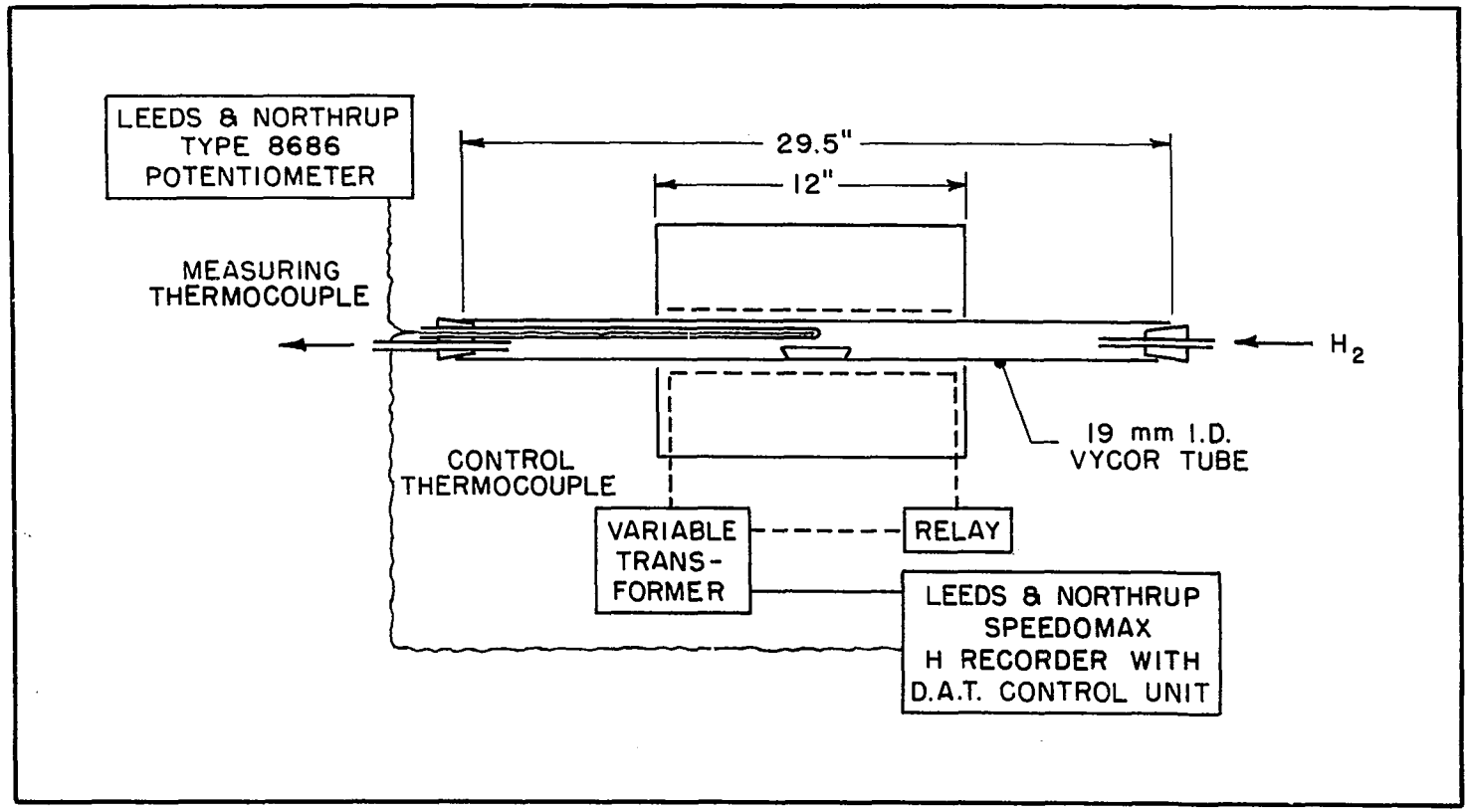

FIG. 5 HIGH TEMPERATURE FURNACE

was removed from the oven, was crushed, and was screened into various particle-size fractions. The fractions were heated in the oven for a second 24-hour period at 200°C. Pyrolysis of the nitrate is reported[11, 19] to yield the beta modification of MnO_2, that is, the pyrolusite form. This was verified by comparing the X-ray diffraction pattern of the product with that reported[11, 19, 22, 30] for pyrolusite.

The oxide was analyzed for available oxygen by reducing the manganese dioxide with an excess of sodium oxalate in acid solution and determining the excess by titration with a standard potassium permanganate solution. The available oxygen determined in this manner was found to be 18.41% ± 0.07%, as compared to a calculated value of 18.40% for stoichiometric MnO_2. The manganese content was determined according to the bismuthate method. Samples of the oxide were dissolved by treatment with 30% hydrogen peroxide and dilute nitric acid; manganous ion was then oxidized to permanganate ion by addition of excess sodium bismuthate, and the excess was removed by filtration. The permanganate was subsequently reduced to manganous ion by the addition of excess ferrous ammonium sulfate; and finally, the excess ferrous ion was determined by titration with standard permanganate solution. The manganese analyzed at 63.18% ± 0.08%, compared to a calculated value of 63.19%

for MnO_2. The composition of the synthetic pyrolusite was therefore very close to stoichiometric manganese dioxide.

Reduction experiments were conducted using both single compressed pellets and small particles of pyrolusite. Two batches of the oxide were prepared in seemingly identical fashion; however, the pore structure of the two preparations differed slightly. The initial B. E. T. surface areas, as determined on a modified Nelson and Eggertsen[23] continuous-flow apparatus, were all relatively low, as shown in Table 1. It will be observed from the data on Batch A that the surface area did not vary significantly with particle size. Obviously, the granules were porous and subdivision of the larger particles did not generate appreciable new surface.

Cumulative micropore volume distributions calculated according to the method of Cranston and Inkley[5] are shown in Figure 6 for two particle-size fractions. It is seen that the porosities associated with micropores are relatively low. Furthermore, the surface area and pore volume data on two particle-size fractions of Batch A indicate that there is virtually no difference in the micropore characteristics between the two particle sizes. The micropore porosity of Batch B is, however, significantly less than that of Batch A; likewise the B. E. T. surface area (Table 1) of Batch A is somewhat greater.

TABLE 1

SYNTHETIC PYROLUSITE

GRANULES USED IN REDUCTION EXPERIMENTS

Batch	Identification	Particle Size (mm.)	Surface Area ($m.^2/g.$)
A	A1	0.15 - 0.21	0.40
	A2	0.11 - 0.15	-
	A3	0.10 - 0.11	-
	A4	0.07 - 0.10	0.52
	A5	<0.07	0.48
B	B1	0.21 - 0.42	-
	B2	0.15 - 0.21	0.26
	B3	0.12 - 0.15	-
	B4	0.10 - 0.12	-
	B5	0.088- 0.10	-
	B6	<0.088	-

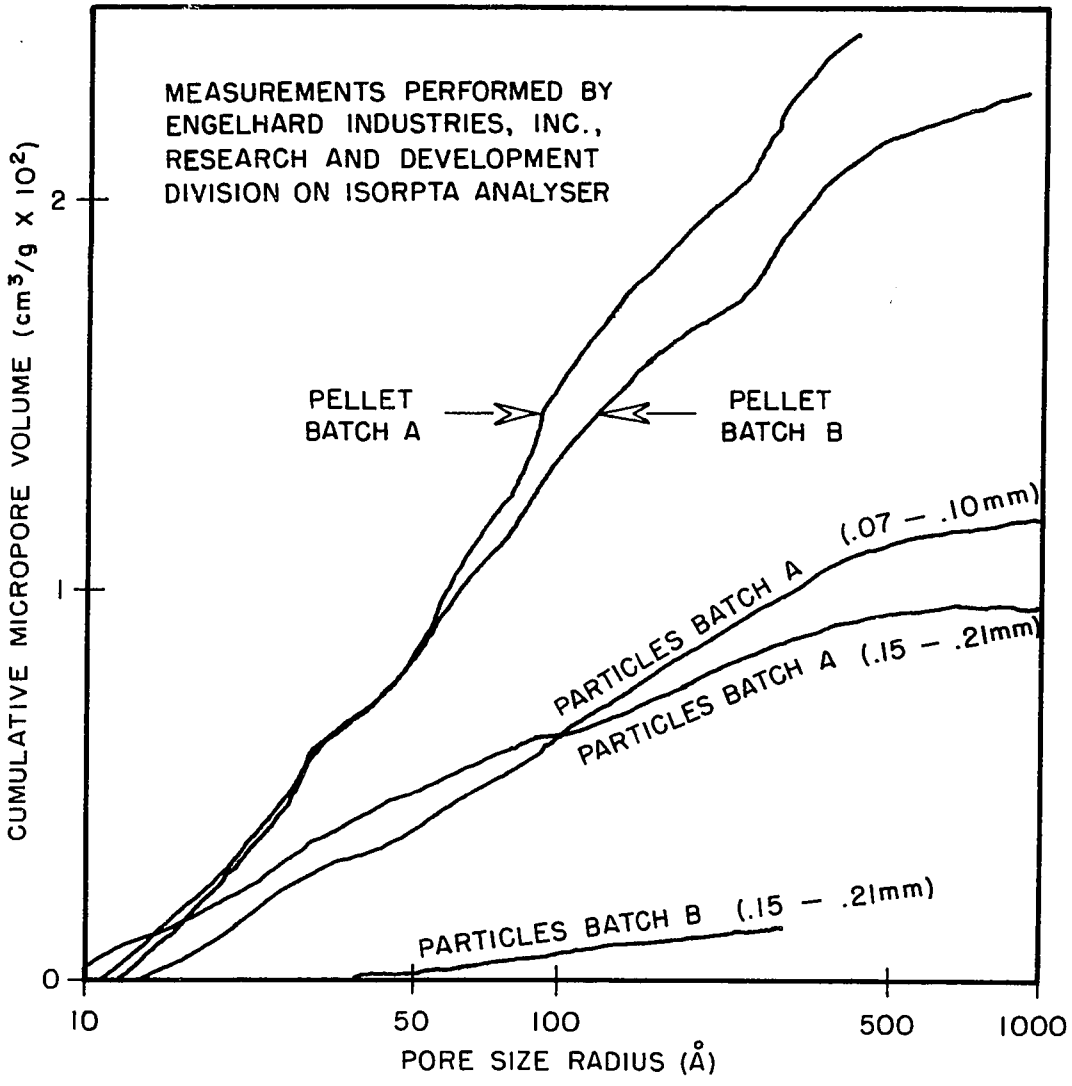

FIG. 6 CUMULATIVE PORE VOLUME

Nominal 1.5-gram pellets were prepared from a minus-200-mesh fraction of Batch A and a minus-170-mesh fraction of Batch B. The pellets were disk-shaped with diameters of 13mm. and thicknesses of approximately 3 mm. It was possible to obtain pellets with sufficient mechanical strength for handling purposes by compressing the fine powder in a stainless steel die at 9000 psi. A single drop of distilled water was added to the charged powder in the die as a lubricant; after compression the pellets were thoroughly dried at a controlled temperature of 200°C. Pellets formed from Batch A and Batch B were found to have B. E. T. surface areas of 1.4 and 1.3 $m.^2/g.$, respectively. The micropore volume distributions of both pellets were, likewise, virtually identical, as can be seen from Figure 6. The total porosity of the pellets was determined to be approximately 22%. This figure is based on a total pore volume estimated by boiling a weighed pellet in water to expel gases, superficially drying and weighing the pellet, and dividing the weight increase by the density of water.

Reduction experiments were also conducted on specimens of a naturally occurring manganese dioxide ore. The sample was obtained from the Union Carbide Corporation (Metals Division) and was identified as a high-grade Belgian Congo pyrolusite. Lumps of the ore were crushed and screened. A size fraction of 0.09 to 0.21 mm. was heated in air at

a controlled temperature of 150°C for 18 hours. The available oxygen analyzed at 15.5% ± 0.1% by reaction with excess sodium oxalate and titration of the excess with potassium permanganate; however, 16.1% available oxygen was found by reduction with hydrogen at approximately 440°C. On the basis of the former analysis, the ore sample was approximately 84% MnO_2.

All gases were purchased from The Matheson Company. The prepurified grade of hydrogen was used, and argon was employed as the purge gas. Mixtures of hydrogen and helium were purchased for the experiments in which the effect of hydrogen partial pressure was investigated.

X-ray Analyses

X-ray diffraction patterns were obtained using a Philips 114.6-mm.-diameter powder camera on a standard Philips Norelco X-ray unit. Filtered iron radiation was used, and the X-ray tube was operated at 40 kv. with a filament current of 10 milliamperes. Under these conditions six-hour exposures produced acceptable patterns.

Experimental Procedure

The procedure for the vertical-tube-furnace runs will be discussed first. Prior to each run the apparatus was purged with a slow stream of hydrogen to decrease traces of water to a negligible level. Shortly before starting

a run the absorption tubes were flushed with the reducing gas to be used (either pure hydrogen, or hydrogen-helium mixture); after this, the U-tubes were disengaged from the apparatus and were tared.

A small quantity of the oxide specimen (granules or a pellet) was carefully weighed into the nickel basket, and the latter was attached to the nickel chain and cylinder. The apparatus was flushed with argon (by-passing the U-tubes), and after approximately 10 minutes (argon flow continuing) the Pyrex cap mounted to the top of the reaction tube was opened and the chain, basket and cylinder assembly was partially lowered into the tube. The external magnet device was then positioned to support the assembly, and the Pyrex cap was replaced. Purging with argon was continued for about 15 minutes; during this interval the sample was gently lowered within approximately 1/4 inch of the thermocouple probe and furnace temperature was stabilized at the control point.

At zero time the argon feed valve was closed, hydrogen flow was started, and the gases leaving the reactor were directed through one of the pairs of U-tubes. After several minutes, hydrogen flow rate and reactor pressure were adjusted to the desired levels. Pressure was maintained constant within a tolerance of approximately $\pm$ 2 or 3 mm. Hg; flow rate was constant within $\pm$ 5%.

The gas stream leaving the reactor was routed to a different pair of U-tubes at intervals of several minutes to two hours. During off-stream periods the U-tubes were weighed, the weight gain corresponding to the reduction experienced during the specific interval. External surfaces of the tubes were always washed with acetone and wiped dry before weighing. That the efficiency of the water recovery tubes was excellent is borne out by the fact that the second tube of each pair never gained more than one or two mg. weight in all experiments.

Rate data could not be based on water recovery in the moist hydrogen runs because the water product was small compared to the water added to the hydrogen in the saturator; consequently, the conversion was determined by oxide weight loss. It was first necessary to establish whether the solid reduction product was stable upon exposure to air; at higher temperatures it was necessary to cool the reduction product to room temperature in argon to avoid appreciable oxidation.

The higher temperature (above 425°C) runs were conducted using the horizontal-tube furnace. The procedure was similar to that described for the vertical-tube furnace with the exception that the Alundum boat containing the sample was manually moved into the hot zone (using a stainless steel rod and chain device) at the time the reaction tube was charged.

CHAPTER V

RESULTS AND DISCUSSION

Preliminary Data

The great majority of runs were conducted in the vertical-tube apparatus using samples of synthetic pyrolusite. Several exploratory experiments, in which single 1.5-gram compressed pellets were reduced in pure hydrogen, were carried out before the furnace temperature controller was available. These data indicated that while the reduction proceeded to 20% completion (based on MnO as the final product) in approximately five hours at 200°C, 67% reduction was realized in approximately three hours at 250°C. Furthermore, at 350°C, the exothermic reduction was found to proceed so rapidly that it was impossible to maintain the oxide specimen at isothermal conditions, and complete conversion to MnO was achieved in several minutes. These preliminary data, although somewhat crude compared to the more quantitative data of later experiments, served as starting points in selecting experimental conditions for later runs.

Low-Temperature Regime

Following the installation of the furnace temperature controller, a series of runs was carried out in pure hydrogen (800 mm. Hg pressure) at 250°C, using a number of size fractions of MnO_2 granules, various hydrogen flow

rates, and several sample sizes. These experimental parameters were varied in order to determine the significance of boundary-layer transport and pore-diffusion resistances, and the extent of retardation due to hydrogen depletion or water vapor accumulation in the reaction zone. Samples of synthetic pyrolusite from Batches A and B were used in this series of runs. The conversion-time curves for these runs are shown in Figure 7.

Results for the two duplicate runs indicate that the conversion at a given time is reproducible within approximately 2%. In terms of the reduction rates (obtained by graphically differentiating the conversion-time curves) the reproducibility is approximately 8%. This variation is apparently caused by small temperature and sample-positioning differences and by accumulated U-tube weighing errors. (Small temperature fluctuation is probably the most influencial factor; an analysis of later data obtained at different temperatures indicates that a $1^{\circ}C$ rise in temperature at $250^{\circ}C$ would raise the observed rate about 5%.)

The initial rate data (below approximately 10% reduction) are somewhat less reliable than the data at higher conversions. Although reaction time was measured from the instant argon flow was terminated and hydrogen flow was started, the oxide specimen was not exposed to pure

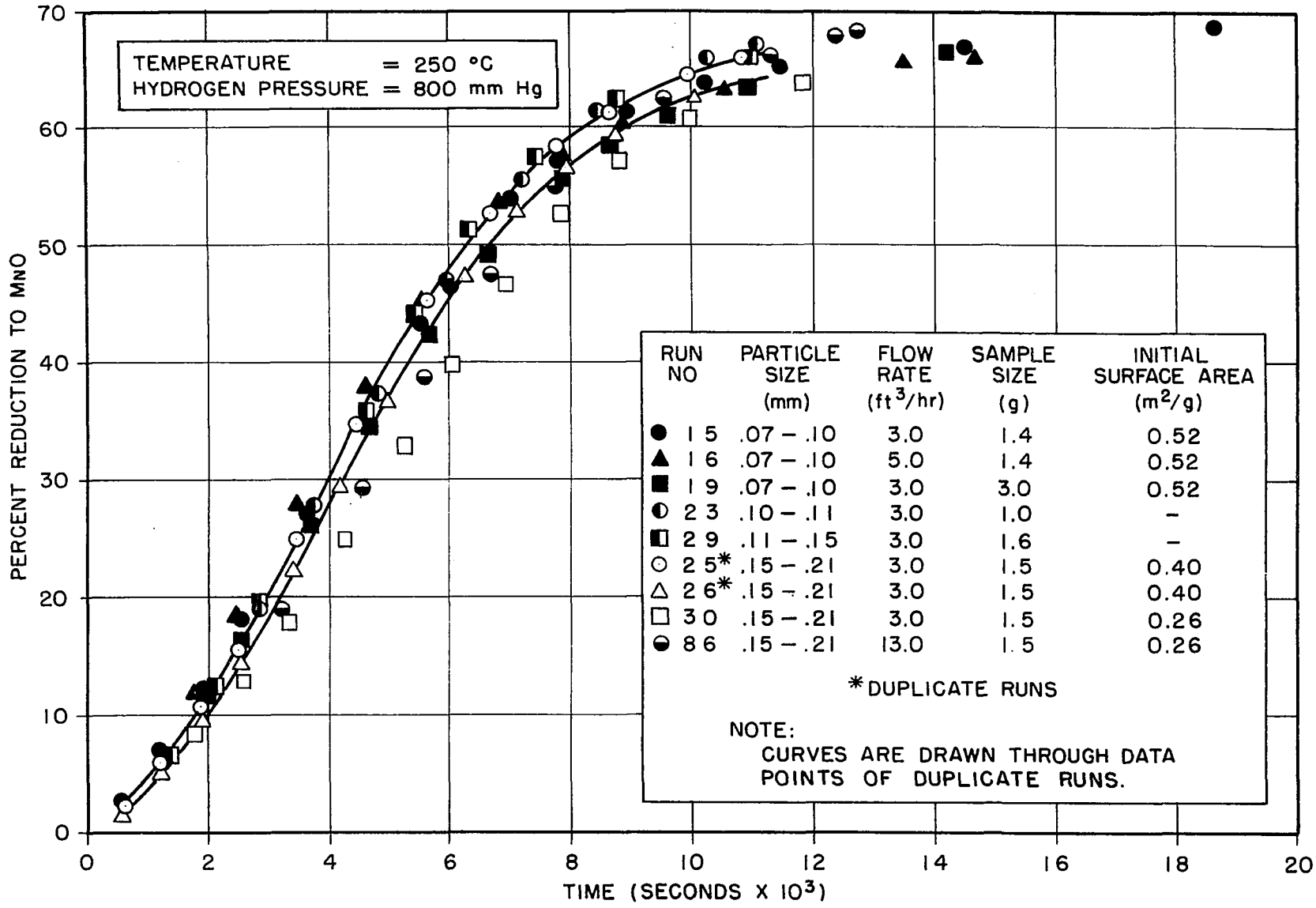

FIG. 7 REDUCTION OF PARTICLES AT 250°C

hydrogen until all of the argon had been purged from the purification and drying tubes and from the reaction zone. This was estimated to take approximately two to three minutes; however, some variability from run to run was encountered. Likewise, some temperature fluctuation usually occurred during the first few minutes, and this also was not generally reproducible from run to run. Therefore, in comparing various reduction curves in Figure 7, the analysis should be restricted to conversions (above about 10% reduction) which are free of these start-up variations.

A careful review of the reduction data plotted in Figure 7 leads to the following conclusions:

(1). The observed rate at 250°C increases slightly as the sample size is reduced from 3 to 1.5 grams; however, no further increase is observed as the sample weight is reduced from 1.5 to 1.0 gram. This indicates that a 1.5-gram bed of oxide placed in the supporting basket is sufficiently shallow to prevent appreciable hydrogen depletion and product water vapor accumulation, which would retard the observed rate. As the sample size is increased to 3.0 grams some retardation is observed. Sample size at 250°C should therefore not exceed 1.5 grams.

(2). Boundary-layer transport resistance at 250°C is negligible for flow rates of 3.0 standard cubic feet per hour or higher. This is evident from the fact that a

fourfold increase in flow rate does not increase the observed reduction rate.

(3). Pore-diffusion resistance and particle temperature gradients at 250° are negligible for granules ranging from 0.07 to 0.21 mm. This is evident from the fact that no significant difference in rate is observed for three different size fractions of granules.

(4). A lower initial surface area decreases the rate only during the early stage of the reduction, and the observed decrease for a 50% change in the initial surface area is, at that, very mild.

Once the 250°C data reported in Figure 7 were available, appropriate operating conditions (flow rate, sample size, etc.) were selected for temperatures below 250°C which insured negligible boundary-layer and pore-diffusion resistances, and negligible retardation due to hydrogen depletion or water vapor accumulation. Data at 200°, 225°, and 238°C were obtained, and the conversion-time curves have been plotted in Figure 8. The final conversions, based on water recovery and oxide weight loss, generally agreed within about 2% in this temperature range. The higher temperature data plotted in Figure 8 will be discussed at a later point.

In order to determine the nature of the reduction products, X-ray powder diffraction patterns were obtained

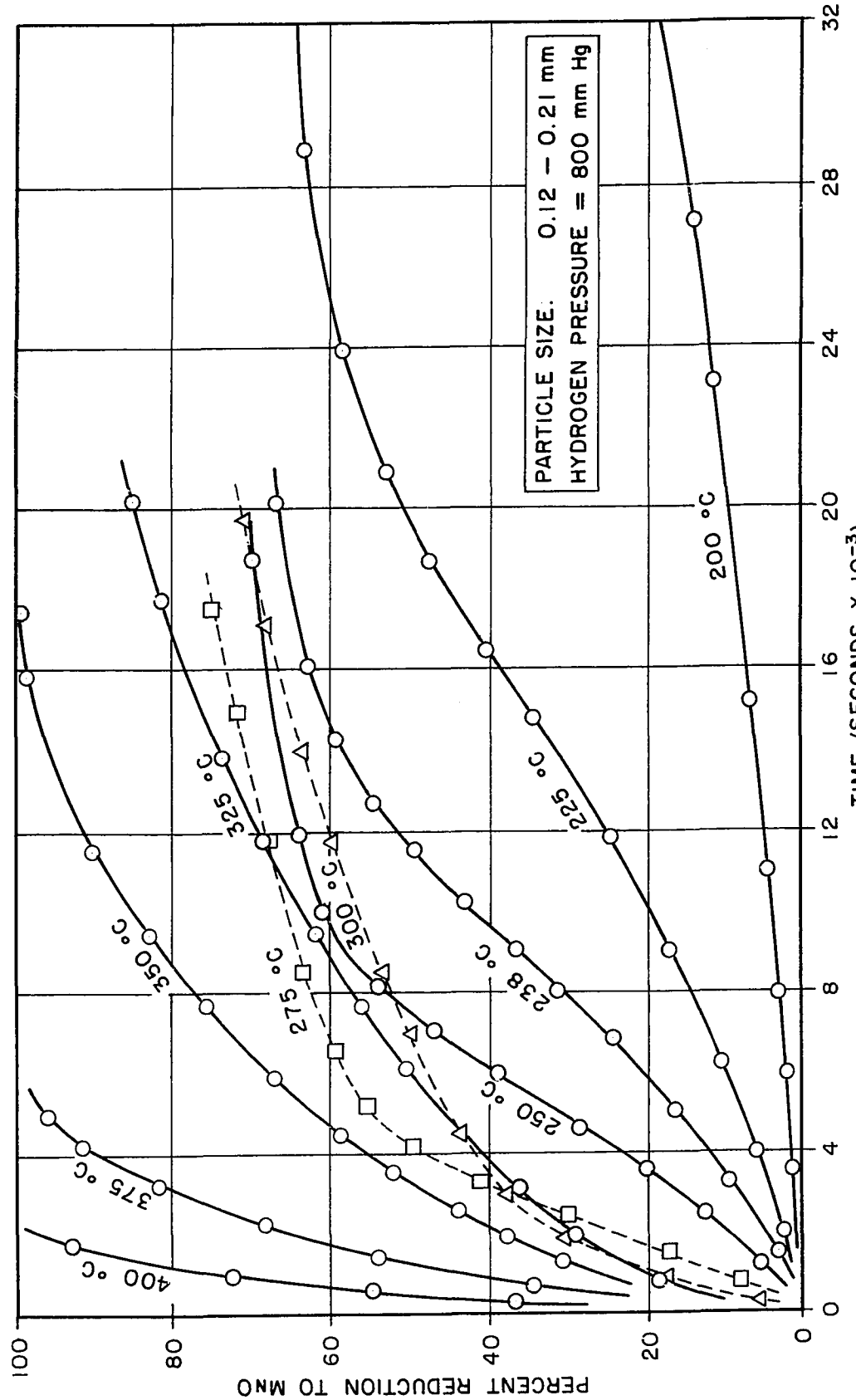

FIG. 8 EFFECT OF TEMPERATURE ON REDUCTION

on a number of partially reduced specimens. The X-ray diagrams have been reproduced in Figure 9 and a summary of the phases identified is given in Table 2. In all of the runs conducted at 250° and 225°C, an oxygen material balance between water product recovered and oxide weight loss agreed within 2 or 3%, indicating that reoxidation of the reduction products upon removal from the furnace was negligible.

The MnO_2 reference pattern shown in Figure 9 was that given by the synthetic pyrolusite, Batch A. The MnO reference pattern was that given by a sample prepared from the MnO_2 by reduction with hydrogen. Reference Mn_2O_3 and Mn_3O_4 samples were prepared by dissociating MnO_2 in air at 540° and 940°C, respectively.

The X-ray pattern of the product of run 16, which was reduced to 66% completion at 250°C, showed predominantly the pattern of Mn_3O_4 (hausmannite)[16], although the strongest lines of the Mn_2O_3 (partridgeite) pattern[32] were also observed. An almost identical pattern was obtained for the product of run 42 which reduced to 68% completion at 225°C. The practically horizontal portions of the reduction curves (at and below 250°C) in Figure 8 correspond then to products which are predominantly Mn_3O_4. It will be observed that the low-temperature conversion curves all tend to

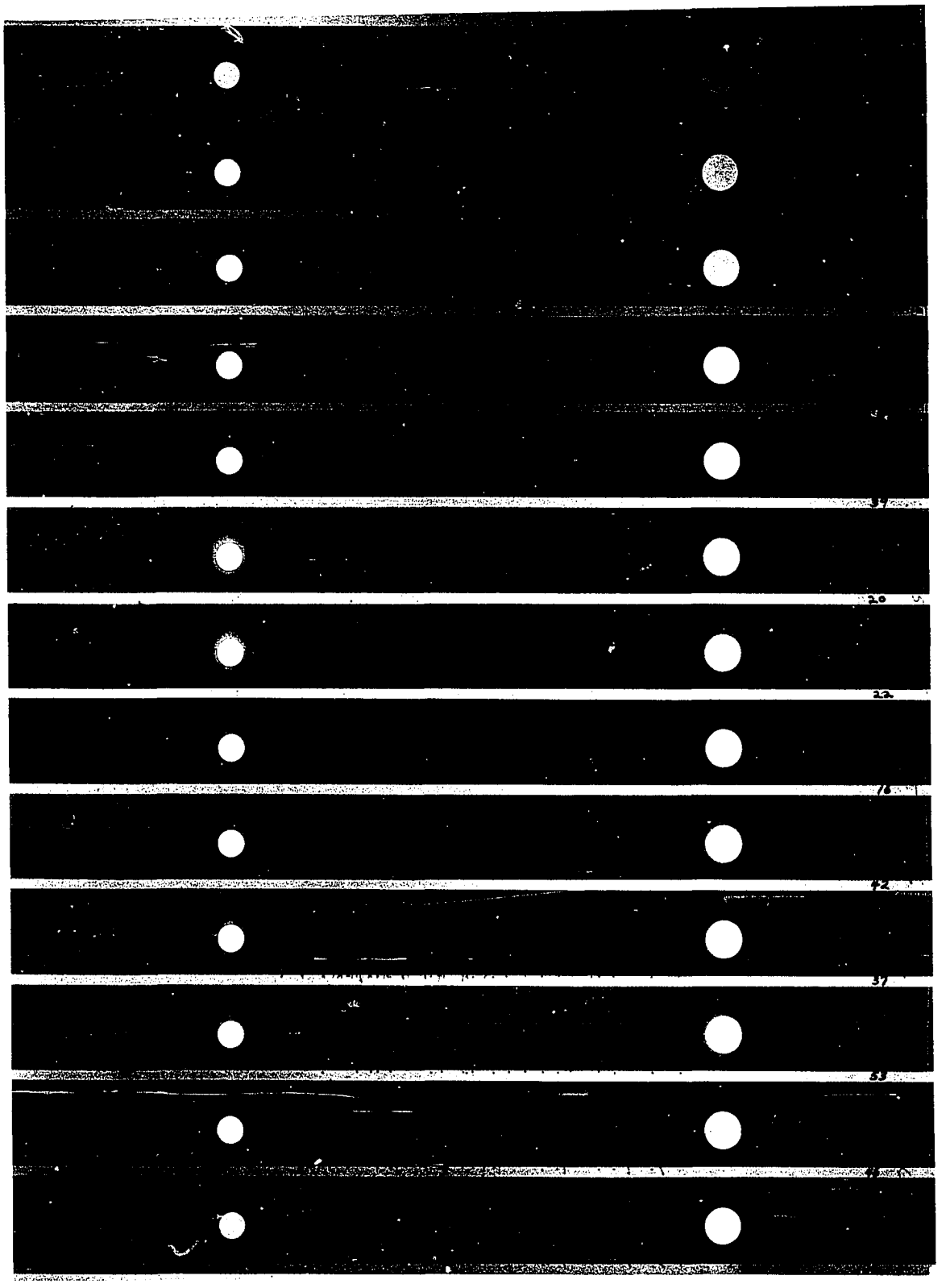

FIG. 9 X-RAY DIFFRACTION PATTERNS

TABLE 2

PHASES FORMED BY REDUCTION WITH HYDROGEN ACCORDING TO X-RAY INVESTIGATIONS

Run No.	Reduction Temp., °C	% Reduction to MnO	Comments	Phases Observed		
				Major	Semi-major	Minor
39	250	11	Reducing agent: H_2	MnO_2		Mn_2O_3, Mn_3O_4
20	250	15	"	MnO_2		Mn_2O_3, Mn_3O_4
22	250	32	"	MnO_2	Mn_3O_4	Mn_2O_3
16	250	66	"	Mn_3O_4		Mn_2O_3
42	225	68	"	Mn_3O_4		Mn_2O_3**
37	315	45	"	MnO_2	MnO, Mn_3O_4, Mn_2O_3	
53	350	21	Reducing agent: 24.9% H_2, balance He	MnO_2		MnO*, Mn_2O_3, Mn_3O_4
46	350	78	Reducing agent: 24.9% H_2, balance He	MnO	MnO_2	Mn_2O_3, Mn_3O_4
106	450	60	Reducing agent: 9.73% H_2, balance He	MnO, MnO_2		Mn_2O_3, Mn_3O_4

*Very weak MnO lines

**Barely detectable

level out at conversions in the range of 65 to 70%. If the reduction were to proceed stoichiometrically from MnO_2 to Mn_3O_4, the extent of reduction (based on complete reduction to MnO) would be 66.67%. Both the X-ray and the kinetic data are therefore consistent with the conclusion that the low-temperature reduction product is chiefly Mn_3O_4. This should not be interpreted to mean that additional reduction to MnO will not occur; further reaction proceeds only at a relatively much slower rate, however.

An attempt was made to determine the composition of a specimen reduced to 68% conversion at 250°C (run 86). If it is assumed that the monoxide is not present (it was not detected in the X-ray pattern), the relative amounts of MnO_2, Mn_2O_3 and Mn_3O_4 can be determined thermogravimetrically[13, 14, 15]. Thus, if the mixture is heated in argon at 700°C, the quantity of oxygen evolved is proportional to the MnO_2 present (the MnO_2 dissociates to Mn_2O_3). If the sample is then heated in air at 700°C, the oxygen consumed is proportional to the Mn_3O_4 content (Mn_3O_4 is oxidized to Mn_2O_3). The amount of Mn_2O_3 is obtained by comparing the active oxygen of the original mixture and the two heated portions. In this manner the product of run 86 was found to contain 91% Mn_3O_4, 7% MnO_2, and 2% Mn_2O_3. In this analysis the MnO_2 percentage (and hence the Mn_2O_3 percentage which is obtained by difference) is

subject to large error in that a trace of water in the original sample would have a very large effect on the calculated MnO_2 content. With the exception that MnO_2 was not detected in the X-ray diagram at this level of reduction, the gravimetric analysis is consistent with the X-ray and kinetic data. Consequently, it is concluded that the low-temperature reduction experiments (at the 65 to 70% conversion level) produced Mn_3O_4 products of approximately 90% purity.

The X-ray patterns obtained on the products of runs 39, 20 and 22, all reduced to various extents at 250°C, show that Mn_3O_4 is formed early in the reduction and that its concentration increases as the reduction proceeds. In all cases, however, minor amounts of Mn_2O_3 were found.

At this point attention was also directed to the reduction of granules of pyrolusite at somewhat higher temperatures. It will be recalled that in an early exploratory run a single compressed pellet of MnO_2 which was initially at 350°C reacted completely to MnO in several minutes, with a consequent large elevation in pellet temperature. In a similar run using 0.15 to 0.21 mm. particles, the indicated temperature increased from 350° to 405°C, and once again, complete reduction was achieved in several minutes. On the other hand, the apparent sample temperature (using granules of the oxide) could be

controlled up to 315°C. Data for two typical runs, 275° and 300°C, are also plotted in Figure 8. It will be observed that the initial rates continued to increase with temperature, but at higher conversions this was no longer true. For example, the reaction rate at 40% reduction is lower at 300°C than at 275°C or even at 250°C.

The low-temperature (200° to 300°C) conversion data were graphically differentiated at constant levels of conversion to obtain quantitative reduction rates, and an Arrhenius plot, Figure 10, was prepared. That the data at 250°C and below are essentially free of boundary-layer transport and pore-diffusion resistances has already been demonstrated. It will be observed that the Arrhenius plot is linear up to approximately 240°C. Furthermore, the 10 and 35% reduction lines exhibit practically identical slopes in this temperature range. This indicates that diffusion resistance through a product layer is also not significant between 200° and 240°C. Equating the slope of the linear portions of the curves to $-E_a/2.3R$, an apparent activation energy of approximately 22.2 kcal./mole is obtained. A value of this magnitude is characteristic of chemical reaction control.

The sharp curvature in the Arrhenius plot beginning at about 250°C is indicative of a drastic change in kinetics; further discussion of the data in this region is postponed

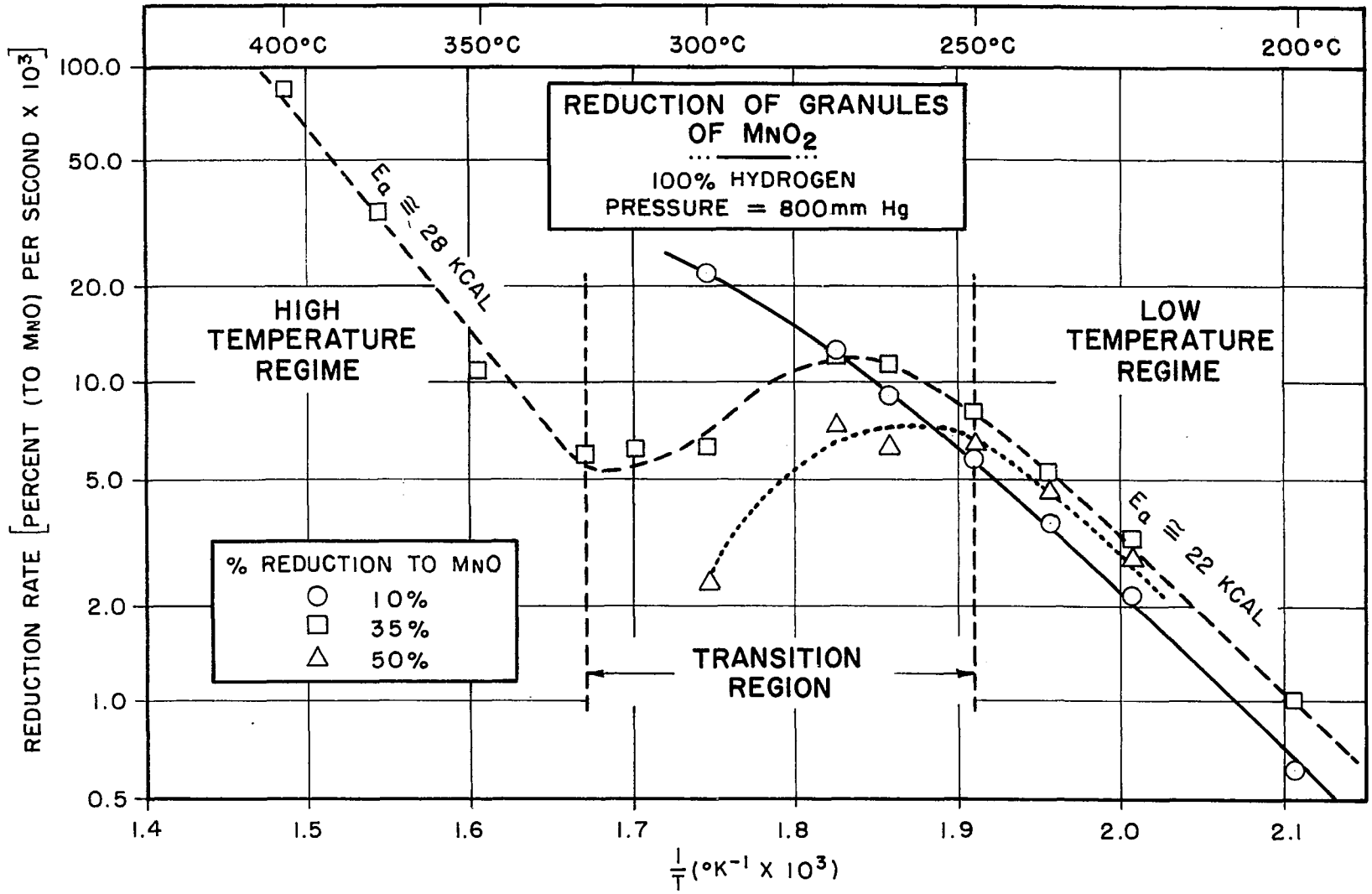

FIG. 10 ARRHENIUS PLOT FOR PARTICLES

until the high-temperature data are reviewed.

Numerous low-temperature reduction runs were also conducted using nominal 1.5-gram porous pellets (Batch B) of synthetic pyrolusite. Several experiments were carried out in pure hydrogen at 226°C to determine the extent of boundary-layer transport and pore-diffusion resistances. These results are plotted in Figure 11 in the form of conversion-time curves. Comparison of runs 44 and 51, in which a fourfold difference in flow rates was used, shows that boundary-layer transport resistance is negligible at this temperature. In order to estimate the extent of pore-diffusion resistance, the pellet reduced in run 64 was sectioned into four more or less equal pie-shaped pieces, thus sharply reducing the pellet dimensions. Comparison with the data of the other two runs indicates that, except possibly initially, no significant difference in rate occurred. In view of the normal variation of initial rate data and the agreement of the rates at higher conversions, it is concluded that the reaction essentially proceeds uniformly on all available surface throughout the pellet. Thus, the reduction of a single pellet at 226°C proceeds without appreciable gaseous diffusion effects if a hydrogen flow rate of 3.0 standard cubic feet per hour or larger is used.

It is interesting to compare the reduction of a single porous pellet with that of a bed of porous granules

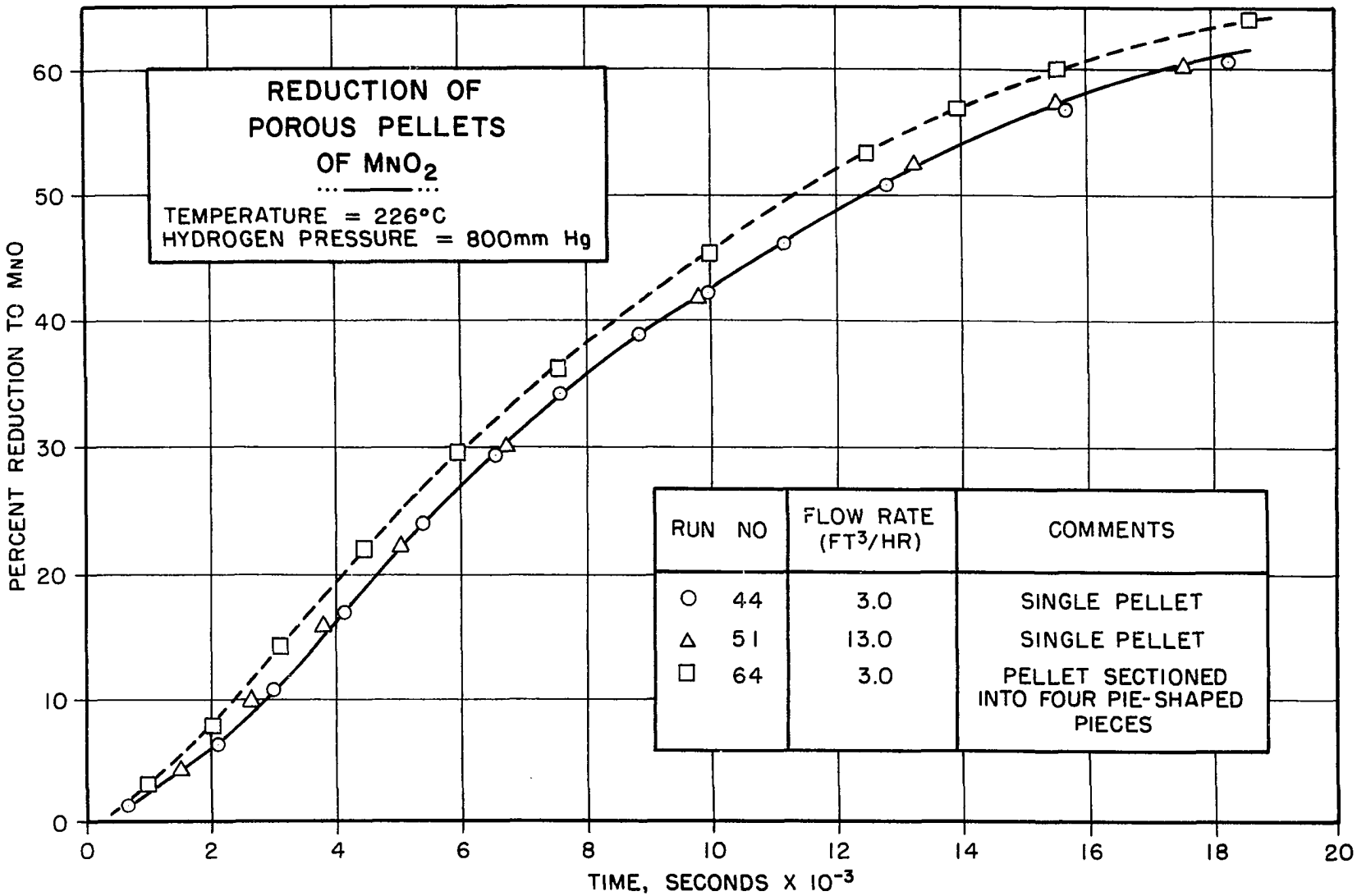

FIG. 11 REDUCTION OF PELLETS AT 226°C

of MnO_2. Such a comparison is shown in Figure 12. In both cases the reduction rate subsides sharply at approximately 65% conversion. However, the early reduction rates are much greater for the pellet than for the bed of particles. In addition, the autocatalytic effect is somewhat less pronounced in the case of the pellet, the maximum rate occurring at a lower conversion. These variations are probably caused by structural differences in the two oxide specimens. A pellet similar to the one used in run 44 had an initial surface area (per gram) approximately five times that of the particles used in run 42. The pore volume distribution data in Figure 6 (Batch B was used in runs 42 and 44) indicated that the micropore volume of a pellet was also much greater than for the particles. These data suggest the existence of some sealed-off pores in the granules. According to this viewpoint, the reduction rate must increase during the initial stages as more and more of the originally sealed-off pores become exposed to hydrogen by virtue of the formation of the more porous lower oxides. Eventually all pore volume becomes exposed and the surface area, and hence the reduction rate, reaches a maximum. Further reduction can then only decrease the amount of surface available for reaction, and therefore, from this point on, the rate subsides. It was observed that the maximum rate of reduction for the particles always occurred at the same level of conversion, regardless

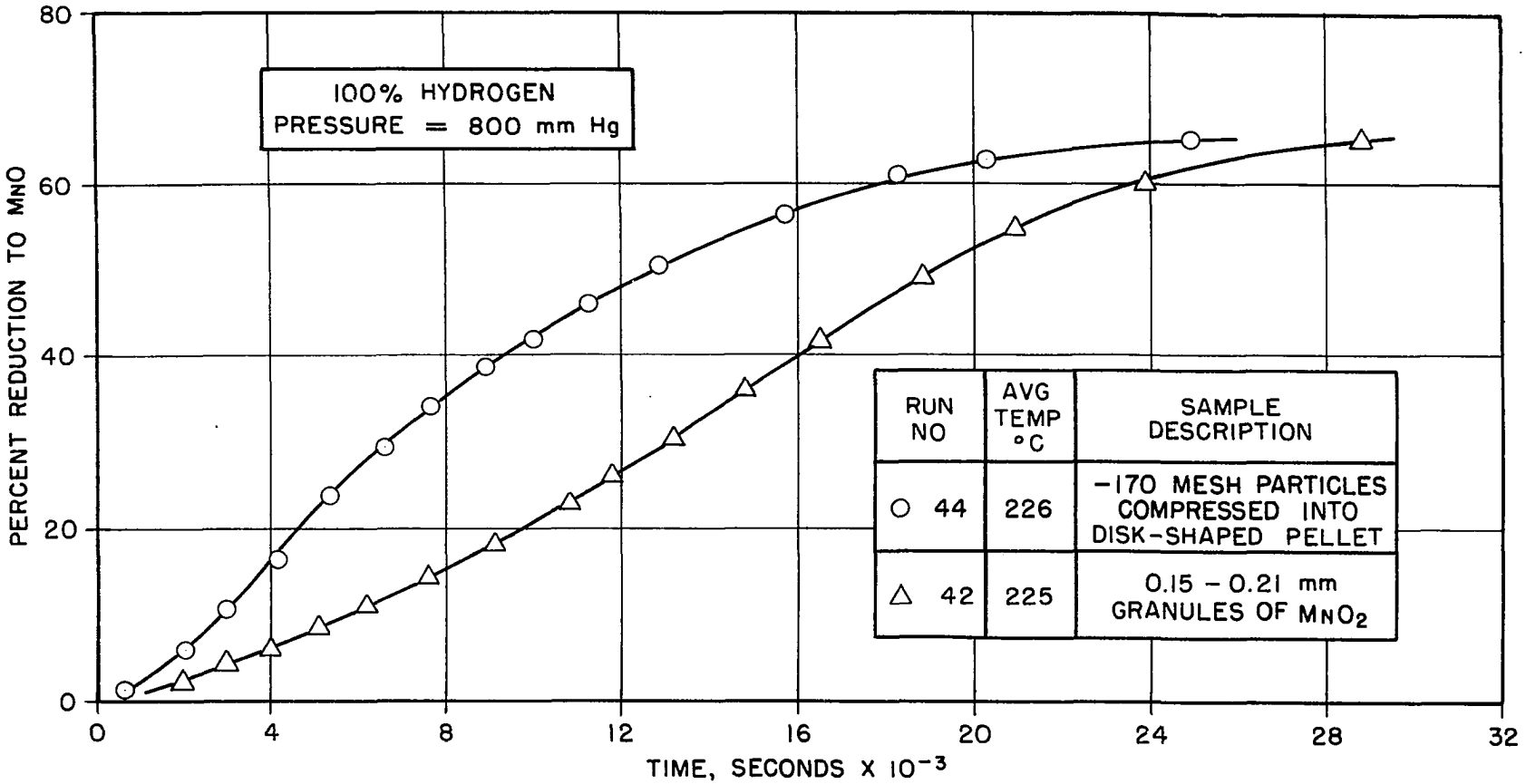

FIG. 12 REDUCTION OF PARTICLES VS. SINGLE PELLET

of the temperature. This also suggests that the autocatalytic behavior resulted from the existence of originally sealed-off pores. This argument does not preclude the existence of some degree of intrinsic autocatalytic behavior. Indeed, as mentioned earlier, when one solid reacts in a gas-solid reaction to form a second solid, the reaction can occur only at the boundary between the two solid phases. Furthermore, if the growth of the interface begins at relatively few points on the surface, the reduction rate will increase until the interface covers the entire surface. Nevertheless, it appears that the primary cause for the autocatalysis observed here lies in the structural characteristics of the oxide and not in the intrinsic kinetic behavior.

It was possible to correlate the reduction data for the porous pellets in terms of the rate model depicted in Figure 13. A porous pellet of MnO_2 may be pictured as an agglomeration (Figure 13a) of numerous dense cubes, each of identical edge x_o. Under conditions where both boundary-layer transport and pore-diffusion resistances are negligible, it suffices to consider the reduction of a single (hypothetical) dense cube (Figure 13b) exposed to the known bulk gas phase hydrogen concentration.

At temperatures of 250°C and lower, the X-ray data have shown that the reaction subsides with the formation

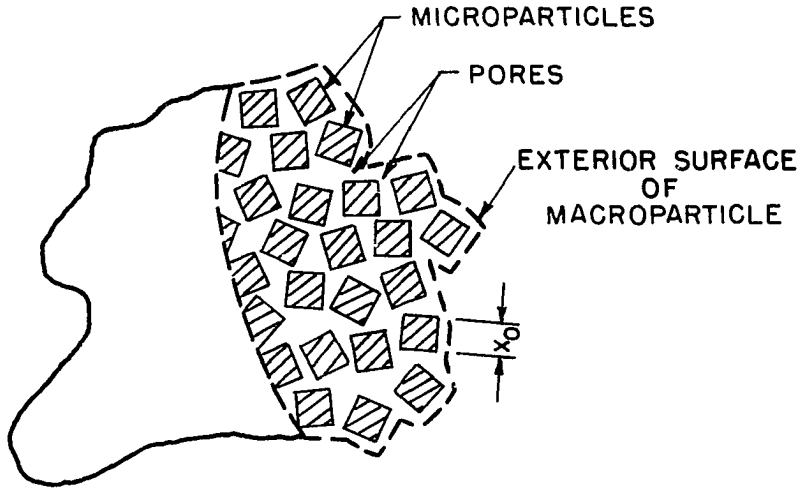

(a) MACROPARTICLE OF MnO_2

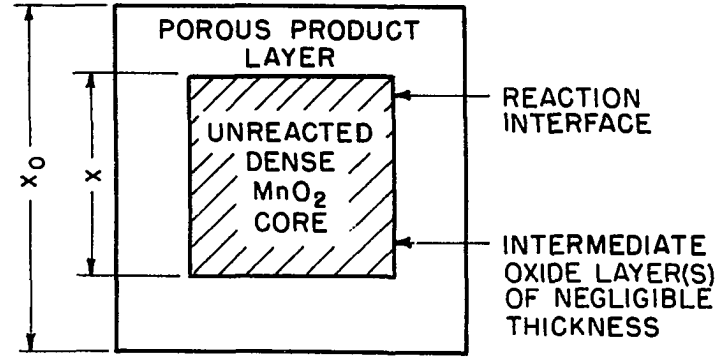

	T < 250°C	T > 325°C
PRODUCT LAYER	Mn_3O_4	MnO
INTERMEDIATE OXIDE LAYERS	Mn_2O_3	Mn_2O_3, Mn_3O_4

(b) PARTIALLY REDUCED MICROPARTICLE

FIG. 13 REDUCTION MODEL

of Mn_3O_4. Moreover, because distinct lower oxide phases appear, the reaction would be expected to proceed in a topochemical fashion. Since the volumes of oxide associated with a gram of manganese are 0.315, 0.319, and 0.287 $cm.^3$ for MnO_2, Mn_2O_3 and Mn_3O_4, respectively, one might expect Mn_2O_3 to form a dense reduction-product layer on MnO_2 (although the specific volumes are admitedly very close), while a porous layer of Mn_3O_4 would, in turn, be expected to form as the reduction product of Mn_2O_3. In view of the X-ray results, it is reasonable to consider the reduction process as occurring topochemically, with MnO_2 in the core, followed by a dense layer of Mn_2O_3, and finally a porous layer of Mn_3O_4. According to this hypothesis the gas-solid reduction occurs only at the Mn_2O_3/Mn_3O_4 boundary, while the reduction of MnO_2 to Mn_2O_3 would presumably proceed by a solid-state process. Furthermore, since Mn_2O_3 is present in relatively small amounts, the thickness of this layer may be neglected. Hence, the model depicted in Figure 13b is obtained. The original dense cube edge is designated x_o, and the cube edge of the unreacted core of MnO_2 is taken as x.

If the fractional conversion based on Mn_3O_4 as the final product is designated Z', and if the chemical reaction step is assumed to control, it has been shown in equations (13) and (14) that

$$\frac{2tr_s'}{\rho_{MnO_2}x_o} = 1 - (1 - Z')^{1/3} = \frac{x_o - x}{x_o} \qquad (17)$$

where t is the time of reaction; r_s', the rate of reaction in moles of MnO_2 per unit of reaction surface area; and ρ_{MnO_2}, the molar density of MnO_2. The quantity, k',

$$k' = \frac{2}{\rho_{MnO_2}x_o}(r_s') \qquad (18)$$

may be designated an apparent rate constant; since r_s' is a function of pressure and temperature, the apparent rate constant will likewise vary with temperature and hydrogen pressure.

A test of this model may be made by examining the linearity of a plot of $1 - (1 - Z')^{1/3}$ versus the time of reaction. Data for four temperatures are plotted in this fashion in Figure 14. With the exception of the low conversion points, excellent linearity is observed. It will be recalled that the low conversion data are characterized by an apparent autocatalytic effect which, of course, has not been considered in formulating the model. For the same reason the straight lines do not pass through the origin.

Apparent rate constants evaluated from the slopes of the lines in Figure 14 are presented in an Arrhenius plot in Figure 15. Setting

$$k' = A' \exp(-E_a/RT) \qquad (19)$$

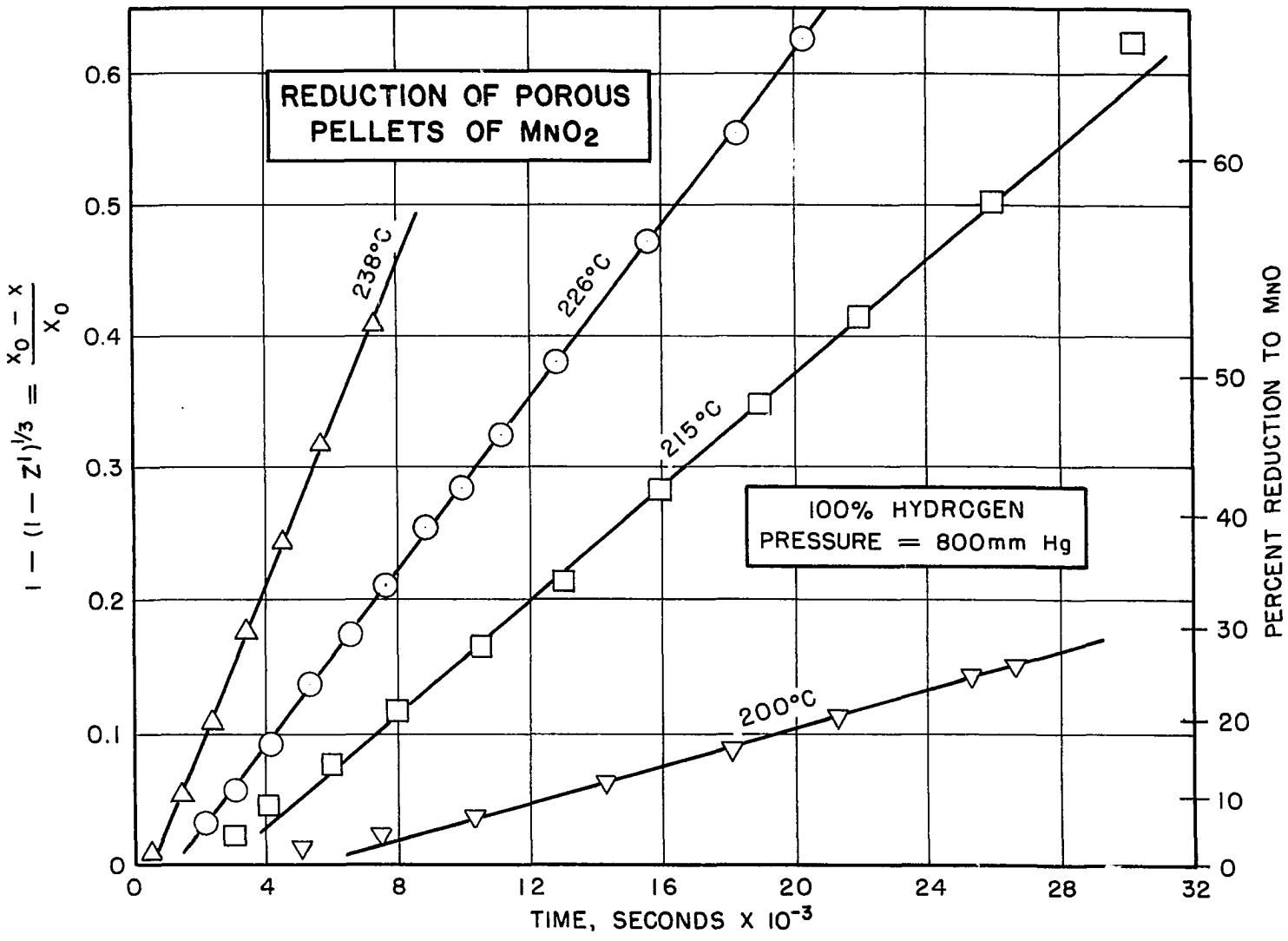

FIG. 14 LOW TEMPERATURE MODEL PLOTS FOR PELLETS

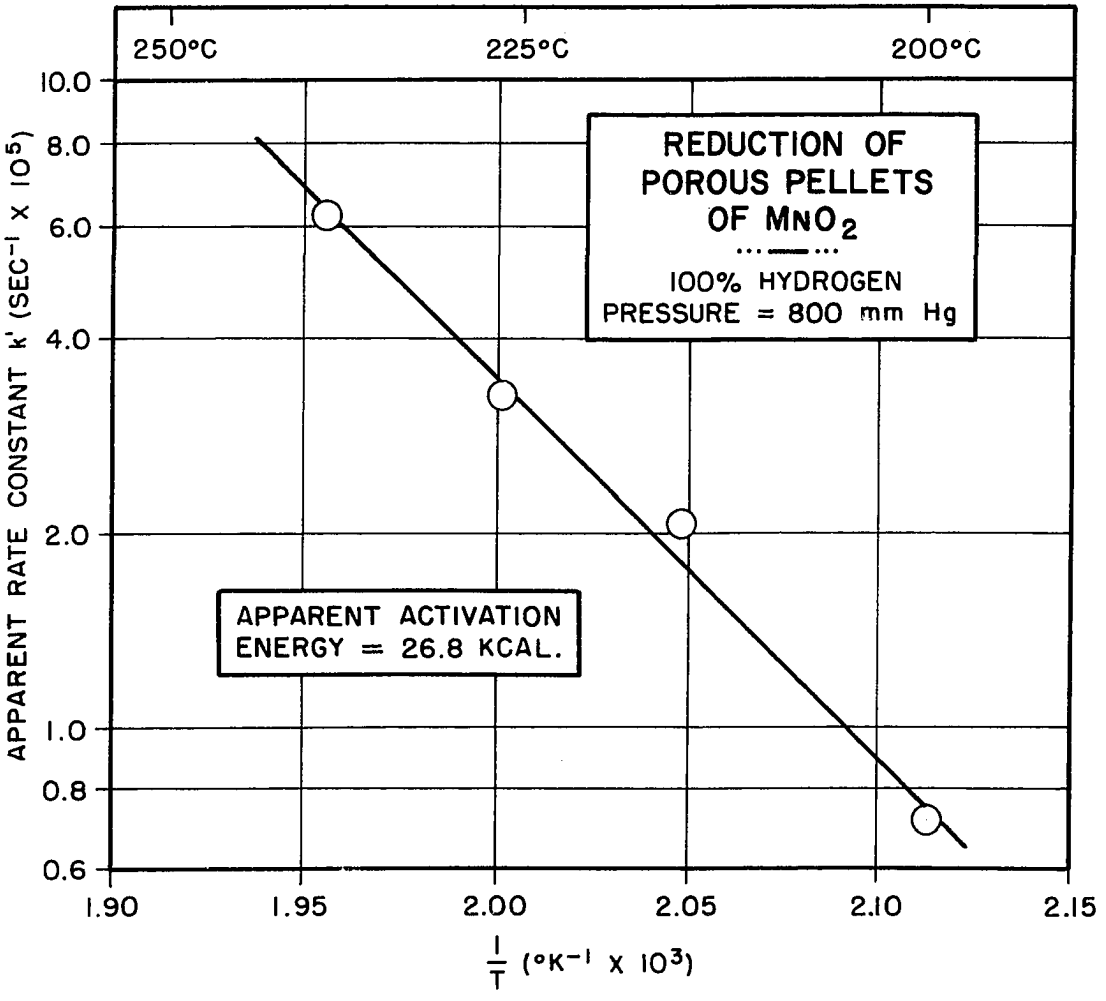

FIG. 15 LOW TEMPERATURE ARRHENIUS PLOT OF APPARENT RATE CONSTANT

an apparent activation energy of E_a = 26.8 kcal./mole is obtained. This value is once again consistent with the premise that the reduction process is controlled by chemical reaction in the temperature range of 200° to 238°C. The activation energy agrees well with the 22.2 kcal./mole value obtained for the reduction of 0.12 to 0.21 mm. granules of MnO_2 in the same temperature range.

The effect of hydrogen partial pressure upon the reduction of pellets was investigated at 226°C. Helium was used as the diluent, and in each case the total pressure was maintained at 800 mm. Hg. Total flow rates in excess of 4.5 standard cubic feet per hour were used to avoid boundary-layer diffusional effects. The results are shown in Figure 16 in terms of the variation of the apparent rate constant, k'. The influence of pressure can be expressed by equation (20).

$$k' = \frac{8.03 \times 10^{-8} \, P_{H_2}}{1 + 1.187 \times 10^{-3} \, P_{H_2}} \qquad (20)$$

This pressure dependence is characteristic of a chemically-controlled solid-gas reaction where the surface is only partially saturated with H_2, and where adsorption of product H_2O is negligible.

The retarding effect of water vapor was also investigated at 226°C. Nominal 1 and 10% (volume or mole %) levels of water vapor concentrations were used, and the

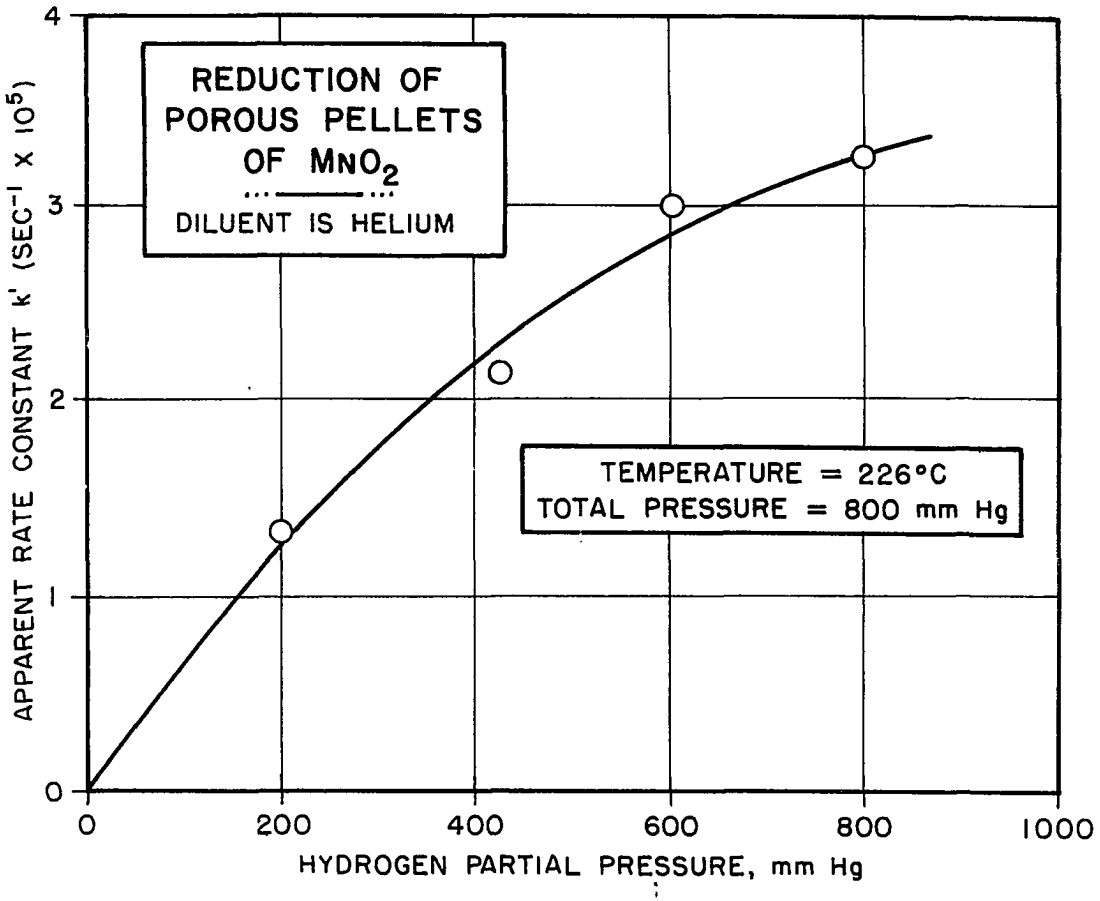

FIG. 16 EFFECT OF H_2 PARTIAL PRESSURE AT 226°C

total pressure was maintained at 800 mm. Hg. Prior to a run the saturator was calibrated by collecting the water from the moist hydrogen stream in the recovery U-tubes over a measured time interval. The extent of reduction was periodically determined by purging the system with argon, removing the sample from the furnace, and weighing the partially reduced oxide. This procedure was valid because the reduction products at 226°C were found to be stable upon removal from the furnace and exposure to the atmosphere. The results are shown in Figure 17. In the first run of this series (number 88), a pellet reacted for 4000 seconds in a hydrogen stream containing 9.9% water vapor, reacted to only 0.8% reduction; in the absence of water vapor the conversion at this point (run 44) was approximately 16%. Thus, the water vapor severely hindered the start of the reduction process. The sample was replaced in the furnace and reacted in dry hydrogen for a second 4000-second period. In this interval the oxide reacted in normal fashion to 18% reduction. After this, the sample was once again reacted in a 9.9% water vapor stream for several intervals of 4000 seconds. The reduction proceeded, but at a highly retarded rate. As will be seen from Table 3, the presence of 9.9% water vapor decreased the apparent rate constant, k', by approximately 71%.

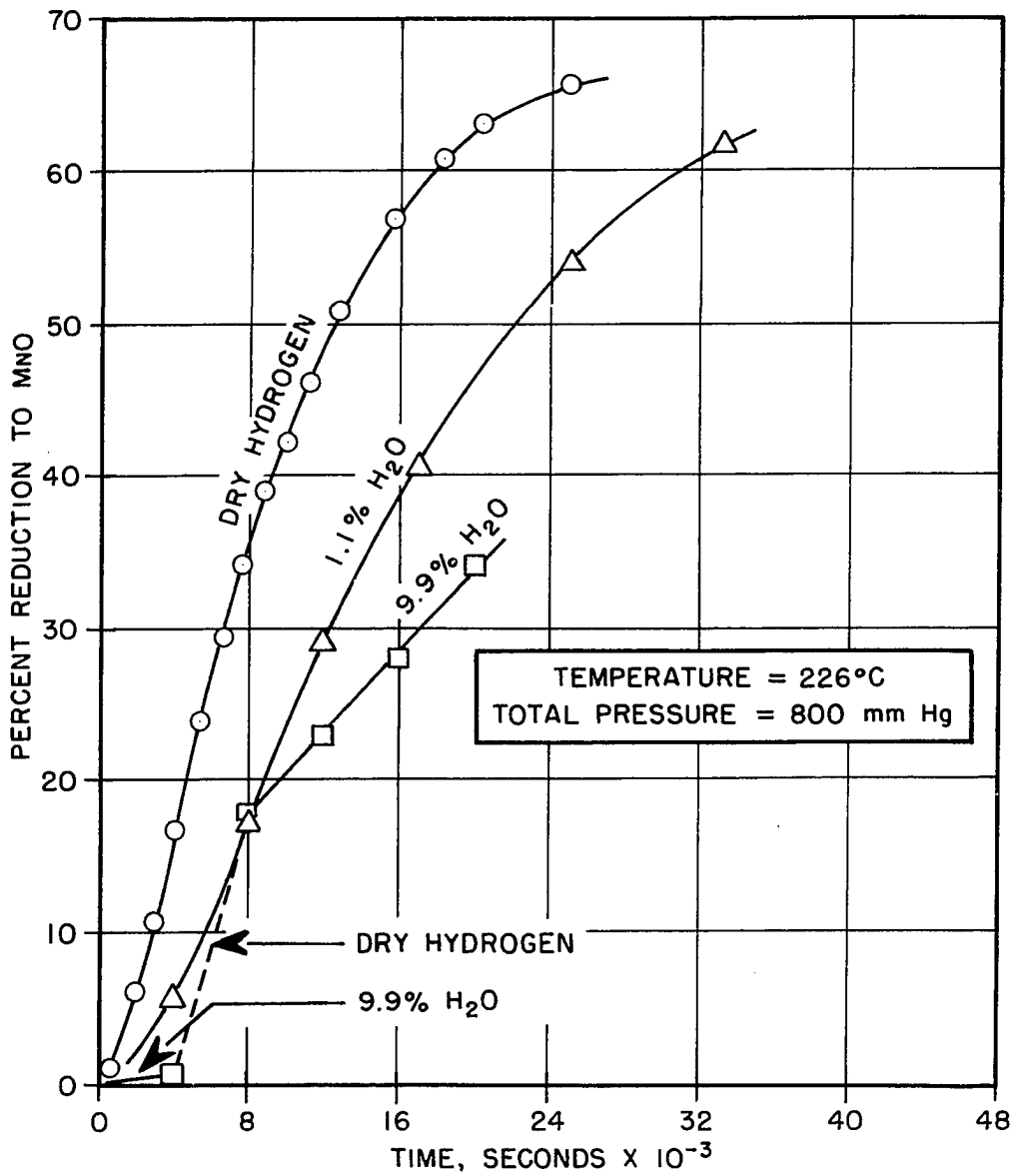

FIG. 17 EFFECT OF WATER VAPOR AT 226°C

TABLE 3

EFFECT OF WATER VAPOR ON REDUCTION RATE

Temperature = 226°C
Total Pressure = 800 mm. Hg

Run No.	% Water Vapor	Apparent Rate Constant $k' \times 10^5$ (sec.$^{-1}$)
44	0.0	3.26
89	1.1	1.80
88	9.9	0.94

Data for a similar run made with a hydrogen stream containing 1.1% water vapor (run 89) are also plotted in Figure 17. The retardation of the initial rate was not nearly as severe as with the 9.9% water run. A second 1.1% water vapor run (number 90, not shown on Figure 17) was made in which the pellet was reacted for a single 14,000-second period of time. The measured conversion at this point was 37%; this compares favorably with the corresponding value of approximately 35% based on the data of run 89. The procedure of periodically removing and weighing the partially reduced pellet did not, therefore, introduce any appreciable error. It will be observed from Table 3 that the presence of 1.1% water vapor in the hydrogen stream decreased the apparent rate constant by approximately 45%.

The strong inhibiting effect of water vapor is once again consistent with the premise that the reduction is controlled by the chemical reaction step. A 10% water vapor concentration at 226°C is apparently effective in essentially preventing the initial formation of Mn_2O_3 or Mn_3O_4 nuclei. This is attributed to the poisoning of active sites by the adsorption of water vapor. In like manner, the retardation at later stages of the reduction is apparently due to appreciable adsorption of water on active sites at the solid-gas reaction interface.

In summary, the data on synthetic MnO_2 indicate that below 250°C the reduction by hydrogen is limited by the chemical reaction step. The reduction practically subsides with the formation of Mn_3O_4 in this region. The rate increases with hydrogen concentration at least up to 800 mm. Hg pressure, and the apparent activation energy is approximately 22 to 27 kcal./mole. Moderate concentrations of water vapor severely inhibit the reduction process. The kinetic and X-ray data are consistent with the hypothesis that the primary gas-solid reaction is controlled at the Mn_2O_3-Mn_3O_4 interface; the mechanism probably consists of adsorption of hydrogen, surface reaction, and water vapor desorption, the slowest step being the surface rearrangement.

High-Temperature Regime

It has been shown (Figure 10) that the low-temperature reduction rates correlate linearly on an Arrhenius plot only up to about 240°C. Above this temperature curvatures appear, and above 275°C the rates of reduction actually decrease at high conversions. This is also evident in Figure 8, where the 300°C conversion curve is seen to intersect both the 275° and 250°C curves. This behavior is characteristic of a drastic change in the reduction kinetics. It should be pointed out, however, that the initial reduction rates continue to increase with temperature; consequently, the Arrhenius plot for the rates at

the 10% reduction level does not deviate greatly from the customary linear relationship in the 200° - 300°C temperature range.

It has already been mentioned that control of sample temperature became a serious problem above 315°C. For example, a sample placed in a pure hydrogen stream at 350°C experienced a very rapid temperature rise (at least 55°C, and probably much higher) with consequent reduction to MnO in several minutes. It was found that temperature stability could be maintained by using hydrogen-helium mixtures sufficiently dilute in hydrogen content. Thus, the reaction could be controlled at 325°C by using a nominal 50% hydrogen (balance, helium) mixture; similarly, control at 375°C was achieved by using a nominal 10% hydrogen (balance, helium) mixture. The conversion curves for these particular conditions, Figure 18, are typical of the high-temperature reduction runs in that they illustrate the characteristic very high initial rate, followed by a much subsided and gradually decreasing rate at higher conversions. These data clearly indicate that the difficulty in temperature control stems from the high initial reaction rate; if control is not maintained during the first few minutes of reaction, particle temperature rises rapidly with consequent escalation of rate to the point where the reduction to MnO is complete in several minutes.

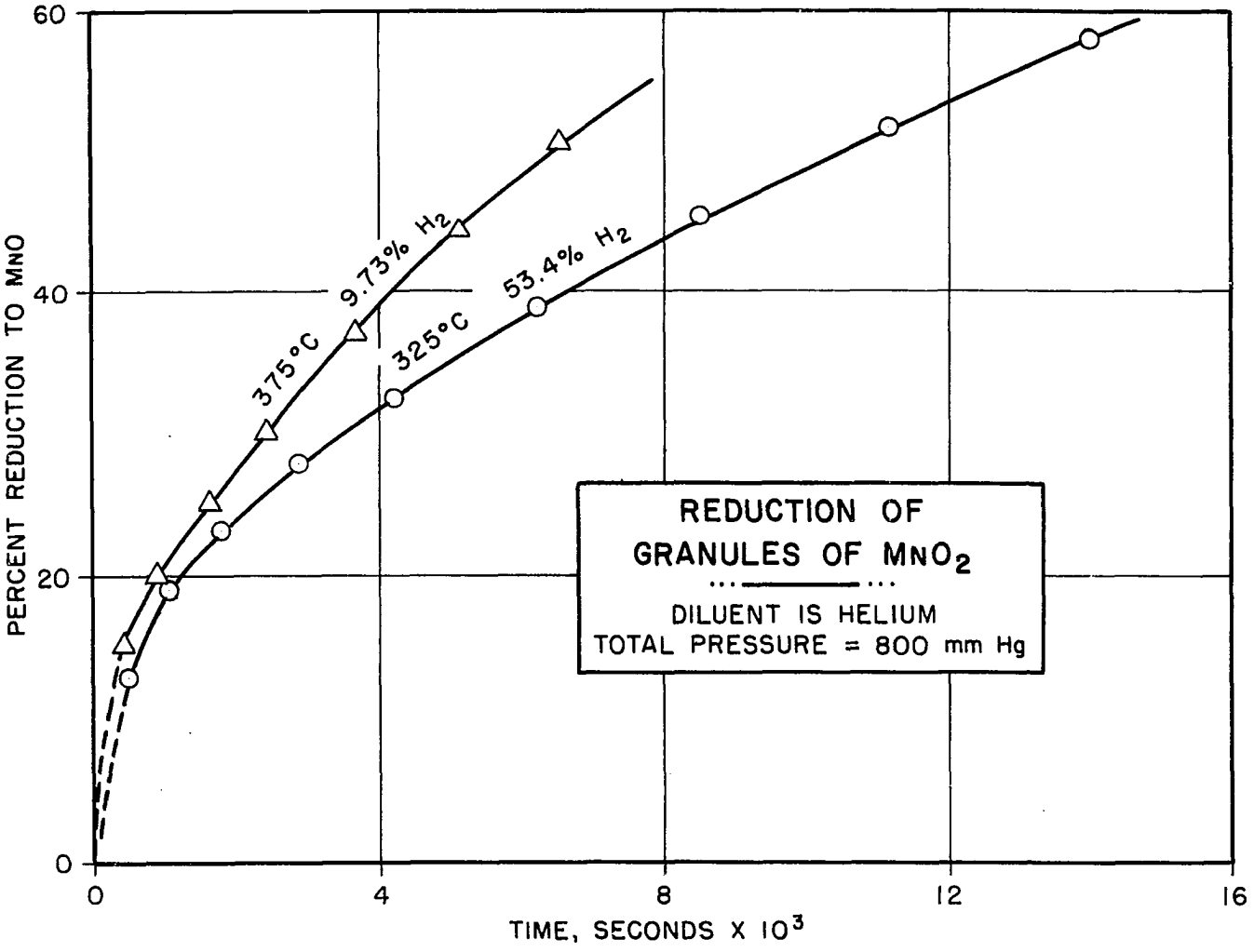

FIG. 18 TYPICAL HIGH TEMPERATURE CONVERSION DATA

In contrast to the data plotted in Figure 18, it was not possible to maintain temperature stability under most high-temperature conditions investigated. This problem was overcome by slowly bleeding hydrogen (or a hydrogen-helium mixture) into a flowing stream of argon during the start of a run. At the same time the flow rate of argon was gradually decreased over an interval of approximately 7 to 10 minutes. Thus, the hydrogen was introduced at a very low, but gradually increasing, partial pressure while the argon, with its relatively high heat capacity, helped to remove the heat liberated during the start of the reaction. Conversions in the range of 15 to 30% were generally obtained during this interval of time. No difficulty in temperature control was experienced after this initial period of reduction.

Because of the relatively poor heat transfer characteristics of large single pellets, the experimental runs in the high-temperature region were limited to the reduction of small granules (0.07 to 0.21 mm.) of pyrolusite. In all cases, specimens from the preparation identified as Batch B were used.

X-ray powder diffraction patterns were obtained on a number of partially reduced oxides in the high-temperature region. These patterns have been reproduced in Figure 9, and the phases identified are summarized in Table 2. In

runs 37 and 53, an oxygen material balance between oxide weight loss and water product recovered agreed within two or three percent, indicating that re-oxidation of the reduction products upon atmospheric exposure was negligible. On the other hand, in runs 46 and 106, the water recovered exceeded the water formed, based on weight loss, by approximately five percent (this, despite the fact that in run 106 the specimen was cooled to room temperature in argon before exposure to the atmosphere). It is very likely that some of the MnO in the products of runs 46 and 106, known to have formed, was re-oxidized as the samples were withdrawn from the furnace.

It will be recalled that MnO was not detected in the products reduced at 250° or 225°C. On the contrary, an appreciable amount of MnO (pattern compared to that of manganosite[31]) was observed in a specimen reduced at 315°C (run 37), even though the conversion was only 45%. The Mn_2O_3[32] and Mn_3O_4[16] patterns were well established in a sample reduced to 21% conversion at 350°C, but the MnO lines in the same sample were noticeably weaker. Inasmuch as the initial high reduction rate subsided at approximately 17% conversion at this temperature, the early stage of the reaction must be associated with the formation of Mn_2O_3 and Mn_3O_4. It is interesting to note that at a conversion of 78% (350°C), minor quantities of

Mn_2O_3 and Mn_3O_4 were again found. It is somewhat surprising still to find an appreciable amount of MnO_2 at this point. Finally, a sample reduced to 60% conversion at 450°C contained both MnO and MnO_2 as major constituents, with once again minor quantities of Mn_2O_3 and Mn_3O_4.

The X-ray data indicate that the initial very high reduction rates result from a very rapid reduction of some MnO_2 to Mn_2O_3 and Mn_3O_4. Contrary to the low-temperature results, however, the formation of Mn_3O_4 apparently subsides after an appreciable amount has formed. This would be the case if the Mn_3O_4 were to become protective; that is, sufficiently dense to severely restrict the counter-diffusion of hydrogen and product water vapor through the layer of reduced oxide formed. The reduction process would then be sharply curtailed, or, in the limit of a perfectly dense layer, stopped altogether. In any event, in this region the temperature is sufficiently high for the Mn_3O_4 itself to undergo reduction to the monoxide. It should be noted that at the higher temperatures Mn_2O_3 and Mn_3O_4 were found only in minor amounts, yet at all levels of conversion. This suggests that the reduction proceeds topochemically through the series $MnO_2 \rightarrow Mn_2O_3 \rightarrow Mn_3O_4 \rightarrow MnO$, with the two intermediate oxides forming relatively small layers between the unreacted dioxide and the reduced monoxide.

A series of runs was conducted in the vertical-tube furnace in pure hydrogen (800 mm. Hg pressure) at 375°C in order to determine the importance of various resistances in the reduction process. Parameters varied were particle size, flow rate, sample size and bed depth. The conversion-time data for these runs have been plotted in Figure 19. Bed depth was varied by using one, two, or three nickel baskets for the support of the oxide specimen; where multiple baskets were used, one was placed above the other in close proximity (bottom-to-bottom distance was approximately 4 to 5 mm.). The bed depth was estimated from the known geometry of the baskets and the measured bulk densities of the oxide samples.

Under these conditions it was necessary to introduce hydrogen slowly in gradually increasing concentrations to maintain temperature stability. No data were taken until the reaction could be controlled at an indicated temperature of 375°C in the presence of pure hydrogen. Consequently, the measured conversion at the first data point for each run was in the vicinity of 30%. There was, as expected, some variability in initial flow rates and hydrogen partial pressures from run to run; this had the effect of shifting the entire conversion curve horizontally in the time coordinate direction. Accordingly, in reviewing Figure 19, it is more meaningful to examine the slopes of the

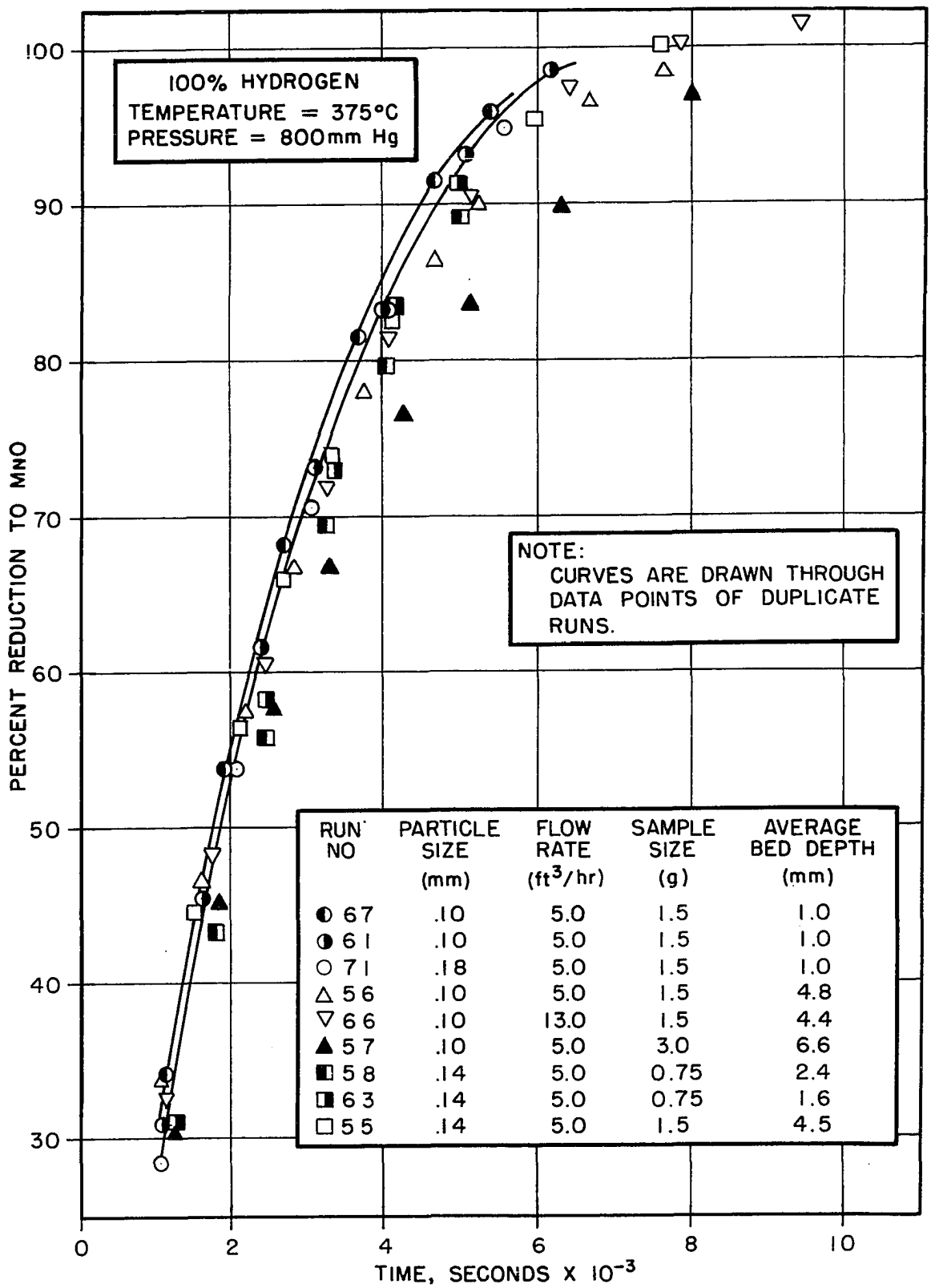

FIG. 19 REDUCTION OF PARTICLES AT 375°C

various conversion-time curves (i.e., the reduction rates) at a given conversion, rather than to compare the conversions of various runs at a given time.

Differences in the reduction curves of Figure 19 are rather minor. A careful analysis of these data leads to the conclusion that the only significant variable is bed depth. Thus, above 45% conversion the reduction rates decrease with an increase in the bed depth. This is apparently due to some hydrogen depletion, or, more likely, to the retarding effect of water vapor, some of which may have accumulated in the bed. The reduction rates appear to be more nearly equal in the 30 to 45% conversion range; in this region, however, other compounding effects may also exist. For instance, since the reaction is exothermic one would expect the temperature to be somewhat higher in a large bed of particles than in a small bed. This effect would be greater in the early stage of the reduction where the rates are higher, and it could conceivably compensate for the other retardation effects. That bed depth is, indeed, the only significant variable will be seen more clearly at a later point when rate constants based on a model of the reduction process will be quantitatively compared.

For reasons previously discussed in the analysis of the low-temperature data, it is concluded that at 375°C

(1) boundary-layer transport resistance is negligible for flow rates of 5.0 standard cubic feet per hour or greater, and (2) pore-diffusion resistance is negligible for granules of average screen size diameters ranging from 0.1 to 0.18 mm.

Based on the data in Figure 19, appropriate flow rates, sample weights, and particle sizes were selected for runs conducted at other temperatures and hydrogen concentrations so as to minimize diffusional resistances. Furthermore, in an attempt to minimize the retarding effect of large beds of particles, bed depths were generally kept at approximately one mm. Reduction experiments were carried out in the vertical-tube furnace at a total pressure of 800 mm. Hg in the temperature range of 325° to 425°C. Hydrogen-helium mixtures with nominal hydrogen concentrations of 10, 25, 50, and 75%, as well as pure hydrogen, were used. Typical high-temperature conversion curves for the pure hydrogen runs have been plotted in Figure 8. At temperatures of 325°C and higher (100% hydrogen runs), the initial hydrogen streams were diluted with argon in order to maintain temperature stability.

It was possible to correlate the high-temperature reduction data in terms of a simple rate model similar to that used for porous pellets at low temperatures. The X-ray data have shown that either MnO or MnO_2, or both of

these oxides, formed the major phase or phases present in a partially reduced specimen. Although the Mn_2O_3 and Mn_3O_4 phases were always found, they were present in relatively minor quantities. On this basis one may postulate that the reduction proceeds topochemically through successive stages of $MnO_2 \rightarrow Mn_2O_3 \rightarrow Mn_3O_4 \rightarrow MnO$, with the intermediate oxides forming relatively small, but dense, layers between unreacted dioxide and reduced porous monoxide. If the thickness of the Mn_2O_3 and Mn_3O_4 layers can be neglected, the modified core model depicted in Figure 13 can be applied. Here, a porous granule is first imagined to consist of an agglomeration of many dense cubes, each of edge x_o. Under conditions where boundary-layer transport and pore-diffusion resistances (as well as temperature gradients) are negligible, it is sufficient to consider the reduction of a single hypothetical dense cube. A partially reduced cube is, in turn, pictured as a dense MnO_2 core surrounded by a porous layer of the monoxide phase; the intermediate layers of Mn_2O_3 and Mn_3O_4 are neglected. According to this model, the gas-solid reduction occurs only at the Mn_3O_4/MnO boundary, the other reductions proceeding by solid-state processes. This implies that the Mn_3O_4 phase becomes protective, that is, it forms as a dense, nonporous layer. Since the volumes of oxide per gram of manganese (based on room-temperature densities) are 0.315, 0.319, 0.287 and 0.238 $cm.^3$ for

MnO_2, Mn_2O_3, Mn_3O_4, and MnO, respectively, one would at first not expect Mn_3O_4 to be able to form as a dense reduction-product layer on Mn_2O_3. However, Frank and van Der Merwe[8, 9] have presented theoretical arguments which show that a dense, nonporous layer of one phase may form on a second phase if the extent of misfit in specific volume is less than about 14%.

The X-ray data have shown that the very high initial reduction rate is associated with the build-up of Mn_2O_3 and Mn_3O_4. This, together with the subsequent sharp decline in rate, also points toward the formation of a dense nonporous protective layer of Mn_3O_4.

If the fractional conversion based on MnO as a final product is designated Z'', and if the chemical reaction step is assumed to control, it has been shown that the proposed model predicts

$$\frac{2\,t r_s''}{\rho_{MnO_2} x_o} = 1 - (1 - Z'')^{1/3} = \frac{x_o - x}{x_o} \qquad (21)$$

where t is the time of reaction; r_s'', the rate of reaction in moles of MnO_2 per unit area; and ρ_{MnO_2}, the molar density of MnO_2. The quantity k'',

$$k'' = \frac{2}{\rho_{MnO_2} x_o} (r_s'') \qquad (22)$$

may be designated an apparent rate constant. Because r_s'' is a function of pressure and temperature, the apparent

rate constant will likewise be temperature- and pressure-dependent.

A test of this model may be made by examining the linearity of a plot of $1 - (1 - Z'')^{1/3}$ versus the time of reaction. Illustrative data for several temperatures are plotted in this manner in Figure 20. These particular runs were carried out in pure hydrogen, but similar results were obtained for reductions conducted in various hydrogen-helium mixtures. As expected, the model does not apply during the initial high rate period of reduction; for this reason, the straight lines do not intersect at the origin. Nevertheless, the model does fit the experimental data very nicely in the range of 30 to 95% conversion. In some runs (for example, runs 75, 84, and 87) where the temperature stabilized more quickly and where data points at lower conversions were taken, the model was valid at conversions as low as 15 to 20%. Because of the success of this simple model, the reduction rate at a given temperature and hydrogen pressure may be represented by a single apparent rate constant, k''. Values of k'' may, of course, be obtained by simply evaluating the slopes of the $1 - (1 - Z'')^{1/3}$ versus time plots. This greatly facilitates the comparison and correlation of the rate data.

The pure hydrogen, 375°C data previously discussed (Figure 19), in which numerous experimental parameters were

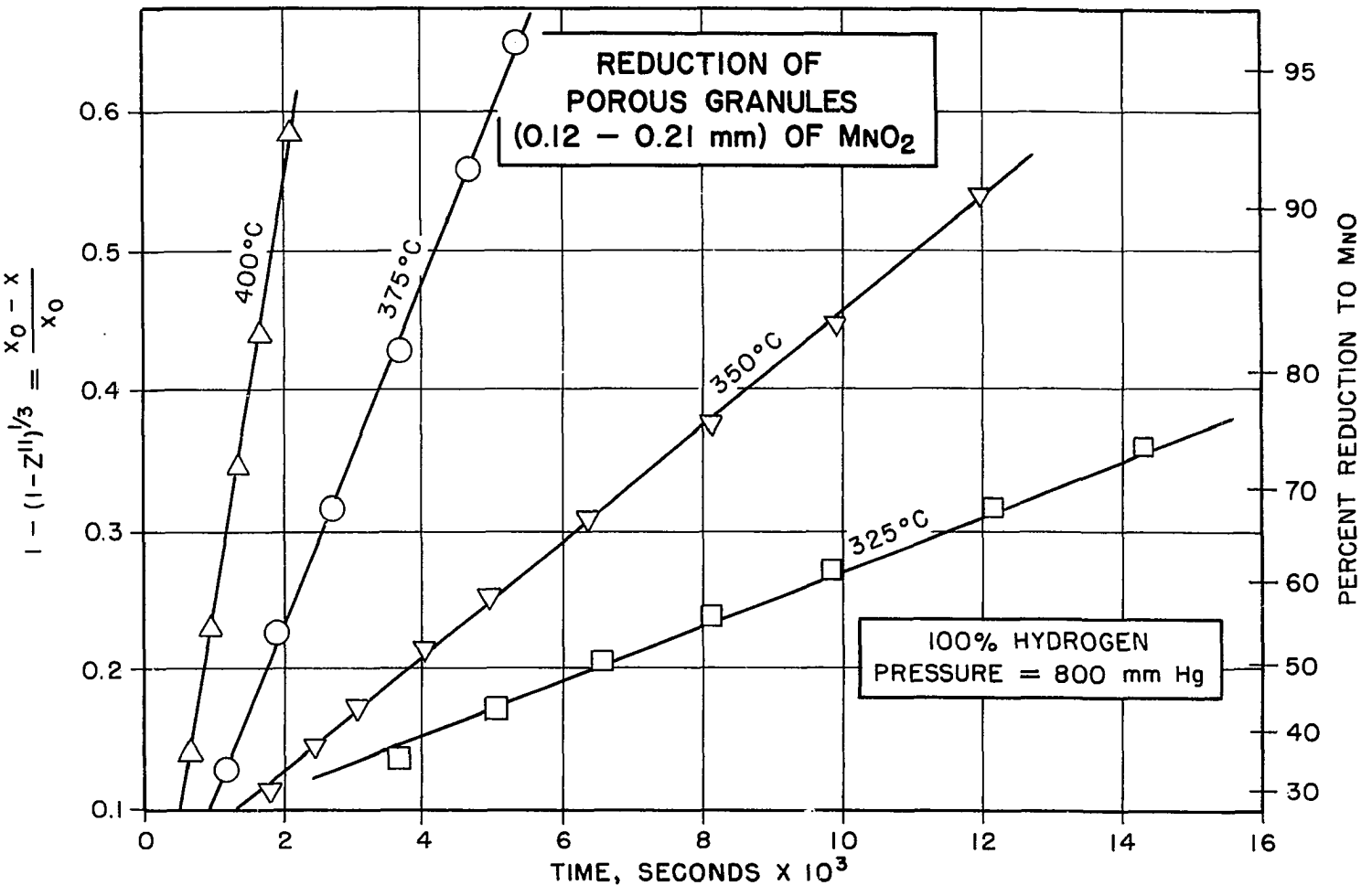

FIG. 20 HIGH TEMPERATURE MODEL PLOTS FOR PARTICLES

varied, can be analyzed in terms of the apparent rate constants. For this comparison values of k'' were calculated for the nine runs by linear least-squares analysis, using the data in the range of 30 to 95% conversion. The 95% confidence limits for these rate constants were approximately plus or minus three percent of the magnitude of the rate constants themselves. That the apparent rate constants for these runs were a function of bed depth alone (and not flow rate, particle size, etc.) is evident from Figure 21. As suggested earlier, the decrease in rate as the bed depth is increased is presumably due to the retarding effect of water vapor. In any event, Figure 21 shows that the observed rate at a bed depth of one mm. is within approximately five percent of the rate extrapolated to zero bed depth. At lower temperatures or lower hydrogen concentrations the rates would be less and the differences between one mm. and zero bed depths would probably also be less. Consequently, observed rates for reductions at other conditions where bed depths were generally kept at approximately one mm. should be within five percent of the true reduction rates.

Several runs in which the bed depth, flow rate and particle size varied were also conducted at 425°C in a 9.73% hydrogen (balance, helium) mixture. The rate constants for these runs are given in Table 4. These data

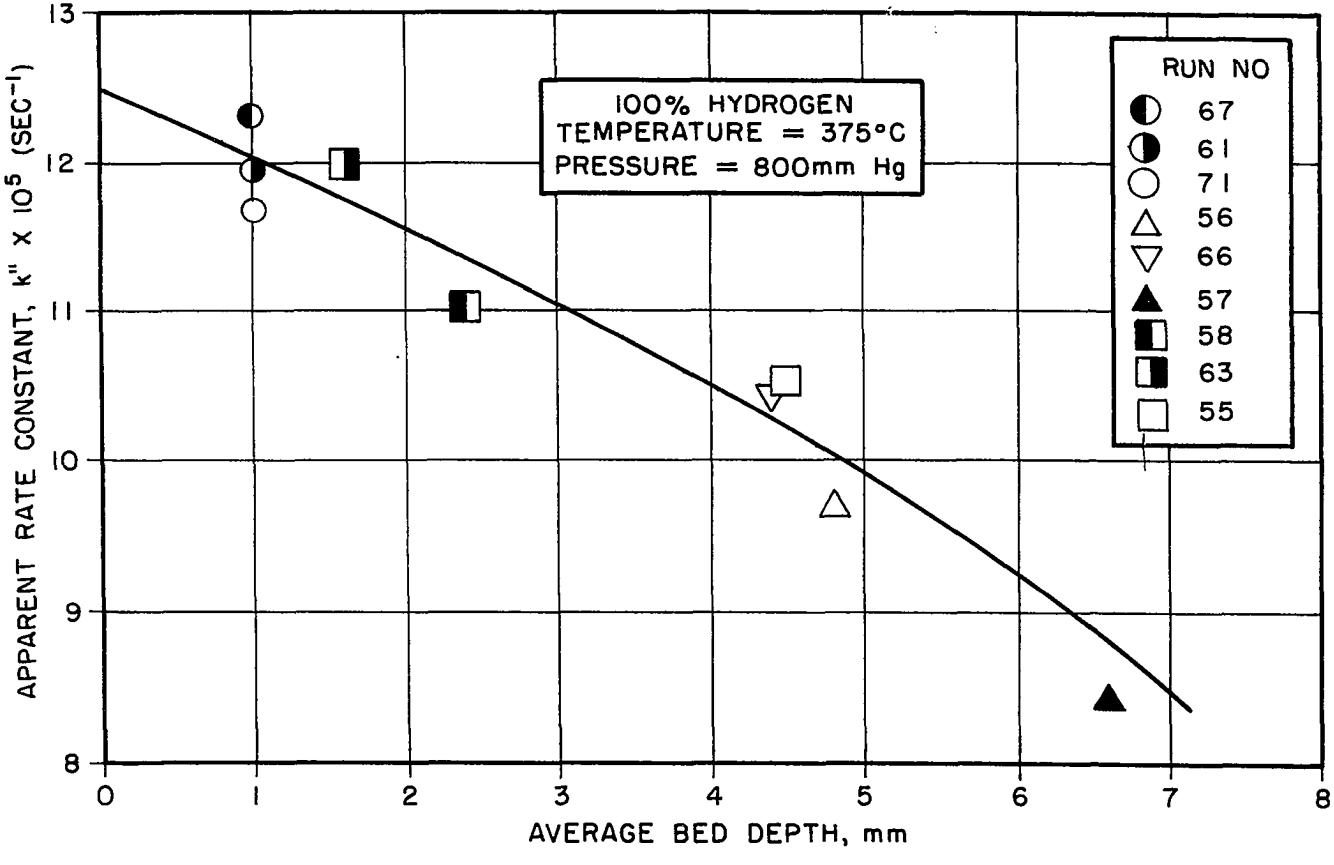

FIG. 21 EFFECT OF BED DEPTH

TABLE 4

REDUCTION RATES AT 425°C
IN 9.73% H_2 - 90.27% He MIXTURE

Run No.	Particle Size (mm.)	Flow Rate (cu. ft./ hr.)	Estimated Bed Depth (mm.)	Apparent Rate Constant $k'' \times 10^5$ ($sec.^{-1}$)
79	0.15-0.21	5.5	1.0	11.3 ± 0.6*
80	0.15-0.21	8.0	1.0	11.4 ± 0.4*
77	0.10-0.12	10.5	2.3	10.6 ± 0.6
81	0.10-0.12	8.0	1.0	11.6 ± 0.6

* 95% Confidence Limits of k''

show once again that the only significant variable is bed depth.

The variation of the apparent rate constant with temperature is shown in Figure 22. It will be observed that the slope of the Arrhenius plot does not vary appreciably with hydrogen partial pressure; the apparent activation energies are in the range of 26 to 29 kcal./mole. This strong temperature dependency is consistent with the basic hypothesis that the reduction process is limited by chemical reaction, and not by any diffusion step.

The excellent fit of the model to the kinetic data, together with an entirely reasonable temperature coefficient for the apparent rate constant, does not insure the absence of significant gas diffusion resistance through the MnO product layer. This is because the model (and the straight-line model plots in Figure 20) is not very sensitive to a moderate diffusion resistance through the product layer. (The initial reduction period, corresponding to the formation of Mn_2O_3 and Mn_3O_4, obviously does involve the build-up of protective layers of Mn_2O_3 and Mn_3O_4, and during this stage diffusion through the intermediate oxides does play a most important role. However, the present concern is directed toward the reduction process <u>after</u> the initial build-up of the intermediate oxides

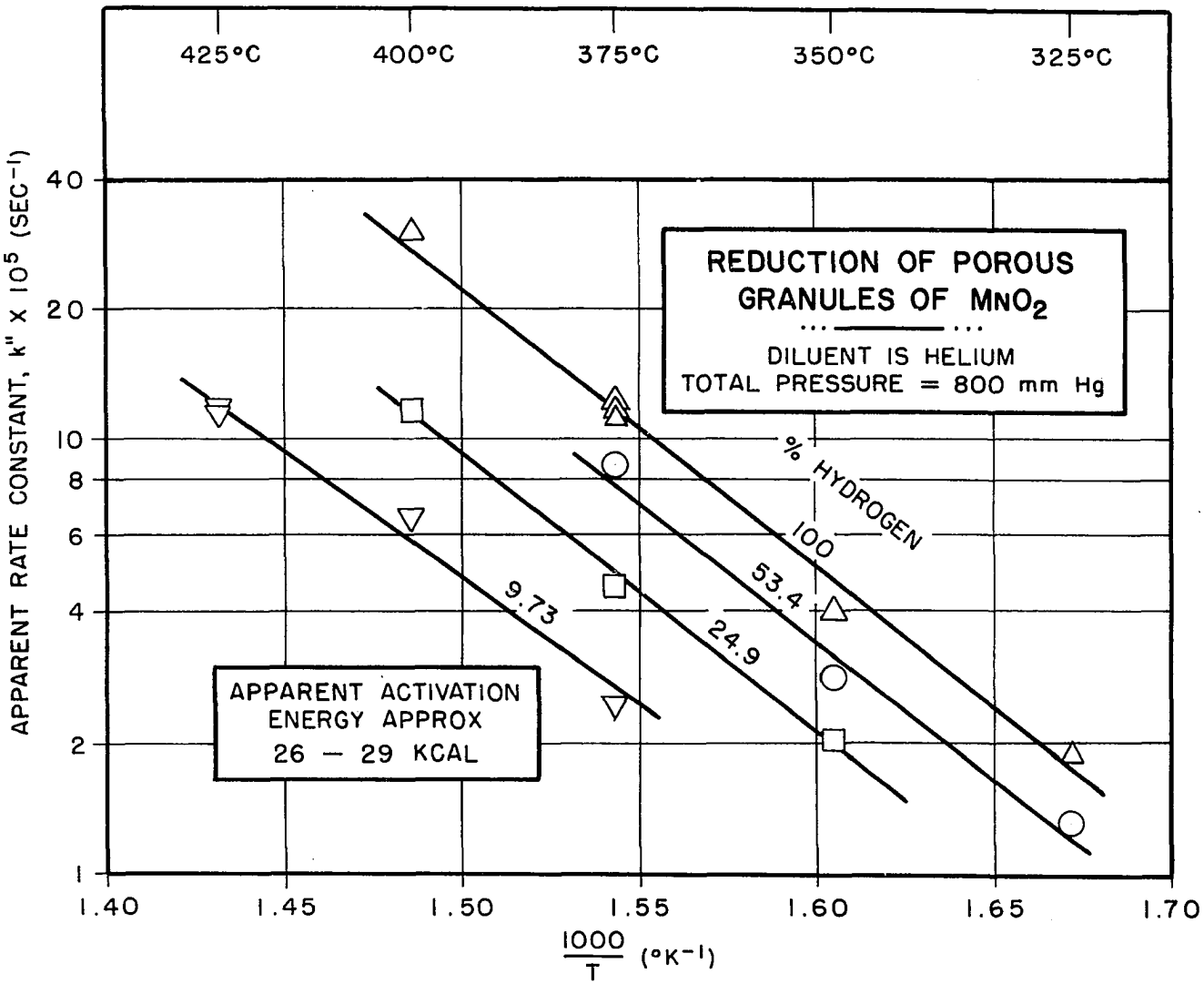

FIG. 22 HIGH TEMPERATURE ARRHENIUS PLOT FOR PARTICLES

is complete.) Consequently, it is best to analyze the data in another manner as well. If diffusion resistance through the MnO layer were significant, its importance would increase as more MnO is formed. Hence, the apparent activation energy for rates at a high level of conversion would be appreciably less than at a lower level. In Figure 23 the reduction rates in pure hydrogen at 45 and 85% conversions (obtained by graphically differentiating the conversion-time curves) are plotted against reciprocal temperature. Inasmuch as the two activation energies are practically identical, it is unlikely that the MnO layer provided appreciable resistance to the diffusion of hydrogen and water vapor. It is concluded, therefore, that the simple reduction model is in all aspects reasonable and consistent with the experimental data.

The apparent rate constant, k'', was correlated by the following equation:

$$k'' = \frac{aP_{H_2}}{1 + bP_{H_2}} \qquad (23)$$

The coefficients were evaluated by first calculating the least-squares values of $\underline{a}$ and $\underline{b}$ at a given temperature in the equation

$$k''/P_{H_2} = a - bk'' \qquad (24)$$

Equation (24) is merely a rearrangement of equation (23). Secondly, the constants $\underline{a}$ and $\underline{b}$ were fitted to Arrhenius

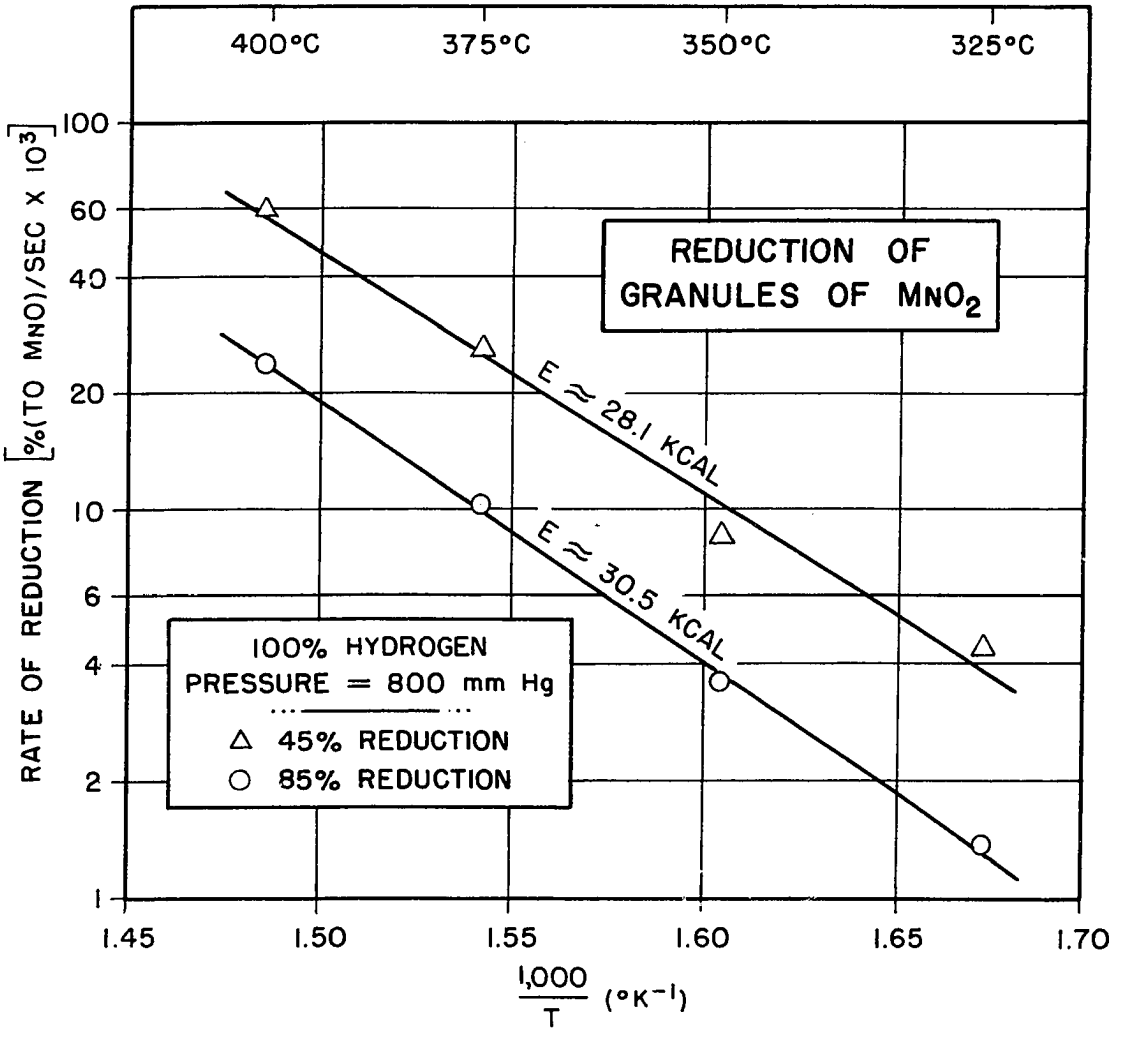

FIG. 23 HIGH TEMPERATURE ARRHENIUS PLOTS AT CONSTANT CONVERSION

temperature dependencies, again using the least-squares technique. The results are:

$$a = 8.81X10^{3} \exp(-30,700/RT) \quad (mm.\ Hg^{-1})(sec.^{-1}) \qquad (25)$$

$$b = 1.015X10^{-2} \exp(-2,300/RT) \quad (mm.\ Hg^{-1}) \qquad (26)$$

The apparent rate constants are plotted in Figure 24; the curves shown were generated from equation (23), using $\underline{a}$ and $\underline{b}$ defined by equations (25) and (26). Because the 425°C data covered only a single hydrogen partial pressure, the points at this temperature were not included in evaluating the coefficients. The 425°C curve therefore represents an extrapolation of the rate expression. Equation (23) correlated the data from 325° to 400°C with an average deviation of 7.0%. The temperature variations of the coefficients $\underline{a}$ and $\underline{b}$ are depicted graphically in Figure 25.

It will be recalled that

$$k'' = \frac{2}{\rho_{MnO_2} x_o} (r_s'')$$

where r_s'' is the rate of reaction of MnO_2 (g.-moles MnO_2 reduced per unit area of unreacted oxide per second). If it is assumed that the solid-gas reaction at the interface follows the Langmuir-Hinshelwood model in which adsorption of hydrogen and water is postulated to occur without dissociation and on only one kind of site, and if the surface reaction is assumed to be rate-controlling, it can

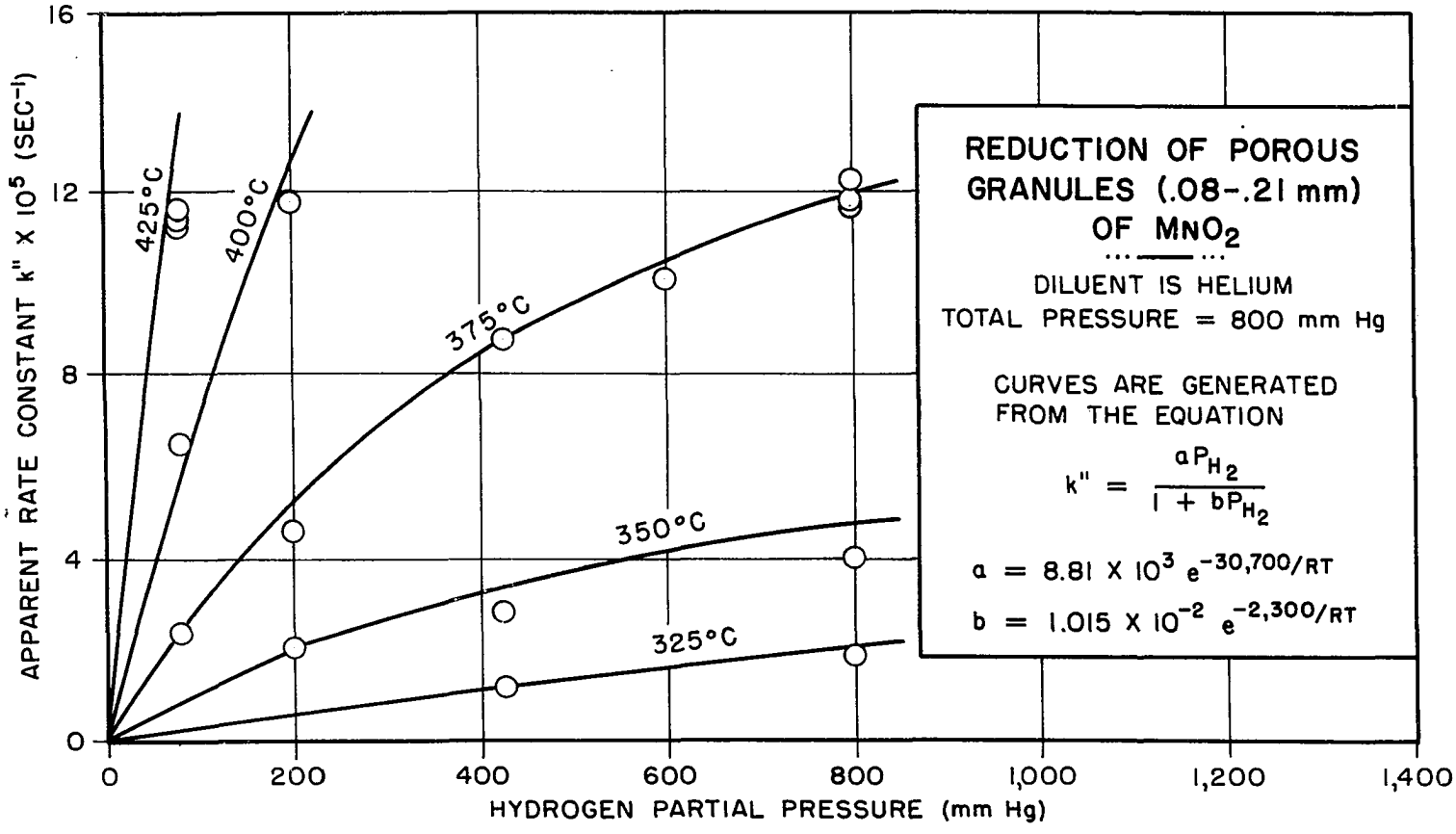

FIG. 24 EFFECT OF H_2 PARTIAL PRESSURE IN THE RANGE 325° – 425°C

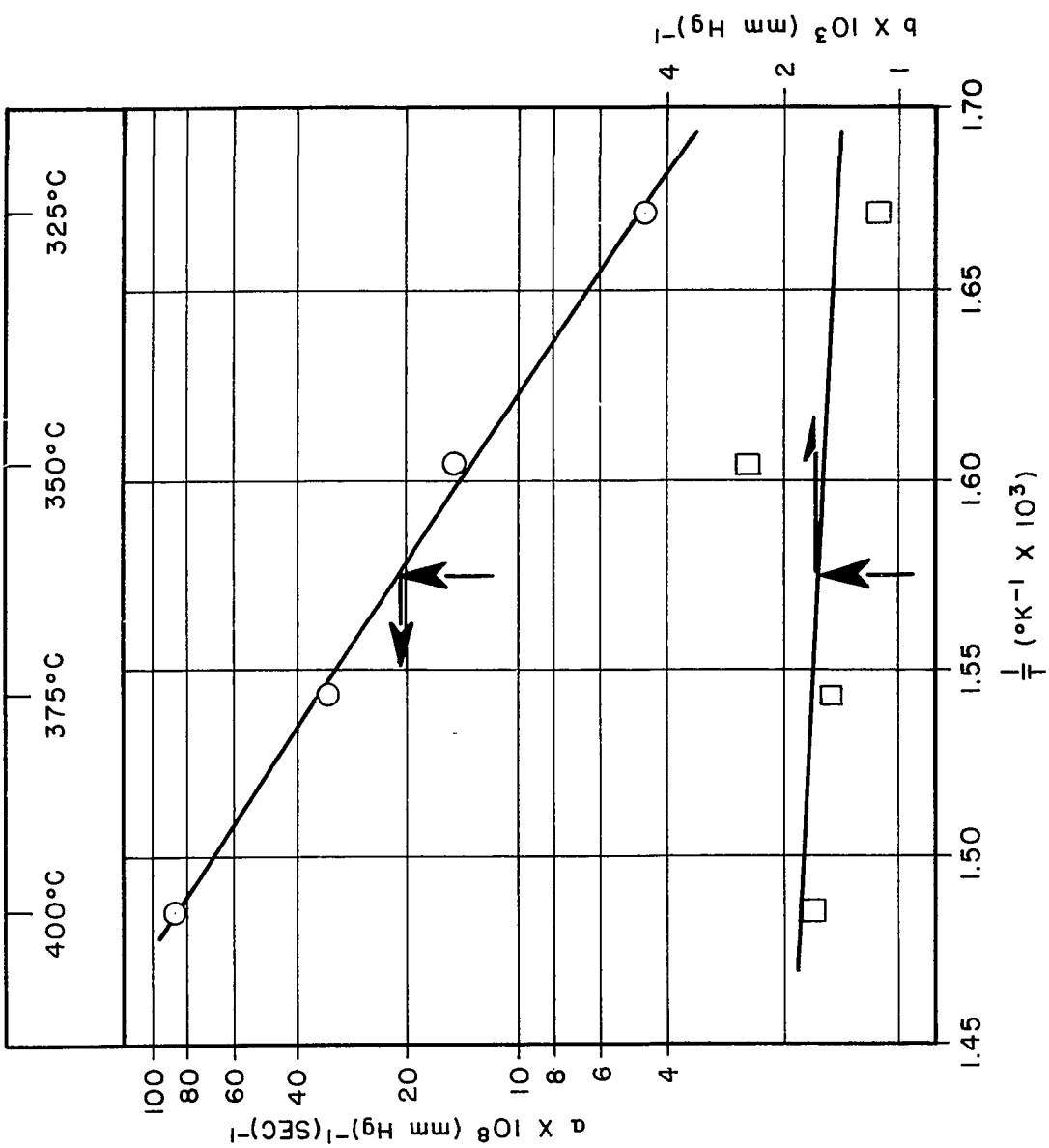

FIG. 25 ARRHENIUS PLOTS FOR PARAMETERS IN RATE EXPRESSION

be shown that

$$r_s'' = \frac{g P_{H_2}}{1 + K_{H_2} P_{H_2} + K_{H_2O} P_{H_2O}} \qquad (27)$$

where

$$g = k_s'' C_t K_{H_2} \qquad (28)$$

and k_s'' is the reaction rate constant for the surface reaction, C_t is the concentration of total active sites per unit of reaction surface, and K_{H_2} and K_{H_2O} are adsorption equilibrium constants. At low water vapor concentrations, the rate expression reduces to

$$r_s'' = \frac{g P_{H_2}}{1 + K_{H_2} P_{H_2}} \qquad (29)$$

Hence, the empirical rate expression, equation (23), may be interpreted in terms of a Langmuir-Hinshelwood model for the interfacial solid-gas reaction.

If the Langmuir-Hinshelwood model is realistic, the coefficients in equation (23) should exhibit temperature dependencies consistent with the model. Thus, the a coefficient should have a positive activation energy with a magnitude characteristic of a chemical reaction, and the b coefficient, being an adsorption equilibrium constant, should have a negative activation energy. The activation energies of the a and b coefficients, together with the 95% confidence limits, were determined to be, respectively, $+30.7 \pm 5.7$ kcal./mole and $+2.3 \pm 2.4$ kcal./mole. (In

calculating these values by the least-squares method, equal weight was assigned to the a and b coefficients at each temperature, regardless of the number of experiments on which the coefficients were based.) The activation energy of a is thus entirely consistent with the postulated Langmuir-Hinshelwood model. It is difficult to state reliably, however, whether the activation energy of the b coefficient is really positive or negative. If negative, the small magnitude of the activation energy suggests that the adsorption is physical, rather than chemical. Alternatively, if the activation energy is positive, the correlating rate expression, equation (23), should be considered strictly empirical.

The effect of water vapor on the rate of reduction was examined at 375°C. Several runs were conducted with hydrogen containing nominal one and ten percent water vapor concentrations. The results have been summarized in Table 5. A control experiment was first carried out using water-free hydrogen for a period of 900 seconds (together with appreciable argon content during the first 700 seconds to stabilize the temperature). At the conclusion of this time interval the reaction tube was purged with argon. The conversion was determined to be 28.9% by water recovery and 29.4% by weight loss. This experiment thus shows that the hot reduction product at

TABLE 5

EFFECT OF WATER VAPOR ON REDUCTION AT 375°C

Total Pressure = 800 mm. Hg

% Water Vapor in Hydrogen	% Reduction After 900 Seconds Reaction Time (by weight loss)	% Reduction After 6200 Seconds Reaction Time (by weight loss)
0	29.4 (Run 91)*	94.0 (Run 95)**
1.1	-	77.1 (Run 94)
9.9	26.2 (Run 92)	52.2 (Run 93)

* 28.9% by water recovery

** 97.9% by water recovery

Note: Partially reduced specimens in runs 93, 94 and 95 were cooled to room temperature in an argon atmosphere prior to removal from furnace.

a conversion of about 30% (375°C) is stable upon exposure to air. The experiment was then repeated with the exception that the hydrogen (diluted with argon during the first 700 seconds, as in the control experiment) contained 9.9% water vapor. The conversion for this run (after 900 seconds) was 26.2%, based on weight loss. (Because of the large amount of water in the feed stream, conversion could not be determined by water recovery with any degree of precision.) Consequently, the water vapor did not appreciably hinder the start of the reduction process, nor did it have much effect on the very rapid initial reduction rate.

The influence of water vapor at higher levels of conversion, i.e., beyond the high initial rate period, was also investigated. In a second water-free control experiment (run 95) at 375°C the conversion after 6200 seconds was found to be 97.9% by water recovery. The reduction product was cooled to room temperature in argon before it was removed from the furnace in order to minimize reoxidation. Immediately thereafter, the weight of the product was determined, and the conversion based on weight loss was determined to be 94.0%. Apparently, the reduced specimen still picked up some oxygen upon atmospheric exposure; however, the 94.0 and 97.9% reduction figures were considered to be in close enough agreement to permit the conversion to

be estimated by weight loss alone. Therefore, two additional runs (numbers 93 and 94) were conducted using hydrogen streams with nominal one and ten percent water vapor concentrations. Except for the water content, these runs were carried out under conditions identical to the dry hydrogen control run, all products being cooled to room temperature in argon. Table 5 shows that the conversion decreased from the 94.0% dry hydrogen figure to 77.1% for the 1.1% water run and to 52.2% for the 9.9% water run. In terms of the apparent rate constant, these data indicate that (at 375°C, total pressure of 800 mm. Hg) one percent moisture in the hydrogen stream will decrease the reduction rate approximately 45%, while ten percent moisture will decrease the rate approximately 75%. Inasmuch as these figures are based on only one conversion at each of two water vapor levels, they should be interpreted as somewhat crude estimates. Nevertheless, these data clearly show that water vapor severely retards the reduction rate at conversions above approximately 30%.

The large retarding effect of water vapor is probably the main cause for the variation of the observed rate with bed depth (Figure 21). As the bed depth is increased, the average water vapor concentration in the bed would also increase, thus causing the rate to decrease.

The strong inhibiting effect of water vapor is consistent with the premise that the reduction process is controlled by the chemical reaction step. The large retardation caused by relatively small percentages of water vapor is apparently due to adsorption of water on active reaction sites at the solid-gas reaction interface.

It was desirable to determine whether the kinetic data could be reasonably well extrapolated to higher temperatures which would be more applicable to industrial practice and where reduction times on the order of one or two minutes would be encountered. Since the vertical-tube furnace was constructed of Pyrex, the runs above 425°C were conducted in the horizontal-tube furnace using a Vycor combustion tube. In order to maintain temperature control during the initial high reduction rate period, the samples were prereduced to approximately 12% reduction at 325°C. The furnace was then purged with argon while the temperature was raised to the desired level. Hydrogen flow was again initiated after the furnace had leveled out at the proper temperature. In these runs no attempt was made to determine the relative importance of noniso-thermal effects or diffusional resistances. Several conversion-time curves were simply generated, and from these data the reaction times required to achieve 95% reduction to MnO were estimated. Because of the rapid

reduction rates, as few as three points were obtained to define a conversion-time curve. Since the samples were prereduced at a lower temperature, the conversion curves at the temperature of interest had to be extrapolated to zero conversion; furthermore, some allowance had to be made for the time required to purge the reactor of argon. As a result, the reaction times deduced from these data are crude compared to the lower temperature data generated on the vertical-tube furnace; however, they are estimated to be correct within 20%. The reaction times are plotted on Figure 26. It will be observed that the vertical-tube furnace data fall on a straight line, as would be predicted from equations (21) and (22), as long as k'' follows an Arrhenius relationship. Extrapolation of the lower-temperature data indicates that the reduction time at 500°C should be somewhat less than a minute and a half. The horizontal-tube data, on the other hand, show that the reduction time at this temperature is in excess of three minutes. The discrepancy is probably due to severe diffusional and water retardation resistances in the horizontal-tube furnace; in this arrangement the oxide is clearly restricted from free access to hydrogen. As the temperature is decreased, the data from the two furnaces appear to merge, as would be expected.

It is concluded that, for engineering purposes, extrapolation of the lower temperature data to temperatures

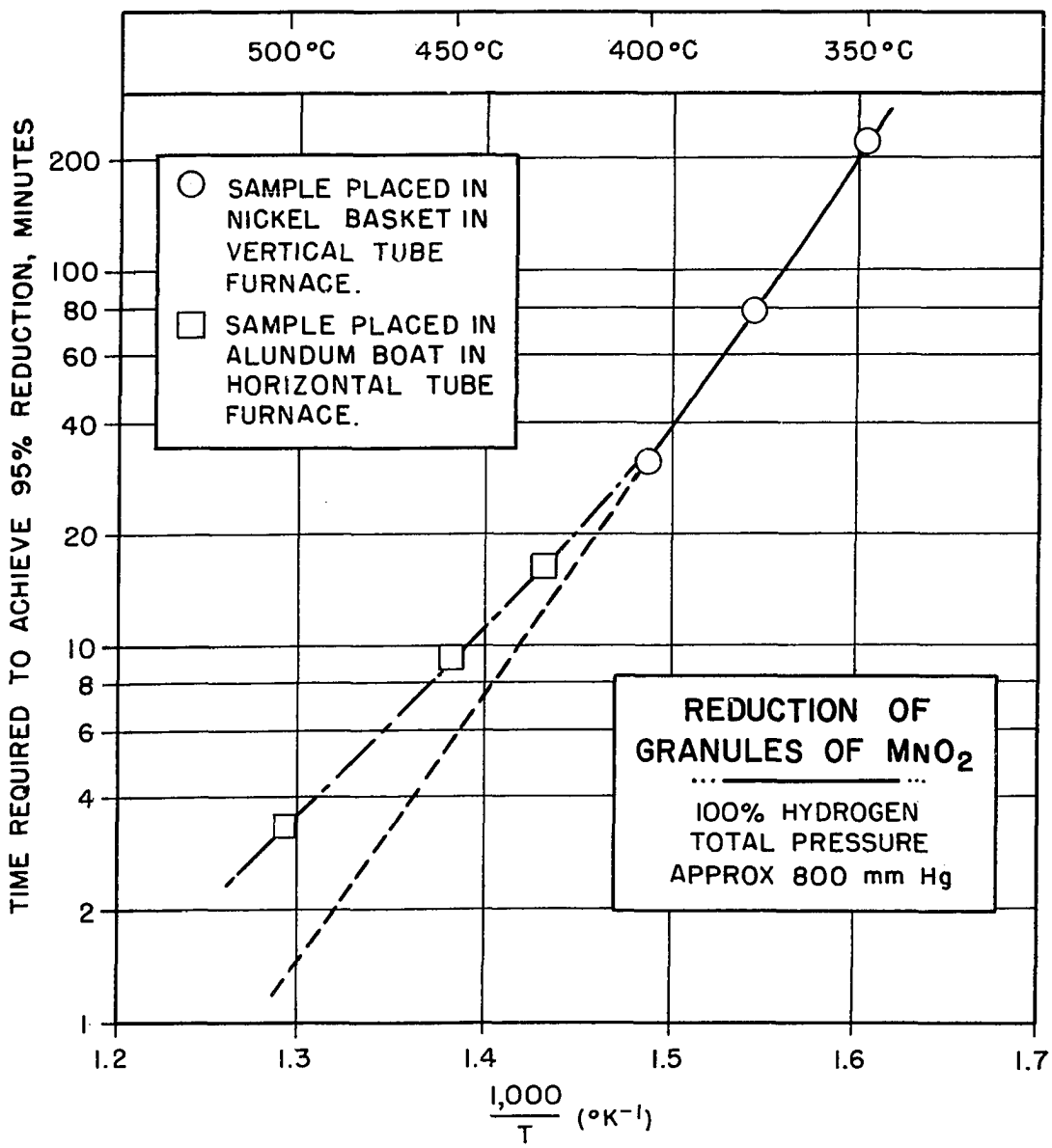

FIG. 26 REDUCTION TIME — TEMPERATURE RELATIONSHIP

as high as 500°C does not seem unreasonable as long as other resistance limitations are taken into account. That is to say, it is unlikely that the intrinsic kinetics undergo a major transition between 400° and 500°C (as does occur in the 250° - 325°C range).

In a reduction experiment conducted at an apparent temperature of 600°C (with no prereduction at lower temperature), the sample decomposed almost completely to stoichiometric Mn_2O_3 during the short period required to charge the reactor and stabilize the temperature. The MnO reduction product formed at this temperature was stable in air and retained its characteristic green appearance. Likewise, a sample reduced at 700°C was found to be stable. This is in contrast to the products formed at temperatures of 500°C and lower, where some re-oxidation of the MnO was always experienced. For example, at a reaction temperature of 425°C, the green MnO product turned a very distinct brown-black color after the reaction tube was opened, and the final conversion, based on weight loss, was only 93%. It appears, then, that a reduction temperature on the order of at least 600°C is required to produce an MnO product which is stable in air.

Reduction of a Pyrolusite Ore

Several runs were conducted with samples of the Belgian Congo pyrolusite ore. Flow rates of 5.0 standard

cubic feet per hour and particles in the size range of 0.09 to 0.21 mm. were used. The conversion-time data have been plotted in Figure 27. Although the effects of flow rate, particle size, etc., were not investigated, a comparison of the ore reduction data with those in Figure 19 indicates that nonisothermal and gas diffusional effects were probably negligible.

The ore samples reacted considerably faster than did the synthetic pyrolusite specimens at all conditions investigated. For example, at 275°C, the ore was reduced to approximately 42% completion in 15 minutes in pure hydrogen, while the synthetic pyrolusite reduced to only 10% completion during the same period.

It was difficult to maintain temperature stability above 275°C (even when the initial hydrogen stream was diluted with argon). For this reason the 325°C run was prereduced to 50% conversion at 275°C.

In one run, a single 8.5-gram lump of the ore was reduced, first to 2.8% conversion at 225°C, and then to 9.3% conversion at 250°C; finally, the reaction was continued at 300°C. Argon was passed through the reaction tube while the temperature was raised from one level to another.

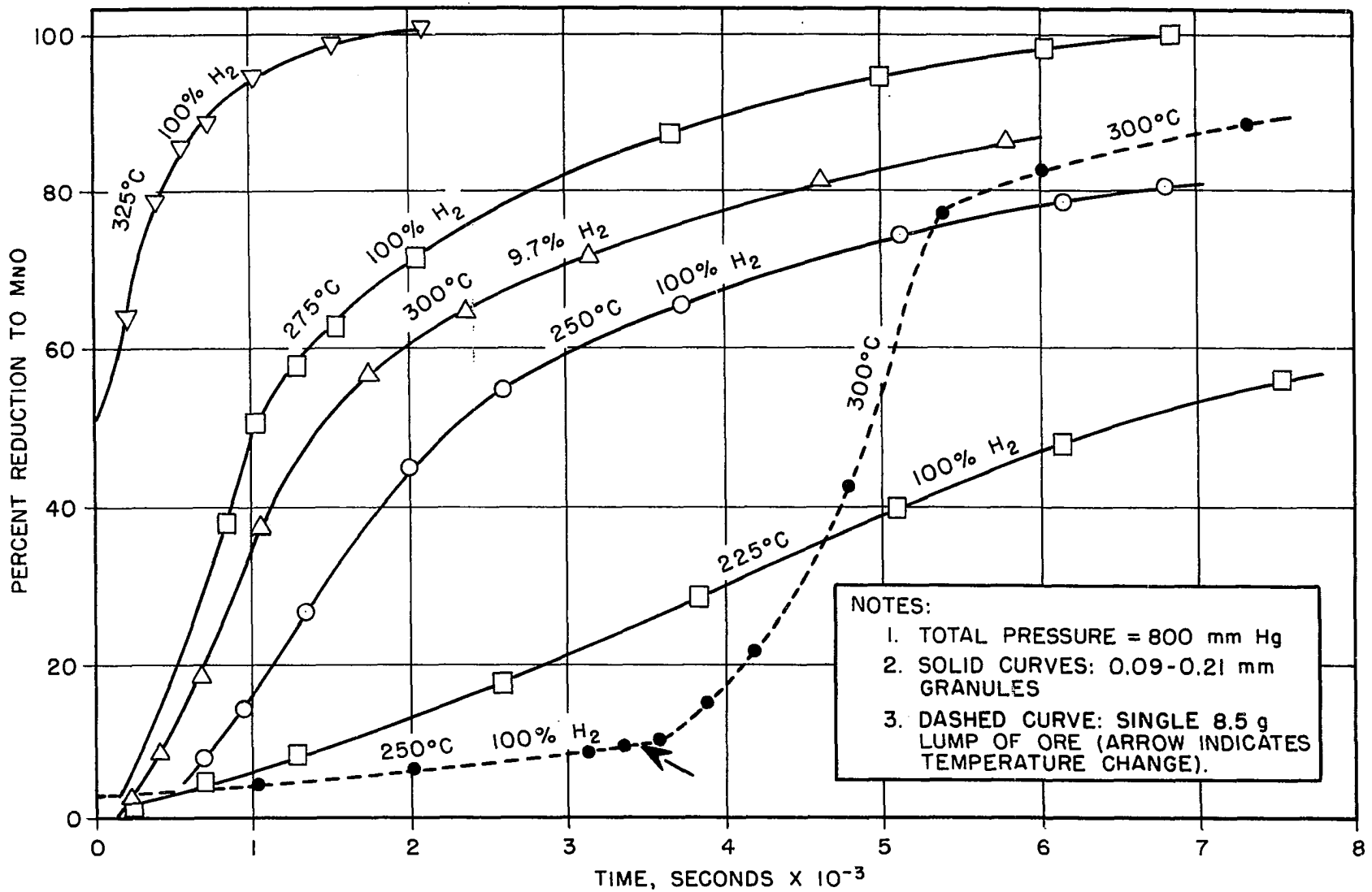

FIG. 27 REDUCTION OF A BELGIAN CONGO PYROLUSITE ORE

The ore data qualitatively exhibited reduction characteristics similar to those of the synthetic MnO_2. It will be observed from Figure 27 that the reaction rate was relatively high in the 0 to 40% reduction range. Thereafter, a rather sharp decline in the rate was experienced. Similar curves were obtained for the synthetic samples (Figure 8).

Data on the synthetic pyrolusite have indicated that the transition from low- to high-temperature regime, and the intersection of reduction curves in Figure 8, are caused by the intermediate Mn_3O_4 oxide becoming progressively more protective as the temperature is raised. Because of the much higher reduction rate of the ore and the resulting temperature instability during the initial reduction period, it was not possible to generate ore data in the region where such a transition would be expected to be most evident (low conversion range above 275°C). Nevertheless, the ore reduction data which were obtained do suggest that diffusional resistances in the oxide become significant as the reduction proceeds. This is evident from the Arrhenius plots in Figure 28, where the reduction rates at constant levels of conversion have been plotted. It is seen that the apparent activation energies decrease from 28.1 to 21.2 to 17.5 kcal./mole at conversions of, respectively, 10, 40, and 60%. A progressive decrease in activation energy would be

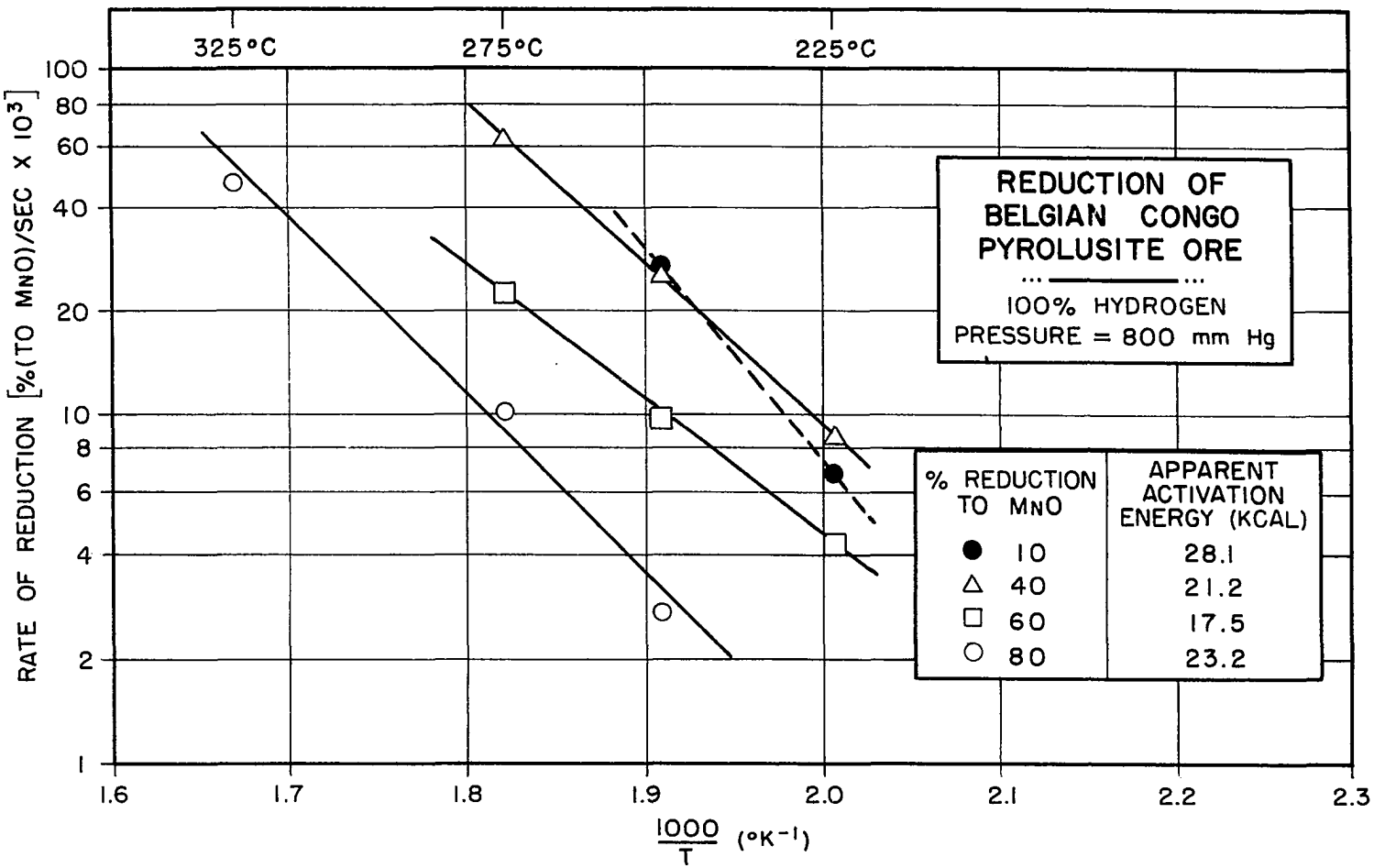

FIG. 28 ARRHENIUS PLOTS FOR REDUCTION OF ORE

anticipated if a product layer contributes significant resistance to the counterdiffusion of H_2 and H_2O to and from the reaction interface. At 80% conversion, where presumably the primary solid-gas reaction involves the reduction of Mn_3O_4 to MnO, the activation energy is once again higher, namely 23.2 kcal./mole.

The low and high conversion activation energies for the ore compare reasonably well with the activation energies calculated for the synthetic samples (approximately 22 to 30 kcal./mole) over somewhat different temperature ranges.

The reason for the faster rate of reduction of the ore specimens compared to the synthetic samples was not unequivocally established. Impurities in the ore undoubtedly play some role; it is also likely that the ore was considerably more porous and consequently contained more surface area available for reaction.

CHAPTER VI

CONCLUSIONS

The following conclusions may be drawn from the results and discussion in Chapter V.

1. The reduction of synthetic pyrolusite with hydrogen proceeded through the sequence $MnO_2 \rightarrow Mn_2O_3 \rightarrow Mn_3O_4 \rightarrow MnO$. Below 250°C the partially reduced products consisted primarily of a mixture of MnO_2 and Mn_3O_4, with some Mn_2O_3. In this region MnO was not detected, and the reaction practically terminated with the formation of Mn_3O_4. Above 250°C the Mn_3O_4 became progressively more protective and the reduction of Mn_3O_4 to MnO became appreciable. Above approximately 300°C all four oxides were detected in the partially reduced products, although the MnO_2 and MnO phases were usually the major components. The kinetic data were conveniently separated into two temperature regimes.

2. Low-Temperature Regime. The reduction of single porous pellets and small beds of porous particles was investigated. Quantitative kinetic data were obtained under conditions which minimized boundary-layer and pore-diffusion resistances. Conclusions specific to this regime follow.

(a) The reaction practically subsided with the formation of Mn_3O_4; a reduction product stable in air and consisting of approximately 90% Mn_3O_4 could be formed

at 250°C.

(b) The apparent activation energy at a hydrogen pressure of 800 mm. Hg for the pellets and particles was, respectively, 26.8 and 22.2 kcal./mole in the range of 200° to 240°C.

(c) The reduction rate increased nonlinearly with hydrogen partial pressure at 226°C.

(d) The reduction rate at 226°C was sharply retarded by the addition of water vapor to the hydrogen stream.

(e) The experimental data for the pellets were correlated with a core reaction model, in which the reduction process was considered to approximate the system MnO_2(core)-Mn_3O_4(product layer), with an intermediate layer of Mn_2O_3 of negligible thickness. The solid-gas reaction was postulated to occur only at the Mn_2O_3/Mn_3O_4 interface, and the $MnO_2 \rightarrow Mn_2O_3$ reaction was assumed to proceed by a solid-state diffusion process. The solid-gas reaction at the Mn_2O_3/Mn_3O_4 interface was taken as the rate-controlling step. Conclusions (a) through (d) are consistent with this model and with the concept that the solid-gas reaction involves adsorption of H_2, surface reaction, and desorption of H_2O, with the surface reaction being the slowest step.

3. High-Temperature Regime. The reduction of small beds of particles was investigated. Quantitative rate data were obtained under conditions where boundary-layer and

pore-diffusion resistances were minimized. Conclusions specific to this regime follow.

(a) Above approximately 300°C, the reduction was characterized by a very high initial rate; this was attributed to a rapid build-up of layers of Mn_2O_3 and Mn_3O_4. The Mn_3O_4 became protective and was itself further reduced to MnO in this temperature regime.

(b) The apparent activation energy at conversions above 20% and in the temperature range of 325° to 425°C was approximately 26 to 30 kcal./mole. This agrees well with the 24 kcal./mole activation energy reported by Chufarov[34] at hydrogen pressures generally lower than those investigated in this work.

(c) The reduction rates at conversions above 20% increased nonlinearly with hydrogen partial pressure in the range of 325° to 425°C.

(d) The reduction rate at 375°C (after the initial build-up of Mn_2O_3 and Mn_3O_4) was sharply retarded by the addition of water vapor to the hydrogen stream.

(e) The experimental data above 20% conversion were correlated with a core reaction model, in which the reduction process was considered to approximate the system MnO_2(core)-MnO(product layer), with intermediate layers of Mn_2O_3 and Mn_3O_4 of negligible thickness. The solid-gas reaction was postulated to occur only at the Mn_3O_4/MnO interface, and the $Mn_2O_3 \rightarrow Mn_3O_4$ and

$MnO_2 \rightarrow Mn_2O_3$ reactions were assumed to proceed by solid-state diffusional processes. The solid-gas reaction at the Mn_3O_4/MnO interface was taken as the rate-controlling step. Conclusions (a) through (d) are consistent with this model and with the concept that the solid-gas reaction involves adsorption of H_2, surface reaction, and desorption of H_2O, with the surface rearrangement being the slowest step.

4. Reduction data on a Belgian Congo pyrolusite ore showed characteristics similar to the synthetic pyrolusite reduction data. The apparent activation energies at a hydrogen pressure of 800 mm. Hg varied from approximately 18 to 28 kcal./mole, depending on the extent of conversion.

CHAPTER VII

RECOMMENDATIONS

At temperatures above 500°C pyrolusite rapidly decomposes to form Mn_2O_3, and as a result, MnO_2 is virtually eliminated as the stable starting oxide for the reduction process. In view of this it would be of considerable interest to initiate experimental studies in two related areas:

(1). The kinetics of decomposition of pyrolusite.

(2). The high-temperature reduction kinetics of Mn_2O_3.

NOMENCLATURE

A	apparent frequency factor
a, b	coefficients defined by equations (25) and (26)
C_t	concentration of active sites per unit area
E_a	apparent activation energy
g	coefficient defined by equation (28)
K_i	adsorption equilibrium constant of component i
K	chemical reaction equilibrium constant
k	apparent reaction rate constant
k_s	reaction rate constant for surface reaction
N_i	moles of solid i
P_i	partial pressure of component i
R	gas constant
r_s	rate of reaction of solid per unit area of reaction surface
T	temperature
t	time
x_o	original edge length of cube in reaction model
x	cube edge length of unreacted core in reaction model
Z	fractional conversion of solid reactant
θ	reaction time for complete conversion (chemical reaction controlling process)
θ_1	reaction time for complete conversion (boundary-layer transport controlling process)
θ_2	reaction time for complete conversion (ash-diffusion controlling process)
ρ_i	molar density of solid i
$'$	superscript denoting low-temperature regime
$''$	superscript denoting high-temperature regime

APPENDIX I: X-RAY DATA

TABLE I-1
X-RAY DIFFRACTION PATTERNS OF PYROLUSITE

This Work (synthetic sample)

d	
3.09	VS
2.39	S
2.18	W
2.10	M
1.96	W
1.62	S
1.55	M
1.44	W
1.39	W
1.30	S

Glemser[11] (synthetic sample)

θ	d	
18.8	3.02	S+
23.8	2.40	M
26.2	2.19	VW
27.2	2.12	M-
37.0	1.61	S
38.8	1.55	M

McMurdie[17] (Caucasia sample)

θ	d	
18.0	3.13	VS
23.7	2.41	M
26.2	2.19	W
27.1	2.12	M
29.2	1.98	W
36.5	1.63	M
38.4	1.56	M

Sorem[30] (natural sample)

d	I/I_{max}
3.48	.1
3.14	1.0
2.41	.5
2.21	.1
2.13	.25
1.98	.15
1.81	.05?
1.63	.5
1.56	.25

Moore[22] (synthetic sample)

d	I/I_{max}
3.11	1.0
2.41	.6
2.20	.2
2.11	.2
1.98	.1
1.62	.9
1.56	.2
1.44	.1
1.39	.2
1.30	.4

McMurdie[19] (Egyptian sample)

θ	d	
18.2	3.09	VS
23.7	2.41	M+
26.0	2.21	W
27.1	2.12	M
29.3	1.98	W
36.7	1.62	M+
38.4	1.56	W

NOTES:

(1). Intensity designations: VW, very weak; W, weak; M, medium; S, strong; VS, very strong.

(2). The Glemser and McMurdie data are presented in the literature in graphical form. These data were converted from the angle, θ, to the d value tabulations by the present author.

(3). The θ values are the angles of diffraction and are related to the d values shown by the Bragg equation,

$$d = \lambda / 2 \sin(\theta),$$

where λ = wavelength of Fe Kα radiation (1.936A).

TABLE I-2
X-RAY PATTERNS OBTAINED FOR OXIDE STANDARDS

MnO*		Mn_3O_4**		Mn_2O_3***	
d		d		d	
2.565	M	4.91	W	4.70	VVW
2.226	S	3.09	M-	3.84	W
1.575	S-	2.88	VW	2.72	S+
1.34	W	2.775	M+	2.51	M+
1.283	M-	2.495	S	2.35	M-
1.111	W	2.36	W	2.22	VVW
1.02	W	2.03	W	2.10	VVW
0.9935	M	1.83	VW	2.01	W
		1.80	W	1.845	W
		1.70	VW	1.719	VVW
		1.64	VVW	1.664	M
		1.58	W	1.615	VVW
		1.54	M	1.528	VW
		1.475	VVW	1.487	VVW
		1.44	W	1.452	W

*Pattern is substantially in agreement with that of manganosite as given by Swanson, et al.(31)

**Pattern is substantially in agreement with that of hausmannite as given by Hanawalt, et al.(16)

***Pattern is identical to that of partridgeite as as given by Swanson, et al.(32)

TABLE I-3
X-RAY PATTERNS OF REDUCTION PRODUCTS

Run 16		Run 20		Run 22		Run 37		Run 39		Run 42	
d		d		d		d		d		d	
4.90	S	3.105	S+	3.10	S+	3.10	S++	3.095	S++	4.90	S
3.08	S	2.75	W	2.76	W++	2.76	S	2.767	W++	3.08	S
2.87	M-	2.72	W	2.72	W+	2.71	S-	2.716	W++	2.87	M-
2.75	S+	2.48	W	2.48	W++	2.56	M+	2.480	W++	2.76	S+
2.71	W--	2.40	M+	2.40	M	2.48	S-	2.401	S+	2.48	S++
2.48	S++	2.11	M	2.11	M-	2.40	S	2.105	S	2.36	M-
2.359	M-	1.620	M+	1.620	M	2.22	S-	1.619	S+	2.03	M-
2.20	W---	1.552	M-	1.552	W++	2.10	S-	1.552	S-	1.79	M--
2.03	M-					1.661	W+			1.70	W
1.793	M--					1.620	S+			1.64	W
1.695	W					1.569	M+			1.62	W-
1.664	W---									1.58	M--
1.638	W--	Run 46		Run 53		Run 53 (Cont.)		Run 106		1.54	S
1.626	?										
1.575	M--	d		d		d		d			
1.539	S	3.10	S	4.90	W+	2.04	W--	3.12	S		
		2.75	M-	3.85	W	2.01	W---	2.72	W-		
		2.70	M	3.11	S++	1.966	M+	2.716	W		
		2.56	S+	2.87	W-	1.842	W--	2.57	M-		
		2.48	M-	2.76	M-	1.797	W-	2.49	W+		
		2.40	M	2.71	M	1.700	W--	2.41	M--		
		2.21	S++	2.55	W--	1.661	W+	2.23	S+		
		1.656	W+	2.48	M	1.621	S+	2.12	W++		
		1.617	M+	2.40	S	1.570	W-	1.975	W		
		1.566	S+	2.22	W+	1.553	M	1.63	S-		
				2.20	W+	1.540	W-	1.575	S		
				2.11	S-			1.56	W+		

APPENDIX II

The numerical data for all reduction experiments have been summarized. A listing of the runs is given in Table II-1, and the conversion and other pertinent data for each experiment are given in Table II-2.

Synthetic pyrolusite specimens are identified by the designations given in Table 1 of the text. In those cases where the oxide was compressed into a pellet, the letter "P" (in parentheses) was added to the designation. The Belgian Congo pyrolusite with a particle size range of 0.09 to 0.21 mm. was designated "C1", and the "C2" and "C3" designations were assigned to, respectively, single 5 and 8 gram lumps of the ore. The Pyrex vertical-tube reactor has been identified by "V", the Vycor horizontal-tube reactor, by "H".

In the early runs using the horizontal-tube reactor, namely runs 96 through 106, the control and measuring thermocouples were placed near the external surface of the 25 mm. diameter Vycor tube. It later became apparent that this arrangement was not satisfactory for accurate temperature control. The thermocouples were, therefore, placed inside the reaction tube (in a shield) in the manner shown in Figure 5, and the essential runs were repeated.

TABLE II-1
LISTING OF EXPERIMENTAL RUNS

Run No.	Oxide Specimen	Reactor	Temp. (°C)	Reducing Gas	Remarks
1-10	--	-	-	-	Equipment check-out
11	A5(P)	V	350	100% H_2	Rapid temperature escalation
12	A5(P)	V	200	"	Temperature manually controlled
13	A5(P)	V	250	"	Temperature manually controlled
14	A5(P)	V	250	"	Temperature manually controlled
15	A4	V	250	"	Temperature controller installed
16	A4	V	250	"	
17	-	-	-	-	Equipment check-out
18	-	-	-	-	Equipment check-out
19	A4	V	250	100% H_2	
20	A4	V	250	"	
21	-	-	-	-	Equipment check-out
22	A4	V	250	100% H_2	
23	A3	V	250	"	
24	-	-	-	-	Equipment check-out
25	A1	V	250	100% H_2	
26	A1	V	250	"	
27	-	-	-	-	Equipment check-out
28	A5(P)	V	250	100% H_2	
29	A2	V	250	"	
30	B2	V	250	"	
31	B2	V	300	"	
32	B2	V	350	"	Rapid temperature escalation
33	B2	V	201	"	
34	B2	V	265	"	
35	B2	V	315	"	
36	B2	V	315/350	"	Prereduced at 315°C

TABLE II-1 (Continued)

Run No.	Oxide Specimen	Reactor	Temp. (°C)	Reducing Gas	Remarks
37	B2	V	315	100% H_2	
38	A4	V	250	"	
39	B2	V	250	"	
40	B2	V	250	"	
41	B2	V	250	53.4% H_2	
42	B2	V	225	100% H_2	
43	B2	V	238	"	U-tube mishap
44	B6(P)	V	226	"	
45	B6(P)	V	215	"	
46	B3	V	350	24.9% H_2	Flow rate too low
47	B2	V	238	100% H_2	
48	B6(P)	V	238	"	U-tube leak
49	B6(P)	V	226	53.4% H_2	
50	B6(P)	V	226	24.9% H_2	
51	B6(P)	V	226	100% H_2	
52	B6(P)	V	200	"	
53	B3	V	350	24.9% H_2	
54	B3	V	350	100% H_2	
55	B3	V	375	"	
56	B5	V	375	"	
57	B5	V	375	"	
58	B3	V	375	"	
59	B3	V	350	"	
60	B6(P)	V	350	"	
61	B5	V	375	"	
62	B5	V	375	"	
63	B3	V	375	"	

TABLE II-1 (Continued)

Run No.	Oxide Specimen	Reactor	Temp. (°C)	Reducing Gas	Remarks
64	B6(P)	V	226	100% H_2	
65	B6(P)	V	226	75.2% H_2	
66	B5	V	375	100% H_2	
67	B5	V	375	"	
68	B5	V	375	75.2% H_2	
69	B5	V	375	53.4% H_2	
70	B5	V	375	24.9% H_2	
71	B2	V	375	100% H_2	
72	B2	V	275	"	
73	B2	V	325	"	
74	B4	V	400	24.9% H_2	
75	B4	V	350	"	
76	B4	V	425	9.73% H_2	
77	B4	V	425	"	
78	B2	V	425	"	Specimen incorrectly positioned in reactor
79	B2	V	425	"	
80	B2	V	425	"	
81	B4	V	425	"	
82	B4	V	400	"	
83	B4	V	400	100% H_2	
84	B4	V	325	53.4% H_2	
85	B4	V	350	"	
86	B2	V	250	100% H_2	
87	B3	V	375	9.73% H_2	
88	B6(P)	V	226	90.1% H_2	Reducing gas contained 9.9% H_2O
89	B6(P)	V	226	98.9% H_2	Reducing gas contained 1.1% H_2O
90	B6(P)	V	226	"	Reducing gas contained 1.1% H_2O
91	B1	V	375	100% H_2	
92	B1	V	375	90.1% H_2	Reducing gas contained 9.9% H_2O
93	B3	V	375	"	Reducing gas contained 9.9% H_2O

TABLE II-1 (Continued)

Run No.	Oxide Specimen	Reactor	Temp. (°C)	Reducing Gas	Remarks
94	B3	V	375	98.9% H_2	Reducing gas contained 1.1% H_2O
95	B3	V	375	100% H_2	
96	B6	H	325/470	100% H_2	
97	B1	H	325/470	"	
98	B4	H	325/490	"	Prereduced to approximately 20 - 25 %
99	B4	H	325/525	"	conversion at 325°C. Temperatures at
100	B4	H	325/525	"	second stage of reduction are approximate
101	B1	H	325/525	"	(probably plus or minus 20°C).
102	B4	H	325/490	"	
103	B1	H	325/570	"	
104	B1	H	550	Argon	Decomposition run
105	B5	H	400	100% H_2	Rapid temperature escalation
106	B4	H	450	9.73% H_2	
107	B1	H	325/425	100% H_2	
108	B1	H	325/450	"	Prereduced to approximately 12% conversion
109	B1	H	325/500	"	at 325°C
110	B1	H	325/500	"	
111	C1	H	325	100% H_2	Rapid temperature escalation
112	C1	H	440	"	Rapid temperature escalation
113	B1	H	600	100% H_2	No kinetic data. Runs conducted to in-
114	B1	H	700	"	vestigate stability of MnO product
115	B1	H	700	Argon	Decomposition run
116	C2	V	350	100% H_2	Temperature unstable during run
117	C1	V	300	"	Rapid temperature escalation
118	C1	V	250	"	
119	C1	V	275	"	
120	C1	V	275/325	"	Prereduced to 50% conversion at 275°C
121	C1	V	225	"	
122	C3	V	225/250/300	"	Initial reduction at 225°C
123	C1	V	300	9.73% H_2	

TABLE II-2
EXPERIMENTAL REDUCTION DATA

RUN 11

350°C; 100% H_2

Flow rate: 3.0 cu.ft./hr.

Specimen A5(P) (1.5091 g.)

Final % reduction (to MnO), based on water recovery was 98%.

Comments: Temperature could not be controlled. Sample reduced to MnO in several minutes.

RUN 12

202°C; 100% H_2

Flow rate: 3.0 cu.ft./hr.

Specimen A5(P) (1.4927 g.)

Comments: Temperature controlled manually. Final % reduction based on weight loss was 23.0%.

Time (sec.)	% Reduction (to MnO)
590	0.58
1,970	1.39
3,950	2.05
8,635	6.66
13,580	12.36
17,300	16.8
20,720	20.9
22,500	24.5

RUN 13

250°C; 100% H_2

Flow rate: 3.0 cu.ft./hr.

Specimen A5(P) (1.4495 g.)

Comments: Temperature controlled manually. Final % reduction based on weight loss was 63.8%.

Time (sec.)	% Reduction (to MnO)
600	3.3
1,335	20.0
2,140	33.7
2,885	40.6
4,080	48.9
5,265	55.6
6,260	59.0
8,180	62.2
10,120	65.1

TABLE II-2 (Continued)

RUN 14

250°C; 100% H_2

Flow rate: 5.0 cu.ft./hr.

Specimen A5(P) (1.4925 g.)

Comments: Temperature controlled manually. Final % reduction based on weight loss was 70.2%

Time (sec.)	% Reduction (to MnO)
600	4.6
1,310	29.5
2,140	41.8
2,880	48.4
4,080	54.2
5,265	58.1
6,260	60.4
8,190	63.0
10,400	64.8
12,870	66.4
16,400	68.6
20,540	70.6

RUN 15

250°C; 100% H_2

Flow rate: 3.0 cu.ft./hr.

Specimen A4 (1.4392 g.)

Comments: Temperature controller installed prior to this run. Final % reduction based on weight loss was 66.8%.

Time (sec.)	% Reduction (to MnO)
600	2.54
1,220	7.02
1,950	12.4
2,590	18.4
3,630	27.2
5,580	43.5
6,020	46.5
7,080	54.0
7,807	57.3
8,980	61.4
10,240	64.1
11,460	65.4
14,540	67.2
18,680	68.9
20,600	69.0

TABLE II-2 (Continued)

RUN 16

$250^{o}C$; 100% H_2

Flow rate: 5.0 cu.ft./hr.

Specimen A4 (1.4465 g.)

Comments: Final % reduction based on weight loss was 66.0%.

Time (sec.)	% Reduction (to MnO)
600	2.24
1,200	7.34
1,800	12.1
2,520	18.6
3,500	28.2
4,620	38.1
5,560	45.4
6,850	53.7
7,890	57.8
8,840	60.5
10,540	63.5
13,520	65.9
14,700	66.2

RUN 19

$250^{o}C$; 100% H_2

Flow rate: 3.0 cu.ft./hr.

Specimen A4 (2.9154g.)

Comments: Final % reduction based on weight loss was 64.9%.

Time (sec.)	% Reduction (to MnO)
600	1.50
1,230	6.28
2,000	12.0
2,560	16.6
3,690	26.2
4,690	34.8
5,660	42.5
6,640	49.4
7,900	55.8
8,680	58.7
9,640	61.2
10,930	63.6
14,270	66.7

TABLE II-2 (Continued)

RUN 20

250°C; 100% H_2	Time (sec.)	% Reduction (to MnO)
Flow rate: 3.0 cu.ft./hr.		
	600	2.7
Specimen A4 (1.0078 g.)	1,320	8.1
	2,200	14.8
Comments: Reduction product spilled upon removal from reactor.		

RUN 22

250°C; 100% H_2	Time (sec.)	% Reduction (to MnO)
Flow rate: 3.0 cu.ft./hr.		
	640	2.20
Specimen A4 (0.8674 g.)	1,380	8.03
	2,190	14.7
Comments: Final % reduction based on weight loss was 32.5%.	3,000	21.7
	4,280	32.4

RUN 23

250°C; 100% H_2	Time (sec.)	% Reduction (to MnO)
Flow rate: 3.0 cu.ft./hr.		
	630	2.04
Specimen A3 (0.9949 g.)	1,220	6.12
	2,040	12.33
Comments: Final % reduction based on weight loss was 63.2%.	2,890	19.3
	3,810	28.0
	4,840	37.5
	5,992	47.3
	7,220	55.7
	8,490	61.7
	10,290	66.3
	11,130	67.4

TABLE II-2 (Continued)

RUN 25

250°C; 100% H_2

Flow rate: 3.0 cu.ft./hr.

Specimen A1 (1.4933 g.)

Comments: Final % reduction by weight loss was 64.1%, and by chemical analysis (for available oxygen) was 64.8%.

Time (sec.)	% Reduction (to MnO)
650	2.26
1,240	6.00
1,900	10.7
2,500	15.8
3,490	25.1
4,480	34.9
5,650	45.4
6,680	52.7
7,780	58.5
8,670	61.4
9,940	64.7
10,860	66.2

RUN 26

250°C; 100% H_2

Flow rate: 3.0 cu.ft./hr.

Specimen A1 (1.4959 g.)

Comments: Final % reduction by weight loss was 62.2%.

Time (sec.)	% Reduction (to MnO)
600	1.26
1,250	5.04
1,930	9.60
2,560	14.62
3,420	22.6
4,190	29.8
4,980	36.9
6,280	47.6
7,130	53.1
7,940	56.8
8,760	59.6
10,050	62.8

TABLE II-2 (Continued)

RUN 28

250°C; 100% H_2

Flow rate: 3.0 cu. ft./hr.

Specimen A5(P) (1.5095 g.)

Comments: Final % reduction based on weight loss was 64.9%.

Time (sec.)	% Reduction (to MnO)
650	5.47
1,385	21.7
1,945	31.2
2,660	40.7
3,270	46.5
4,170	53.2
4,985	57.2
6,000	60.4
6,990	62.8
7,905	64.5
9,545	66.1
10,770	66.8

RUN 29

250°C; 100% H_2

Flow rate: 3.0 cu. ft./hr.

Specimen A2 (1.6245 g.)

Comments: Final % reduction based on weight loss was 65.5%. Prior to run, sample was preheated in air at 345°C for two hours.

Time (sec.)	% Reduction (to MnO)
600	1.25
1,380	6.74
2,120	12.52
2,900	19.82
3,610	26.8
4,650	36.0
5,440	44.4
6,360	51.5
7,420	57.6
8,770	62.6
10,970	66.3

TABLE II-2 (Continued)

RUN 30

250°C; 100% H_2

Flow rate: 3.0 cu.ft./hr.

Specimen B2 (1.5418 g.)

Comments: Final % reduction based on weight loss was 63.5%.

Time (sec.)	% Reduction (to MnO)
600	1.32
1,250	5.08
1,810	8.37
2,590	13.01
3,370	18.02
4,305	25.1
5,260	33.1
6,060	39.9
6,940	46.8
7,860	52.8
8,830	57.3
10,000	60.9
11,870	64.0

RUN 31

300°C; 100% H_2

Flow rate: 3.0 cu.ft./hr.

Specimen B2 (1.9492 g.)

Comments: Final % reduction based on weight loss was 68.8%.

Time (sec.)	% Reduction (to MnO)
335	5.71
610	11.92
910	17.56
1,305	23.9
1,855	30.4
2,550	35.5
2,950	37.8
3,750	41.2
4,480	43.7
5,700	47.0
6,910	49.9
8,460	53.3
11,700	59.8
13,950	63.6
17,150	68.3
19,710	71.2

TABLE II-2 (Continued)

RUN 32

350°C; 100% H_2

Flow rate: 3.0 cu.ft./hr.

Specimen B2 (1.8940 g.)

Comments: Rapid temperature escalation. Specimen reacted to MnO in several minutes. Final % reduction based on weight loss was 101.8%.

Time (sec.)	% Reduction (to MnO)
?	100.2%

RUN 33

201°C; 100% H_2

Flow rate: 3.0 cu.ft./hr.

Specimen B2 (3.0422 g.)

Comments: Final % reduction based on weight loss was 33.1%.

Time (sec.)	% Reduction (to MnO)
3,570	0.94
5,980	1.99
7,960	3.00
10,980	4.64
15,170	6.96
23,110	11.70
27,070	14.24
33,280	19.08
37,230	22.6
41,290	26.6
45,000	30.1
49,600	34.8
50,650	35.6

RUN 34

265°C; 100% H_2

Flow rate: 3.0 cu.ft./hr.

Specimen B2 (1.8921 g.)

Comments: Final % reduction based on weight loss was 66.8%.

Time (sec.)	% Reduction (to MnO)
525	2.07
1,280	8.39
1,650	12.07
2,110	16.62
2,670	22.9
3,250	30.2
3,800	36.8
4,350	42.7
5,175	49.6
6,050	54.3
7,000	57.8
8,380	60.7
9,680	62.5
14,180	66.5
15,980	67.8

TABLE II-2 (Continued)

RUN 35

315°C; 100% H_2

Flow rate: 6.0 cu.ft./hr.

Specimen B2 (0.9547 g.)

Time (sec.)	% Reduction (to MnO)
600	15.78
1,200	25.3
2,015	32.5
3,050	38.6
4,100	43.8
5,750	50.2
7,650	56.6
10,250	63.6

Comments:

(1). Final % reduction based on weight loss was 58.3%. Product probably picked up oxygen upon exposure to atmosphere.

(2). Reduction product was stored in air (desiccator) at room temperature for 48 hours. No oxidation occurred during this period as revealed by negligible weight increase.

(3). The product was then heated in air at 120°-140°C for two hours, cooled, and weighed. A weight increase was observed; the corresponding "% reduction" at this point was 55.7%, indicating that appreciable oxidation occurred during the two hour heating period.

RUN 36

315°/350°C; 100% H_2

Flow rate: 3.0 cu.ft./hr.

Specimen B2 (1.0206 g.)

Comments: Specimen pre-reduced to 50.6% at 315°C. Reactor was purged with argon during the period 6175 to 10,100 sec. while furnace temperature was raised to 350°C. The final % reduction based on weight loss was 75.0%. Product partially oxidized upon contact with air.

Time (sec.)	% Reduction (to MnO)	
1,000	21.4	
2,050	30.8	
3,060	37.1	315°C
4,440	43.9	
6,175	50.6	
10,415	51.9	
11,020	57.1	
11,950	65.1	
13,050	71.8	
14,050	77.1	350°C
15,200	82.3	
16,750	87.9	
18,530	92.6	
21,000	96.2	

TABLE II-2 (Continued)

RUN 37

315°C; 100% H_2

Flow rate: 5.0 cu.ft./hr.

Specimen B2 (0.9960 g.)

Comments: Reduction product was cooled in reactor to approximately 380°F prior to removal from furnace (argon atmosphere). Final % reduction based on weight loss was 46.4%.

Time (sec.)	% Reduction (to MnO)
500	13.10
1,005	20.85
1,650	27.0
2,200	30.7
2,820	34.5
3,575	38.6
4,575	43.5
5,005	45.4

RUN 38

250°C; 100% H_2

Flow rate: 3.0 cu.ft./hr.

Specimen A4 (0.8253 g.)

Comments: Final % reduction based on weight loss was 11.4%.

Time (sec.)	% Reduction (to MnO)
925	5.39
1,800	12.64

RUN 39

250°C; 100% H_2

Flow rate: 3.0 cu.ft./hr.

Specimen B2 (0.8558 g.)

Time (sec.)	% Reduction (to MnO)
1,000	4.74
2,000	10.8

RUN 40

250°C; 100% H_2

Flow rate: 3.0 cu.ft./hr.

Specimen B2 (1.4490 g.)

Comments: Final % reduction based on weight loss was 66.5%.

Time (sec.)	% Reduction (to MnO)
625	1.73
1,260	5.13
1,900	8.84
2,530	12.67
3,610	19.90
4,610	28.7
5,975	39.0
7,015	46.8
8,125	53.9
9,270	59.3
18,750	70.0

TABLE II-2 (Continued)

RUN 41

250°C; 53.4% H_2 (balance, He)

Flow rate: 3.0 cu.ft./hr.

Specimen B2 (1.4700 g.)

Comments: Final % reduction based on weight loss was 62.7%.

Time (sec.)	% Reduction (to MnO)
700	0.92
1,200	2.37
1,870	4.51
2,610	7.24
3,525	10.56
4,500	14.40
5,825	20.0
6,750	24.3
7,675	29.0
8,850	35.0
10,350	42.8
11,600	48.2
13,060	53.5
14,850	58.0
16,510	60.7
17,760	62.3
20,330	64.0

RUN 42

225°C; 100% H_2

Flow rate: 2.7 cu.ft./hr.

Specimen B2 (1.5157 g.)

Comments: Final % reduction based on weight loss was 65.9%.

Time (sec.)	% Reduction (to MnO)
1,000	0.48
2,020	2.25
3,000	3.98
4,000	5.92
5,110	8.25
6,200	10.68
7,560	13.84
9,080	17.32
10,780	21.9
11,780	24.8
13,070	28.9
14,790	34.6
16,470	40.2
18,740	47.5
20,925	53.0
23,900	58.4
28,850	63.2
32,550	64.7
34,050	65.0

TABLE II-2 (Continued)

RUN 43

238°C; 100% H_2

Flow rate: 3.4 cu.ft./hr.

Specimen B2 (1.4488 g.)

Comments: U-tube mishap at 11,460 sec.

Time (sec.)	% Reduction (to MnO)
1,000	2.07
2,000	6.20
3,020	10.20
4.050	14.0
5,230	19.02
6,415	24.9
7,470	30.8
8,460	36.5
9,420	42.0
10,540	48.4
11,460	53.2

RUN 44

226°C; 100% H_2

Flow rate: 3.0 cu.ft./hr.

Specimen B6(P) (1.4343 g.)

Comments: Final % reduction based on weight loss was 65.3%.

Time (sec.)	% Reduction (to MnO)
680	1.247
2,110	6.30
3,000	10.73
4,130	16.9
5,360	23.9
6,570	29.4
7,590	34.2
8,860	39.0
9,970	42.2
11,180	46.2
12,840	50.9
15,670	56.9
18,300	60.8
20,315	63.1
24,900	65.7

TABLE II-2 (Continued)

RUN 45

215°C; 100% H_2

Flow rate: 3.0 cu.ft./hr.

Specimen B6(P) (1.4420 g.)

Comments: Final % reduction based on weight loss was 64.2%.

Time (sec.)	% Reduction (to MnO)
2,000	3.28
4,025	8.91
6,000	14.77
8,000	20.9
10,550	28.1
13,000	34.5
16,020	42.2
19,000	48.4
22,000	53.4
26,000	58.5
30,300	63.1
35,530	66.5
38,530	67.6

RUN 46

350°C; 24.9% H_2 (balance, He)

Flow rate: 2.8 cu.ft./hr.

Specimen B3 (1.5672 g.)

Comments: Final % reduction based on weight loss was 74.0%. Flow rate too low. See run 75.

Time (sec.)	% Reduction (to MnO)
970	18.5
2,010	24.2
3,225	28.9
5,610	37.9
7,800	45.5
11,400	54.8
16,000	65.8
19,930	74.0
22,150	77.8

TABLE II-2 (Continued)

RUN 47

238°C; 100% H_2

Flow rate: 3.0 cu.ft./hr.

Specimen B2 (1.9459 g.)

Comments: Final % reduction based on weight loss was 65.2%.

Time (sec.)	% Reduction (to MnO)
1,500	3.15
3,340	9.65
5,040	16.38
6,770	24.4
8,025	31.3
9,000	36.5
10,240	43.1
11,490	49.2
12,710	54.5
14,300	59.3
16,070	62.8
20,130	66.8

RUN 48

238°C; 100% H_2

Flow rate: 6.0 cu.ft./hr.

Specimen B6(P) (1.4444 g.)

Comments: Developed leak in U-tube; data valid up to reaction time of 7260 sec.

Time (sec.)	% Reduction (to MnO)
500	1.84
1,530	10.43
2,400	19.72
3,440	29.6
4,530	37.8
5,700	45.7
7,260	52.9

RUN 49

226°C; 53.4% H_2 (balance, He)

Flow rate: 6.0 cu.ft./hr.

Specimen B6(P) (2.7582 g.)

Comments: Two nominal 1.4-gram pellets were used. Final % reduction based on weight loss was 55.5%.

Time (sec.)	% Reduction (to MnO)
1,840	2.61
4,075	8.81
6,155	16.04
8,370	23.4
10,170	28.8
12,400	35.0
14,450	39.9
16,500	44.8
19,320	49.9
22,125	54.3
23,950	56.8

TABLE II-2 (Continued)

RUN 50

226°C; 24.9% H_2 (balance, He)

Flow rate: 6.5 cu.ft./hr.

Specimen B6(P) (2.6865 g.)

Comments: Two nominal 1.4-gram pellets were used. Final % reduction based on weight loss was 35.8%.

Time (sec.)	% Reduction (to MnO)
3,600	3.76
5,880	8.10
8,290	13.19
10,670	18.46
13,200	23.8
16,210	29.5
21,245	38.1

RUN 51

226°C; 100% H_2

Flow rate: 13.0 cu.ft./hr.

Specimen B6(P) (1.2990 g.)

Comments: Final % reduction based on weight loss was 59.9%.

Time (sec.)	% Reduction (to MnO)
1,525	4.20
2,640	9.78
3,810	15.9
5,050	22.2
6,750	30.1
9,800	41.8
13,250	52.6
15,520	57.5
17,570	60.5

RUN 52

200°C; 100% H_2

Flow rate: 3.0 cu.ft./hr.

Specimen B6(P) (3.3924 g.)

Comments: Two nominal 1.7-gram pellets were used. Final % reduction based on weight loss was 25.0%.

Time (sec.)	% Reduction (to MnO)
2,000	0.97
5,000	2.68
7,440	4.67
10,260	7.44
14,230	11.87
18,080	16.3
21,330	20.1
25,330	24.6
26,640	25.9

TABLE II-2 (Continued)

RUN 53

350°C; 24.9% H_2 (balance, He)	Time (sec.)	% Reduction (to MnO)
Flow rate: 3.8 cu.ft./hr.	1,650	21.0%
Specimen B3 (0.9430 g.)		

Comments: Final % reduction based on weight loss was 21.2%.

RUN 54

350°C; 100% H_2	Time (sec.)	% Reduction (to MnO)
Flow rate: 5.0 cu.ft./hr.	1,810	30.7
Specimen B3 (1.5045 g.)	2,430	37.7
	3,050	43.8
Comments: Average bed depth	3,990	51.7
was 4.4 mm. H_2 stream	4,920	58.4
was diluted with argon	6,370	67.0
during first 1400 seconds.	8,125	75.6
Final % reduction based on	9,900	83.0
weight loss was 77.6%.	12,010	90.2
Product partially re-	16,300	98.6
oxidized upon exposure	17,400	99.4
to air.		

RUN 55

375°C; 100% H_2	Time (sec.)	% Reduction (to MnO)
Flow rate: 5.0 cu.ft./hr.	1,040	31.6
Specimen B3 (1.4967 g.)	1,520	44.6
	2,100	56.4
Comments: Average bed depth	2,700	66.1
was 4.5 mm. H_2 stream	3,310	74.0
was diluted with argon	4,090	82.5
during first 700 seconds.	5,020	90.2
Final % reduction based on	5,955	95.6
weight loss was 76.0%,	7,590	100.5
indicating that product		
was partially reoxidized upon		
contact with air.		

TABLE II-2 (Continued)

RUN 56

375°C; 100% H_2	Time (sec.)	% Reduction (to MnO)
Flow rate: 5.0 cu.ft./hr.		
	1,100	33.8
Specimen B5 (1.5828 g.)	1,600	46.6
	2,180	57.4
Comments: Average bed depth	2,820	66.9
was 4.8 mm. H_2 stream was	3,730	78.0
diluted with argon during	4,650	86.3
first 750 seconds. Final	5,200	90.1
% reduction based on weight	6,670	96.6
loss was 76.5%, indicating	7,630	98.6
that product was partially		
reoxidized upon contact with air.		

RUN 57

375°C; 100% H_2	Time (sec.)	% Reduction (to MnO)
Flow rate: 5.0 cu.ft./hr.		
	1,250	30.6
Specimen B5 (3.0150 g.)	1,820	45.3
	2,550	57.8
Comments: Average bed depth	3,290	67.0
was 6.6 mm. H_2 stream was	4,250	76.6
diluted with argon during	5,110	83.6
first 950 seconds. Final	6,150	90.2
% reduction based on weight	8,000	97.2
loss was 93.4%.		

RUN 58

375°C; 100% H_2	Time (sec.)	% Reduction (to MnO)
Flow rate: 5.0 cu.ft./hr.		
	1,300	30.5
Specimen B3 (0.7841 g.)	1,810	43.3
	2,430	55.8
Comments: Average bed depth	3,265	69.7
was 2.4 mm. H_2 stream was	4,020	79.7
diluted with He during first	5,000	89.3
900 seconds.		

TABLE II-2 (Continued)

RUN 59

350°C; 100% H_2

Flow rate: 5.0 cu.ft./hr.

Specimen B_3 (2.8817 g.)

Comments: Average bed depth was 6.4 mm. H_2 stream was diluted with He during first 800 seconds. Final % reduction based on weight loss was 75.6%.

Time (sec.)	% Reduction (to MnO)
1,500	26.8
2,800	40.0
3,900	48.7
5,350	58.0
6,950	66.5
8,100	71.6
10,450	80.5

RUN 60

350°C; 100% H_2

Flow rate: 5.0 cu.ft./hr.

Specimen $B_6(P)$ (1.4509 g.)

Comments: H_2 stream was diluted with He during first 1500 seconds. Final % reduction based on weight loss was 87.5%. Surface temperature of solid was probably much higher than 350°C.

Time (sec.)	% Reduction (to MnO)
1,775	55.1
2,360	66.2
3,020	74.2
3,550	78.9
4,190	83.1
4,910	86.7
5,730	89.6
7,060	92.8

RUN 61

375°C; 100% H_2

Flow rate: 5.0 cu.ft./hr.

Specimen B_5 (1.4925 g.)

Comments: H_2 stream was diluted with He during first 750 seconds. Final % reduction based on weight loss was 91.7%. Average bed depth was 1.0 mm.

Time (sec.)	% Reduction (to MnO)
1,100	30.6
1,630	45.4
2,410	61.6
3,100	73.0
4,000	83.1
5,060	93.2
6,150	98.4

TABLE II-2 (Continued)

RUN 62

375°C; 100% H_2

Flow rate: 5.0 cu.ft./hr.

Specimen B5 (0.7281 g.)

Comments: H_2 stream was diluted with He during first 850 seconds. Product could not be weighed due to sample spillage after removal from furnace

Time (sec.)	% Reduction (to MnO)
1,160	33.8
1,650	48.0
2,420	65.3
3,100	77.1
4,000	88.8
5,125	97.1

RUN 63

375°C; 100% H_2

Flow rate: 5.0 cu.ft./hr.

Specimen B3 (0.7319 g.)

Comments: H_2 stream was diluted with He during first 900 seconds. Average bed depth was 1.6 mm. Final % reduction based on weight loss was 83.9%.

Time (sec.)	% Reduction (to MnO)
1,300	31.0
1,830	45.0
2,470	58.2
3,330	73.0
4,150	83.6
4,950	91.4

RUN 64

226°C; 100% H_2

Flow rate: 3.0 cu.ft./hr.

Specimen B6(P) (1.5143 g.)

Comments: Pellet was sectioned into four more or less equal pie-shaped pieces. Final % reduction based on weight loss was 63.7%.

Time (sec.)	% Reduction (to MnO)
1,010	2.91
2,025	7.82
3,110	14.14
4,460	22.0
5,960	29.6
7,570	36.2
10,010	45.4
12,520	53.5
14,000	57.1
15,580	60.2
18,630	64.3
23,000	68.0
24,430	68.9

TABLE II-2 (Continued)

RUN 65

226°C; 75.2% H_2 (balance, He)

Flow rate: 4.6 cu.ft./hr.

Specimen B6(P) (1.8718 g.)

Comments: Final % reduction based on weight loss was 60.2%.

Time (sec.)	% Reduction (to MnO)
1,960	5.06
4,000	14.07
5,850	22.45
8,000	31.2
10,710	40.6
13,150	47.8
16,330	55.1
19,350	60.0
22,400	63.6

RUN 66

375°C; 100% H_2

Flow rate: 13.0 cu.ft./hr.

Specimen B5 (1.4791 g.)

Comments: H_2 diluted with He during first 900 seconds. Average bed depth was 4.4 mm. Final % reduction based on weight loss was 93.5%.

Time (sec.)	% Reduction (to MnO)
1,145	32.7
1,760	48.3
2,450	60.6
3,247	72.1
4,060	81.5
5,100	90.4
6,390	97.5
7,870	100.6
9,430	101.5

RUN 67

375°C; 100% H_2

Flow rate: 5.0 cu.ft./hr.

Specimen B5 (1.4551 g.)

Comments: H_2 diluted with argon during first 750 seconds. Reactor cooled to 150°F prior to removing reduction product. Average bed depth was 1.0 mm. Final % reduction based on weight loss was 95.7%.

Time (sec.)	% Reduction (to MnO)
1,170	34.1
1,900	53.8
2,705	68.2
3,670	81.5
4,660	91.4
5,365	95.8
11,960	102.1

TABLE II-2 (Continued)

RUN 68

375°C; 75.2% H_2 (balance, He)	Time (sec.)	% Reduction (to MnO)
Flow rate: 7.8 cu.ft./hr.		
	1,125	33.6
Specimen B5 (1.5014 g.)	1,790	48.2
	2,650	62.4
Comments: H_2 diluted with	3,360	72.0
argon during first 800 sec.	4,250	82.2
Average bed depth was 1.0 mm.	5,260	90.4
Final % reduction based on	6,340	96.0
weight loss was 75.5%.	7,210	98.8
Product partially re-oxidized upon exposure to air.		

RUN 69

375°C; 53.4% H_2 (balance, He)	Time (sec.)	% Reduction (to MnO)
Flow rate: 10.0 cu.ft./hr.		
	1,175	30.2
Specimen B5 (1.5156 g.)	2,140	49.2
	2,780	58.9
Comments: H_2 diluted with	3,810	71.8
argon during first 850 sec.	4,925	82.6
Average bed depth was 1.0 mm.	5,930	90.0
	7,335	97.1

RUN 70

375°C; 24.9% H_2 (balance, He)	Time (sec.)	% Reduction (to MnO)
Flow rate: 12.5 cu.ft./hr.		
	1,120	24.6
Specimen B5 (1.4931 g.)	1,890	34.3
	2,830	44.2
Comments: H_2 diluted with	4,165	55.4
argon during first 700 sec.	5,730	66.9
Average bed depth was 1.0 mm.	7,550	76.9
	9,265	85.4

TABLE II-2 (Continued)

RUN 71

375°C; 100% H_2

Flow rate: 5.0 cu.ft./hr.

Specimen B2 (1.5120 g.)

Comments: H_2 diluted with argon during first 750 sec. Average bed depth was 1.0 mm.

Time (sec.)	% Reduction (to MnO)
1,080	28.4
2,080	53.8
3,060	70.7
4,040	83.2
5,530	94.8

RUN 72

275°C; 100% H_2

Flow rate: 5.0 cu.ft./hr.

Specimen B2 (1.5602 g.)

Comments: Final % reduction based on weight loss was 68.4% (probably some re-oxidation of product upon exposure to atmosphere). Average bed depth was 1.0 mm.

Time (sec.)	% Reduction (to MnO)
805	8.05
1,490	17.32
2,400	30.1
3,240	41.0
4,130	49.5
5,130	55.2
6,480	59.4
8,520	63.3
11,740	67.8
14,950	71.8
17,540	75.2

RUN 73

325°C; 100% H_2

Flow rate: 5.0 cu.ft./hr.

Specimen B2 (1.9420 g.)

Comments: Final % reduction based on weight loss was 67.6% (probably some re-oxidation of product upon exposure to atmosphere). H_2 diluted with argon during first 800 sec. Average bed depth was 1.3 mm.

Time (sec.)	% Reduction (to MnO)
1,300	18.58
2,540	29.3
3,620	35.9
5,040	43.6
6,560	50.3
8,125	56.1
9,870	61.8
12,170	68.3
14,320	73.9
18,180	81.5
20,650	85.3

TABLE II-2 (Continued)

RUN 74

400°C; 24.9% H_2 (balance, He)

Flow rate: 12.5 cu.ft./hr.

Specimen B4 (1.4756 g.)

Comments: Average bed depth was 1.0 mm. Reactor was cooled to 102°F (argon atmosphere) prior to oxide product removal. Final % reduction based on weight loss was 95.3%.

Time (sec.)	% Reduction (to MnO)
840	27.2
1,260	38.9
1,940	54.1
2,795	68.9
4,015	84.7
5,240	94.7
6,260	99.3
11,000	102.0

RUN 75

350°C; 24.9% H_2 (balance, He)

Flow rate: 11.3 cu.ft./hr.

Specimen B4 (1.5777 g.)

Comments: Average bed depth was 1.0 mm. Final % reduction based on weight loss was 55.6%.

Time (sec.)	% Reduction (to MnO)
460	12.89
1,110	18.13
1,700	21.6
2,390	25.4
3,360	30.4
4,680	36.9
6,905	46.3
8,700	52.9
10,340	59.0

RUN 76

425°C; 9.73% H_2 (balance He)

Flow rate: 12.0 cu.ft./hr.

Specimen B4 (1.5101 g.)

Comments: H_2 diluted with argon during first 400 sec. Average bed depth was 1.0 mm. Final % reduction based on weight loss was 97.9%.

Time (sec.)	% Reduction (to MnO)
660	27.6
1,130	41.0
1,895	58.2
2,725	73.1
3,790	88.7
5,025	98.1
9,230	102.6

TABLE II-2 (Continued)

RUN 77

425°C; 9.73% H_2 (balance, He)

Flow rate: 10.5 cu.ft./hr.

Specimen B4 (1.5035 g.)

Comments: H_2 diluted with argon during first 400 sec. Average bed depth was 2.3 mm.

Time (sec.)	% Reduction (to MnO)
690	26.1
1,170	38.8
2,003	54.2
3,080	71.7
4,100	85.4

RUN 78

425°C; 9.73% H_2 (balance, He)

Flow rate: 6.9 cu.ft./hr.

Specimen B2 (1.5352 g.)

Comments: Data are not valid. Specimen was incorrectly positioned in reactor -- this was observed at time of oxide product removal.

Time (sec.)	% Reduction (to MnO)
790	18.61
1,290	25.0
1,950	32.7
3,370	49.6

RUN 79

425°C; 9.73% H_2 (balance, He)

Flow rate: 5.5 cu.ft./hr.

Specimen B2 (1.4742 g.)

Comments: H_2 diluted with argon during first 475 sec. Estimated bed depth was 1.0 mm.

Time (sec.)	% Reduction (to MnO)
710	26.8
1,200	39.3
1,900	53.3
2,840	69.4
3,810	82.8
4,370	88.7

RUN 80

425°C; 9.73% H_2 (balance, He)

Flow rate: 8.0 cu.ft./hr.

Specimen B2 (1.4883 g.)

Comments: H_2 diluted with argon during first 400 sec. Estimated bed depth was 1.0 mm.

Time (sec.)	% Reduction (to MnO)
700	26.1
1,240	40.3
1,940	55.1
2,590	66.2
3,570	80.4
4,190	87.3

TABLE II-2 (Continued)

RUN 81

425°C; 9.73% H_2 (balance, He)	Time (sec.)	% Reduction (to MnO)
Flow rate: 8.0 cu.ft./hr.		
	760	29.4
Specimen B4 (1.5019 g.)	1,435	45.8
	2,070	58.5
Comments: H_2 diluted with	2,820	70.7
argon during first 400 sec.	3,605	81.8
Estimated bed depth was	4,330	89.4
1.0 mm.		

RUN 82

400°C; 9.73% H_2 (balance, He)	Time (sec.)	% Reduction (to MnO)
Flow rate: 5.5 cu.ft./hr.		
	850	22.7
Specimen B4 (1.4796 g.)	2,005	40.4
	3,100	53.2
Comments: H_2 diluted with	4,370	65.8
argon during first 570 sec.	5,935	78.4
Estimated bed depth was	8,150	91.5
1.0 mm.		

RUN 83

400°C; 100% H_2	Time (sec.)	% Reduction (to MnO)
Flow rate: 7.5 cu.ft./hr.		
	650	36.7
Specimen B4 (0.7847 g.)	950	54.5
	1,350	72.1
Comments: H_2 diluted with	1,650	82.5
argon during first 430 sec.	2,100	92.8
Estimated bed depth was	2,800	101.1
1.7 mm.		

TABLE II-2 (Continued)

RUN 84

325°C; 53.4% H_2 (balance, He)	Time (sec.)	% Reduction (to MnO)
Flow rate: 9.0 cu.ft./hr.		
	510	12.97
Specimen B4 (1.8219 g.)	1,080	18.96
	1,790	23.1
Comments: H_2 diluted with	2,910	27.8
argon during first 550 sec.	4,240	32.4
Estimated bed depth was	6,280	38.8
1.2 mm. Final % reduction	8,560	45.3
based on weight loss was	11,200	51.7
56.4%.	14,050	58.0
	15,700	61.2

RUN 85

350°C; 53.4% H_2 (balance, He)	Time (sec.)	% Reduction (to MnO)
Flow rate: 9.0 cu.ft./hr.		
	840	18.13
Specimen B4 (1.7158 g.)	1,530	25.1
	2,320	31.3
Comments: H_2 diluted with	3,640	40.6
argon during first 540 sec.	5,310	50.5
Estimated bed depth was	6,980	58.6
1.1 mm. Final % reduction	9,220	68.1
based on weight loss was	11,680	76.9
63.5%.		

RUN 86

250°C; 100% H_2	Time (sec.)	% Reduction (to MnO)
Flow rate: 13.0 cu.ft./hr.		
	1,040	4.84
Specimen B2 (1.5077 g.)	2,000	11.06
	3,210	19.04
Comments: Final % reduction	4,520	29.6
based on weight loss was	5,550	38.7
64.1%. Reduction product was	6,640	47.6
analyzed by thermal decomposi-	7,760	55.1
tion in the manner discussed	9,490	62.6
on page 55 of the text. The	11,300	66.5
analysis indicated a product	12,325	68.1
of 91% Mn_3O_4, 7% MnO_2, and —	12,700	68.6
2% Mn_2O_3.		

TABLE II-2 (Continued)

RUN 87

375°C; 9.74% H_2 (balance, He)

Flow rate: 5.5 cu.ft./hr.

Specimen B_3 (2.0167 g.)

Comments: Estimated bed depth was 1.3 mm. Final % reduction based on weight loss was 49.5%.

Time (sec.)	% Reduction (to MnO)
425	15.19
910	20.0
1,065	25.1
2,480	30.1
3,710	37.0
5,200	44.5
6,610	50.7

RUN 88

226°C; 9.9% H_2O, 90.1% H_2

Flow rate: 3.3 cu.ft./hr.

Specimen $B_6(P)$ (1.8147 g.)

Comments: % reduction calculated from weight loss data.

Time (sec.)	% Reduction (to MnO)
4,010	0.8 (9.9% H_2O)
8,000	18.0 (100% H_2)
12,000	23.1 (9.9% H_2O)
16,000	28.2 "
20,000	34.2 "

RUN 89

226°C; 1.1% H_2O, 98.9% H_2

Flow rate: 3.0 cu.ft./hr.

Specimen $B_6(P)$ (1.5565 g.)

Comments: % reduction calculated from weight loss data.

Time (sec.)	% Reduction (to MnO)
4,000	5.7
8,000	17.18
12,000	29.2
16,960	40.7
25,120	54.2
35,265	61.8

TABLE II-2 (Continued)

RUN 90

226°C; 1.1% H_2O, 98.9% H_2	Time (sec.)	% Reduction (to MnO)
Flow rate: 3.0 cu.ft./hr.	14,000	37.0
Specimen B6(P) (1.8721 g.)		

Comments: Conversion based on weight loss data.

RUN 91

375°C; 100% H_2	Time (sec.)	% Reduction (to MnO)
Flow rate: 5.0 cu.ft./hr.	900	28.9*
Specimen B1 (1.5371 g.)		29.4**

*Based on water recovery
**Based on weight loss

Comments: H_2 diluted with argon during first 700 sec. Estimated bed depth was 4.5 mm.

RUN 92

375°C; 9.9% H_2O, 90.1% H_2	Time (sec.)	% Reduction (to MnO)
Flow rate: 5.5 cu.ft./hr.	900	26.2
Specimen B1 (1.5028 g.)		

Comments: H_2 diluted with argon during first 700 sec. Conversion was based on weight loss. Estimated bed depth was 4.5 mm.

RUN 93

375°C; 9.9% H_2O, 90.1% H_2	Time (sec.)	% Reduction (to MnO)
Flow rate: 5.5 cu.ft./hr.	6,200	52.2
Specimen B3 (1.5330 g.)		

Comments: H_2 diluted with argon during first 700 sec. Conversion was based on weight loss. Estimated bed depth was 1.0 mm. Reactor cooled to room temperature (argon atmosphere) prior to reduction-product removal.

TABLE II-2 (Continued)

RUN 94

375°C; 1.1% H_2O, 98.9% H_2

Flow rate: 5.0 cu.ft./hr.

Specimen B3 (1.5107 g.)

Time (sec.)	% Reduction (to MnO)
6,200	77.1

Comments: H_2 diluted with argon during first 700 sec. Conversion based on weight loss. Estimated bed depth was 1.0 mm. Reactor cooled to room temperature (argon atmosphere) prior to reduction-product removal.

RUN 95

375°C; 100% H_2

Flow rate: 5.0 cu.ft./hr.

Specimen B3 (1.5230 g.)

Comments: H_2 diluted with argon during first 700 sec. Estimated bed depth was 1.0 mm. Reactor cooled to room temperature (argon atmosphere) prior to reduction-product removal. Final conversion based on weight loss was 94.0%.

Time (sec.)	% Reduction (to MnO)
1,100	32.2
1,800	50.6
2,750	67.6
3,800	81.1
5,040	92.1
6,180	97.9

RUN 96

325/470°C; 100% H_2

Flow rate: 6.0 cu.ft./hr.

Specimen B6 (0.6335 g.)

Comments: Horizontal furnace used. Purged with argon while reactor was heated from 325° to 470°C. Temperature of second stage approximately plus or minus 20°C.

Time (sec.)	% Reduction (to MnO)	
600	58.9	(325°C)
842	96.2	(approx.
1,130	102.0	470°C)

TABLE II-2 (Continued)

RUN 97

325/470°C; 100% H_2

Flow rate: 6.0 cu.ft./hr.

Specimen B1 (0.6428 g.)

Comments: Horizontal furnace was used. Purged with argon while furnace temperature was raised from 325° to 470°C. Temperature of second stage approximately plus or minus 20°C. Reactor cooled to room temperature prior to reduction-product removal (argon atmosphere). Final % reduction based on weight loss was 99.3%.

Time (sec.)	% Reduction (to MnO)	
300	28.0	(325°C)
500	67.1	(approx.
708	98.2	
908	100.3	470°C)
1,120	99.9	

RUN 98

325/490°C; 100% H_2

Flow rate: 6.0 cu.ft./hr.

Specimen B4 (0.5909 g.)

Comments: Horizontal furnace was used. Purged with argon while furnace temperature was raised from 325° to 490°C. Temperature of second stage approximately plus or minus 20°C. Final % reduction based on weight loss was 96.9%.

Time (sec.)	% Reduction (to MnO)	
170	27.8	(325°C)
360	59.6	(approx.
452	96.5	
560	104.0	490°C)

RUN 99

325/525°C; 100% H_2

Flow rate: 6.0 cu.ft./hr.

Specimen B4 (0.5791 g.)

Comments:
Horizontal furnace was used. Purged with argon while furnace temperature was raised from 325° to 525°C. Temperature of second stage approximately plus or minus 20°C. Reactor cooled to 200°C (argon atmosphere) prior to reduction-product removal. Final % reduction based on weight loss was 92.4%.

Time (sec.)	% Reduction (to MnO)	
170	25.2	(325°C)
370	101.1	(525°C)

TABLE II-2 (Continued)

RUN 100

325/525°C; 100% H_2

Flow rate: 6.0 cu.ft./hr.

Specimen B4 (0.6646 g.)

Time (sec.)	% Reduction (to MnO)	
170	25.8	(325°C)
270	98.9	(525°C)

Comments:
Horizontal furnace was used. Purged with argon while furnace temperature was raised from lower to higher level. Reactor cooled to 200°C (argon atmosphere) prior to reduction-product removal. Final % reduction based on weight loss was 97.5%. Temperature of second stage approximately plus or minus 20°C.

RUN 101

325/525°C; 100% H_2

Flow rate: 6.0 cu.ft./hr.

Specimen B1 (0.8480 g.)

Time (sec.)	% Reduction (to MnO)	
170	22.7	(325°C)
370	101.8	(525°C)

Comments:
Horizontal furnace was used. Purged with argon while furnace temperature was raised from lower to higher level. Reactor cooled to room temperature (argon atmosphere) prior to reduction-product removal. Final % reduction based on weight loss was 99.7%. Temperature of second stage approximately plus or minus 20°C.

RUN 102

325/490°C; 100% H_2

Flow rate: 6.0 cu.ft./hr.

Specimen B4 (0.6236 g.)

Time (sec.)	% Reduction (to MnO)	
170	22.4	(325°C)
350	57.8	
520	105.1	(490°C)
685	105.2	

Comments:
Horizontal furnace was used. Purged with argon while furnace temperature was raised from 325° to 490°C. Reactor cooled to 200°C (argon atmosphere) prior to reduction-product removal. Final % reduction based on weight loss was 96.2%. Temperature of second stage approximately plus or minus 20°C.

TABLE II-2 (Continued)

RUN 103

325/570°C; 100% H_2

Flow rate: 5.0 cu.ft./hr.

Specimen B1 (0.6580 g.)

Time (sec.)	% Reduction (to MnO)	
170	18.95	(325°C)
670	94.9	(570°C)

Comments:
Horizontal furnace was used. Purged with argon while furnace temperature was raised from 325° to 570°C. Temperature of second stage approximately plus or minus 20°C. Reaction product was green, indicating complete reduction to MnO had been achieved, even though a conversion of only 94.9% had been measured. It is likely that some of the MnO_2 decomposed to Mn_2O_3 while furnace temperature was being raised.

RUN 104

550°C; 100% Argon; decompsition run.

Specimen B1 (3.8927 g.)

Comments: Specimen was heated in a slow stream of argon for approximately 1000 seconds after a temperature of approximately 550°C (possibly, somewhat higher) had been achieved. Based on weight loss (reactor cooled to room temperature prior to contacting the decomposed specimen with air), the % conversion to Mn_2O_3 was 97.3%.

RUN 105

400°C; 100% H_2

Flow rate: 6.0 cu.ft./hr.

Specimen B5 (0.6921 g.)

Time (sec.)	% Reduction (to MnO)
650	77.2
830	91.3

Comments: Horizontal furnace was used. H_2 was diluted with argon during first 550 seconds. Temperature escalated at least 10°C during the run. Reactor cooled to 200°C (argon atmosphere) prior to reduction-product removal. Final % reduction based on weight loss was 97.4%. Reduction product (prior to opening of reaction tube) was green, indicating that reduction to MnO was essentially complete. It is likely that some decompostion of the original MnO_2 to Mn_2O_3 occurred.

TABLE II-2 (Continued)

RUN 106

450°C; 9.73% H_2	Time (sec.)	% Reduction (to MnO)
Flow rate: 8.0 cu.ft./hr.		
	1,000	31.5
Specimen B4 (0.8873 g.)	2,150	62.6

Comments: Horizontal furnace was used. Reactor cooled to room temperature (argon atmosphere) prior to reduction-product removal. Final % reduction based on weight loss was 59.5%.

RUN 107

325/425°C; 100% H_2	Time (sec.)	% Reduction (to MnO)	
Flow rate: 6.0 cu.ft./hr.			
	200	10.5	(325°C)
Specimen B1 (0.6030 g.)			
	405	35.3	
Comments: Horizontal furnace	660	64.7	
was used. Reactor cooled to	925	84.3	(425°C)
room temperature (argon	1,155	92.8	
atmosphere) prior to reduction-	1,355	96.8	
product removal. Purged with	1,855	102.2	
argon while furnace temperature was raised from 325° to 425°C. Final % reduction based on weight loss was 93.0%			

RUN 108

325/450°C; 100% H_2	Time (sec.)	% Reduction (to MnO)	
Flow rate: 6.0 cu.ft./hr.			
	300	12.27	(325°C)
Specimen B1 (0.6227 g.)			
	490	37.4	
Comments: Horizontal furnace	620	61.9	
was used. Reactor cooled to	720	74.9	(450°C)
200°C prior to reduction-	1,020	99.0	
product removal. Purged with	1,300	102.2	
argon while furnace temperature was raised from 325° to 450°C. Final % reduction based on weight loss was 94.5%.			

TABLE II-2 (Continued)

RUN 109

325/500°C; 100% H_2

Flow rate: 6.0 cu.ft./hr.

Specimen B1 (0.5763 g.)

Comments: Horizontal furnace was used. Reactor cooled to 200°C prior to reduction-product removal. Purged with argon while furnace temperature was raised from 325° to 500°C. Final % reduction based on weight loss was 96.9%.

Time (sec.)	% Reduction (to MnO)	
300	13.50	(325°C)
500	59.3	
590	93.6	(500°C)
690	105.2	

RUN 110

325/500°C; 100% H_2

Flow rate: 6.0 cu.ft./hr.

Specimen B1 (0.6667 g.)

Comments: Horizontal furnace was used. Reactor cooled to 200°C prior to reduction-product removal. Purged with argon while furnace temperature was raised from 325° to 500°C. Final % reduction based on weight loss was 96.5%.

Time (sec.)	% Reduction (to MnO)	
300	13.27	(325°C)
495	59.7	
565	85.0	
660	98.6	
945	106.0	
1,320	106.8	

RUN 111

325°C; 100% H_2

Flow rate: 3.5 cu.ft./hr.

Specimen C1 (1.0004 g.)

Comments: Horizontal furnace was used. Temperature increased to 337°C at a reaction time of approximately 200 sec. Therefore, reactor was purged with argon at 250 seconds until temperature stabilized; finally, the reduction was resumed by starting H_2 flow again.

Time (sec.)	% Reduction (to MnO)	
250	75.4	
.	.	
.	.	(See note in comments)
.	.	
.	.	
450	79.5	
800	91.0	
1250	93.6	
2500	103.8	

TABLE II-2 (Continued)

RUN 112

440°C; 100% H_2

Flow rate: 6.0 cu.ft./hr.

Specimen C1 (2.4646 g.)

Comments: Horizontal furnace was used. No kinetic data; run was conducted to determine available oxygen in ore specimen by reduction with H_2. Temperature escalated during run. Reactor cooled to room temperature (argon atmosphere) prior to sample removal. The % available oxygen was determined to be 16.10% by water recovery, and 15.95% by weight loss.

RUN 113

600°C; 100% H_2

Flow rate: 6.0 cu.ft./hr.

Specimen B1 (0.7104 g.)

Comments: Horizontal furnace was used. No kinetic data; stability of MnO product formed at an apparent temperature of 600°C was investigated. Reactor cooled to 200°C (argon atmosphere) prior to sample removal. Final % reduction based on water recovery was 56.5% and based on weight loss was 100.6%. It may be concluded that (1) the product MnO was relatively stable, and (2) some decomposition of MnO_2 to Mn_2O_3 occurred.

RUN 114

700°C; 100% H_2

Flow rate: 6.0 cu.ft./hr.

Specimen B1 (0.6119 g.)

Comments: Horizontal furnace was used. No kinetic data; stability of MnO product formed at an apparent temperature of 700°C was investigated. Reactor cooled to 200°C (argon atmosphere) prior to sample removal. Final % reduction based on water recovery was 56.0% and based on weight loss was 100.9%. It may be concluded that (1) the product MnO was relatively stable, and (2) some decomposition of MnO_2 to Mn_2O_3 occurred.

TABLE II-2 (Continued)

RUN 115

700°C; 100% Argon

Specimen B1 (0.7058 g.)

Comments: Decomposition run in horizontal-tube furnace. Sample was heated in a slow stream of argon for approximately 10 minutes. Reactor was cooled to room temperature prior to exposing product to air. The extent of decomposition (based on weight loss) expressed in terms of "% reduction to MnO" was 54%. Hence, MnO_2 was completely decomposed to Mn_2O_3 in less than 10 minutes.

RUN 116

350°C; 100% H_2	Time (sec.)	% Reduction (to MnO)
Specimen C2 (5.1007 g.)		
	1,430	86.8
Flow rate: 6.0 cu.ft./hr.	1,890	99.6

Comments: Vertical-tube reactor was used. H_2 was diluted with argon during first 550 seconds. Temperature could not be controlled; maximum temperature was approximately 370°C. Final % reduction based on weight loss was 90.6%.

RUN 117

300°C; 100% H_2	Time (sec.)	% Reduction (to MnO)
Specimen C1 (1.4521 g.)		
	950	101.0
Flow rate: 6.0 cu.ft./hr.		

Comments: Vertical-tube reactor was used. H_2 was diluted with argon during first 560 seconds. Temperature escalated rapidly, and entire sample reacted to MnO before any kinetic data were taken. Maximum apparent temperature was approximately 330°C.

TABLE II-2 (Continued)

RUN 118

250°C; 100% H_2

Flow rate: 5.0 cu.ft./hr.

Specimen C1 (1.6641 g.)

Comments: H_2 was diluted with argon during first 490 seconds. Estimated bed depth was 1.0 mm.

Time (sec.)	% Reduction (to MnO)
700	7.90
950	14.18
1,350	26.5
2,010	44.7
2,600	54.6
3,730	65.3
5,140	74.4
6,160	78.3
6,820	80.5

RUN 119

275°C; 100% H_2

Flow rate: 5.0 cu.ft./hr.

Specimen C1 (1.3424 g.)

Comments: Estimated bed depth was 1.0 mm.

Time (sec.)	% Reduction (to MnO)
840	37.8
1,040	50.3
1,300	57.6
1,550	62.8
2,050	71.3
3,680	87.6
5,000	94.7
6,050	98.1
6,850	100.1

TABLE II-2 (Continued)

RUN 120

275/325°C; 100% H_2

Flow rate: 5.0 cu.ft./hr.

Specimen C1 (1.4568 g.)

Comments:
H_2 was diluted with argon during first 660 seconds. Estimated bed depth was 1.0 mm. Purged with argon while furnace temperature was raised from 275° to 325°C. Final % reduction based on weight loss was 65.7%.

Time (sec.)	% Reduction (to MnO)	
950	50.2	(275°C)
1,170	63.2	
1,340	78.2	
1,510	85.2	
1,680	88.4	(325°C)
1,970	94.5	
2,480	98.5	
3,040	100.7	

RUN 121

225°C; 100% H_2

Flow rate: 5.0 cu.ft./hr.

Specimen C1 (2.1044 g.)

Comments:
Estimated bed depth was 1.4mm. Final % reduction based on weight loss was 53.0%.

Time (sec.)	% Reduction (to MnO)
240	1.50
690	4.78
1,300	8.33
2,590	17.48
3,850	28.5
5,100	40.0
6,150	47.9
7,550	55.9
8,460	59.8
9,540	63.7

TABLE II-2 (Continued)

RUN 122

225/250/300°C; 100% H_2

Flow rate: 5.0 cu.ft./hr.

Specimen C3 (8.5814 g.)

Comments:
Single lump of ore was reduced to various stages at three temperatures, starting at 225°C. Purged with argon while furnace temperature was raised from one level to another. Final % reduction based on weight loss was 78.0%; product partially re-oxidized upon contact with air.

Time (sec.)	% Reduction (to MnO)	
900	0.51	
2,030	1.23	(225°C)
3,600	2.23	
4,420	2.75	
4,710	2.99	
5,460	4.25	
6,460	6.26	(250°C)
7,560	8.72	
7,790	9.30	
8,010	10.31	
8,310	15.06	
8,610	21.5	
9,220	42.2	(300°C)
9,810	77.0	
10,440	82.6	
11,790	88.3	
13,350	92.6	

RUN 123

300°C; 9.73% H_2 (balance, He)

Flow rate: 10.0 cu.ft./hr.

Specimen C1 (1.4473 g.)

Comments:
Estimated bed depth was 1.0 mm. Final % reduction based on weight loss was 67.1%; product partially re-oxidized upon contact with air.

Time (sec.)	% Reduction (to MnO)
230	2.75
420	8.51
685	18.30
1,060	37.1
1,750	56.4
2,370	64.5
3,150	71.5
4,630	81.3
5,800	86.3

REFERENCES

1. Anikeev, V. A., Lyubau, A. P., Manchinskii, V. G., Tr. Leningr. Politekh. Inst., No 212, 52 (1960).

2. Chufarov, G. I., Averbukh, B. D., Tatievskaya, E. P., Zh. Fiz. Khim., 26, 834 (1952).

3. Cismaru, I. D., Vass, M., Rev. Chim., Acad. Rep. Populaire Roumaine, 7, No. 1, 101 (1962).

4. Clevenger, G. H., Caron, M. H., U. S. Bur. Mines Bull. 226, 36 (1925).

5. Cranston, R. W. and Inkley, F. A., Advances in Catalysis, IX, Academic Press, New York, 1957, p. 143.

6. Dunoyer, Jean M., Compt. Rend., 208, 1018 (1939).

7. Elliott, J. F. and Gleiser, M., Thermochemistry for Steel Making, Addison-Wesley, Reading, Massachusetts, 1960.

8. Frank, F. C. and van Der Merwe, J., Proc. Roy. Soc. (London) Ser. A, 198, 203 (1949).

9. Ibid., 200, 125 (1950).

10. Gattow, G. and Glemser, O., Z. Anorg. Allgem. Chem., 309, 20 (1961).

11. Ibid., 121.

12. Glemser, O., Gattow, G., Meisieh, H., Z. Anorg. Allgem. Chem., 309, 1 (1961).

13. Grasselly, Gy., Acta Univ. Szeged., Acta Mineral. - Petrog., 8, 13 (1955).

14. Ibid., 9, 41 (1956).

15. Grasselly, Gy. and Klivenyi, E., Acta Univ. Szeged., Acta Mineral. - Petrog., 9, 15 (1956).

16. Hanawalt, et al., Anal. Chem., 10, 475 (1938).

17. Langmuir, I., J. Am. Chem. Soc., 38, 2263 (1916).

18. Levenspiel, O., Chemical Reaction Engineering, Wiley, New York, 1962.

19. McMurdie, H. F. and Golovato, E., J. Res. Natl. Bur. Std., 41, 589 (1948).

20. Minerals Handbook, U. S. Bur. Mines, Div. of Minerals, 1959.

21. Ibid., 1964.

22. Moore, T. E., Ellis, M., Selwood, P. W., J. Am. Chem. Soc., 72, 856 (1950).

23. Nelson, F. M. and Eggertsen, F. T., Anal. Chem., 30, 1387 (1958).

24. Osman, M. A., Manning, F. S., Philbrook, W. O., A. I. Ch. E. J., 12, 685 (1966).

25. Petersen, E. E., Chemical Reaction Analysis, Prentice-Hall, Englewood Cliffs, New Jersey, 1965.

26. Rode, E. Ya., Zh. Neorgan. Khim., 1, 1430 (1956).

27. Satterfield, C. N. and Sherwood, T. K., The Role of Diffusion in Catalysis, Addison-Wesley, Reading, Massachusetts, 1963.

28. Shen, J. and Smith, J. M., Ind. Eng. Chem. Fundamentals, 4, 293 (1965).

29. Soldatkin, A. I., Domennoe Proiz. Sb. Statei, 56 (1957).

30. Sorem,R. and E. Cameron, Econ. Geol., 55, 278 (1960).

31. Swanson, H., et al., Natl. Bur. Std. (U.S.), Circ. 539, 5, 45 (1955).

32. Ibid., 9, 37 (1959).

33. Tatievskaya, E. P., Antonov, V. K., Chufarov, G. I., Dokl. Akad. Nauk S.S.S.R., 68, 561 (1949).

34. Tatievskaya, E. P., Chufarov, G. I., Antonov, V. K., Izv. Akad. Nauk S.S.S.R., Otd. Tekhn. Nauk, 371 (1948).

VITA

Herbert E. Barner was born on in . He attended public schools in Irvington and Union, New Jersey, and in 1958 was graduated from Newark College of Engineering with a B.S. in Chemical Engineering. He served as an officer in the United States Air Force from 1958 to 1961. Following his release from active duty he undertook a year of graduate study at Carnegie Institute of Technology, from which he received his M.S. in Chemical Engineering in 1963.

He was employed as a development engineer by The M. W. Kellogg Company from September, 1962 to September, 1964, and early in 1963 he enrolled in the doctoral program at Newark College of Engineering on a part time basis. From September, 1964 to September, 1966 he served as an Assistant Instructor at Newark College of Engineering, while concurrently pursuing his graduate studies and research. Presently, he is employed as a research engineer in the Research and Engineering Development Division of The M. W. Kellogg Company.